UNIVERSITAT POLITÈCNICA DE CATALUNYA BARCELONATECH

On the fracture behavior of ductile polymer films : notch quality, essential work of fracture, J-integral, and crack tip opening displacement

Noel León Albiter

On the fracture behavior of ductile polymer films: Notch quality, essential work of fracture, J-integral, and crack tip opening displacement

A Thesis by compendium of publications submitted in fulfillment of the requirements for the degree of Doctor by the Universitat Politècnica de Catalunya-BarcelonaTech

Noel León Albiter

Department of Materials Science and Metallurgical Engineering
Doctorate Program in Materials Science and Engineering
Universitat Politècnica de Catalunya-BarcelonaTech

Advisor: Antonio Martínez Benasat

Barcelona, February 2018

Abstract

Polymers have a wide range of applications. Their ability to be shaped into multiple forms makes it possible to obtain polymer films, which are highly used in industries such as food and pharmaceuticals. Characterization of polymer films using the classical mechanical properties is well-defined; however, this is not the case for the fracture properties.

The Linear Elastic Fracture Mechanics (LEFM) approach studies fractures where the plastic deformation is confined to a small zone around the crack tip. However, when the plastic deformation at the crack tip becomes too large, the Elastic Plastic Fracture Mechanics (EPFM) is applied by using the J-integral and crack tip opening displacement (CTOD) fracture parameters. Finally, if the crack propagates through a highly deformed and yielded material, the Post-Yield Fracture Mechanics (PYFM) is used and the Essential Work of Fracture (EWF) is a suitable method to characterize fracture.

The overall aim of this work was to analyze in full-detail the fracture behavior of ductile polymer films by applying the appropriate fracture mechanics approaches. Specific objectives include: i) to provide a better understanding of factors affecting the EWF test, ii) to analyze the effect of the notch sharpening procedure on the fracture parameters values, iii) to clarify the aspects that make the specific essential work of fracture (w_e) and inherent material property and equal to the J-value at crack initiation J_{IC}, and iv) to investigate in detail the effect of the notch quality on the shape of the stress-displacement curves and on the propagation range.

The first part of the thesis aimed to investigate the existing relationships between the w_e, J_{IC}, and $CTOD_C$ (CTOD at crack initiation) values and find clear evidence that makes w_e the specific energy at crack initiation, that is, an initiation value. To do this, the Digital Image Correlation (DIC) technique was applied in double edge notched tension (DENT) specimens. Applying this technique makes it possible to measure the displacement and ligament length at the same time, allowing that the EWF, the J-integral, and the CTOD fracture approaches to be performed in a single set of DENT specimens.

The second part of the thesis was focused on analyzing the influence of the notch quality on the fracture behavior. The specimen preparation, particularly the notch sharpening technique, has been studied in more depth. With the purpose of seeing the influence of the notch sharpening procedure, several techniques have been used, including femtosecond laser ablation, razor blade sliding on specimens at room temperature and frozen by liquid nitrogen, saw cutting, plastically deformed saw cutting, scalpel sliding and drilled holes used as notches. The effects of the non-collinearity of the notches and misalignment of the specimens with respect to the direction of tension have also been

studied. The results revealed that all of the femtolaser sharpened notches had very consistent, sharp notches without plastic deformation in front of the notch tip. Instead, the razor blade sliding technique (the generalized way to sharpen notches in ductile polymer films) produced very sharp cracks, as sharp as the femtolaser ones, but the different compressive component of the sliding force that was applied by the operator generated notches with different levels of plastic deformation ahead of the notch tip.

As different notch sharpening techniques produce different levels of plastic deformation at the crack tip, differences would also be expected in the shape and size of the stress-displacement curves. In the third part of the thesis, the shape and size of the stress-displacement curves that were notched in distinct ways were analyzed to clarify their EWF behavior. In the propagation region, it is also identified the parabolic shape of the stress-displacement curves, which modeled relates the specific non-essential work of fracture with the stress at crack initiation and the extension ratio during the crack growth.

Keywords: polymer films; fracture mechanics; fracture properties; essential work of fracture; J-integral; crack tip opening displacement; notch quality; femtosecond laser ablation; razor blade sliding; digital image correlation; double edge notched tension specimen geometry

Preface

This dissertation has been written to fulfill the requirements for obtaining the degree of Doctor in Materials Science and Engineering at Universitat Politècnica de Catalunya – Barcelona Tech during the period from 15th of September 2014 to the 1st of February 2017. This Ph.D. thesis was performed at the Centre Català del Plàstic (CCP) under the supervision of Antonio Martínez Benasat professor in the Department de Ciència dels Materials I Enginyeria Metal-lúrgica (CMEM) of the Universitat Politècnica de Catalunya (UPC).

This Ph.D. thesis is presented within the modality designated as a compendium of publications. This modality takes into consideration the published articles in international journals as a result of the work performed during the time that this Ph.D. thesis lasted.

The dissertation includes five chapters, which are described henceforward. Chapter 1 presents and defines the main concepts as used to describe the fracture behavior of polymeric materials. Chapter 2 is integrated with the main research performed to evaluate the fracture toughness of ductile polymer films and summarizes the aims of the thesis as well. In chapter 3, the articles obtained from this thesis are presented in full-length. In chapter 4, a discussion comparing the results obtained for the distinct materials is made. Finally, chapter 5 includes a summary of conclusions and future research lines to follow.

List of publications

The following list presents the compendium of the articles that resulted from this thesis.

Article I. Martínez AB, **León N**, Arencón D, Sánchez-Soto M. Essential work of fracture, crack tip opening displacement, and J-integral relationship for a ductile polymer film. Polymer Testing 2016; 55: 247-256. IF: 2.464, Q1 (6/33), area: Materials Science, Characterization & Testing and Q2 (27/86), area: Polymer Science. DOI: 10.1016/j.polymertesting.2016.09.004.

Article II. Martínez AB, **León N**, Arencón D, Sánchez-Soto M. The post-yield fracture of a ductile polymer film: Notch quality, essential work of fracture, crack tip opening displacement, and J-integral. Engineering Fracture Mechanics 2017; 173: 21-31. IF: 2.151, Q2 (41/133), area: Mechanics. DOI: 10.1016/j.engfracmech.2017.01.019.

Article III. Martínez AB, **León N**, Segovia A, Cailloux J, Martínez PP. Effect of specimen notch quality on the essential work of fracture of ductile polymer films. Engineering Fracture Mechanics 2017; 180: 296-314. IF: 2.151, Q2 (41/133), area: Mechanics. DOI: 10.1016/j.engfracmech.2017.06.007.

Article IV. León N, Martínez AB, Castejón P, Arencón D, Martínez PP. The fracture testing of ductile polymer films: Effect of the specimen notching. Polymer Testing 2017; 63: 180-193. IF: 2.464, Q1 (6/33), area: Materials Science, Characterization & Testing and Q2 (27/86), area: Polymer Science. DOI: 10.1016/j.polymertesting.2017.08.022.

Article V. León N, Martínez AB, Castejón P, Martínez PP, Arencón D. Notch effect on the fracture of a polymeric film **(Under review**). Theoretical and Applied Fracture Mechanics 2018. IF:2.659, Q1 (24/130), area: Engineering, Mechanical and Q1 (21/133), area: Mechanics.

Additional contributions include:

Article:

Martínez AB, Salazar A, León N, Illescas S, Rodríguez J. Influence of the notch-sharpening technique on styrene-acrylonitrile fracture behavior. Journal of Applied Polymer Science 2016; 133: 43775. IF: 1.86, Q2 (36/86), area: Polymer Science. DOI: 10.1002/app.43775.

Journal reviewer for:

- Journal of Applied Polymer Science
- Engineering Fracture Mechanics

Table of contents

List of figures and tables

Figures

Tables

Glossary of symbols

a	crack length
BG	scalpel pre-notching + razor blade sliding
CHDM	cyclohexanedimethanol
CTOD	crack tip opening displacement
DENT	double edge notched tension
DIC	digital image correlation
DMTA	dynamic mechanical thermal analysis
ds	element of arc in the contour S
e	engineering strain
E	elastic modulus/Young's modulus
ECOZEN	bio-based amorphous copolyester
EPBC	ethylene-propylene block copolymer
EPFM	Elastic Plastic Fracture Mechanics
EPR	elastomeric particles
ESIS	European Structural Integrity Society
f (θ)	dimensionless calibration factor
F	applied load
FPZ	fracture process zone
G	energy release rate
GPC	gel permeation chromatography
J	J-integral
K	stress intensity factor
l	final length
L	specimen length
LEFM	Linear Elastic Fracture Mechanics
m-LLDPE	metallocene linear low-density polyethylene
MD	machine direction
MFI	melt flow index
n	hardening exponent
NMR	nuclear magnetic resonance
OM	optical microscopy
OPZ	outer plastic zone

P	registered load
PE	polyethylene
PET	polyethylene terephthalate
PETG	polyethylene terephthalate glycol-modified
PMMA	polymethyl methacrylate
PP	polypropylene
PS	polystyrene
PVC	polyvinyl chloride
PYFM	Post-Yield Fracture Mechanics
r	distance from the crack tip
S	arbitrary contour around the crack tip
SD	pre-notches forming saw cut slots + deformed plastically
SEM	scanning electron microscopy
SGN	pre-notches frozen by liquid nitrogen + razor blade sliding
t	specimen thickness
T	traction vector
TC4	ESIS technical committee 4
u	displacement vector
U	energy dissipated in fracture the specimen
V	volume inside the contour S
W	specimen width
Z	distance between clamps
$\mathbf{a_e}$	effective crack length
$\mathbf{A_o}$	original cross-sectional area
$\mathbf{CTOD_C}$	critical crack tip opening displacement
$\mathbf{d_i}$	displacement at crack initiation
$\mathbf{d_r}$	displacement at rupture
$\mathbf{d_{\sigma max}}$	displacement at maximum stress
$\mathbf{G_C}$	critical energy release rate
$\mathbf{G_{IC}}$	critical energy release rate in mode I
$\mathbf{J_{IC}}$	J-integral value at crack initiation in mode I
$\mathbf{K_C}$	critical stress intensity factor
$\mathbf{K_{IC}}$	critical stress intensity factor in mode I
$\mathbf{l_i}$	ligament length at displacement at crack initiation
$\mathbf{l_n}$	integration constant for a n-range

$\mathbf{l_o}$	initial ligament length
$\mathbf{M_n}$	average molecular mass in number
$\mathbf{m_p}$	plastic constraint factor
$\mathbf{M_w}$	average molecular mass in weight
$\mathbf{M_z}$	Z-average molecular weight
$\mathbf{r_p}$	plastic zone radius
$\mathbf{r_y}$	plastic zone correction
$\mathbf{T_g}$	glass transition temperature
$\mathbf{T_m}$	melting temperature
$\mathbf{U_G}$	energy required to grow a crack
$\mathbf{U_{load}}$	potential energy due to applied loads
$\mathbf{U_p}$	energy absorbed during the crack propagation per ligament section
$\mathbf{U_{strain}}$	stored strain potential energy
$\mathbf{u_y}$	crack opening
$\mathbf{w_e}$	specific essential work of fracture
$\mathbf{W_e}$	essential work of fracture
$\mathbf{w_f}$	specific total work of fracture
$\mathbf{W_f}$	total work of fracture
$\mathbf{W_n}$	work of fracture for necking and tearing
$\mathbf{W_p}$	non-essential work of fracture
$\mathbf{W_s}$	strain energy density
$\mathbf{W_v}$	work related to recoverable viscoelastic deformation
$\mathbf{W_y}$	work needed for yielding the ligament area
$\mathbf{W_I}$	irreversible initiation process involving yielding, necking, and crack tip blunting
$\mathbf{W_{II}}$	work related to crack propagation and extended necking in the plastic zone
$\boldsymbol{\alpha}$	extension ratio at rupture
$\boldsymbol{\beta}$	geometrical shape factor related to OPZ
$\boldsymbol{\gamma}$	specific surface energy
$\boldsymbol{\Delta l}$	change in length
$\boldsymbol{\theta}$	angle measured from the crack plane
$\boldsymbol{\upsilon}$	Poisson's ratio
$\boldsymbol{\sigma}$	engineering stress
$\boldsymbol{\beta w_p}$	specific non-essential work of fracture
$\boldsymbol{\Delta a_b}$	increment of crack length at blunting
$\boldsymbol{\varepsilon_{ij}(\theta,n)}$	dimensionless strain function of θ and n

σ_f	stress at the onset of fracture
σ_{fs}	engineering flow stress
σ_i	crack initiation stress
σ_{ij}	stress components
σ_{ij} **(θ,n)**	dimensionless stress function of θ and n
σ_{max}	maximum stress
$\sigma_{max,av}$	mean of the maximum stress
σ_o	initial yield strength
σ_y	uniaxial tensile yield stress
σ_{yield}	effective yield stress
τ_1	in-plane shear stress
τ_2	out-of-plane shear stress

Chapter 1

Introduction

This chapter is integrated by basic concepts will provide the necessary tools for a better understanding of all the aspects related to this thesis work.

1.1 Basic definitions

The word polymer comes from two Greek terms, poly (many) and mer (parts) [1]. A polymer is a very long molecule formed by small molecules called monomers [2], being the monomer the repeating unit in the molecular structure.

A polymer is termed homopolymer if only one kind of monomer appears in its molecular structure; if there is more than one type of monomer, then the polymer is termed copolymer [3].

Polymers can be naturally occurring (DNA, silk, wool) or synthetic (Teflon, nylon, polyester) [4]. In synthetic polymers, the process through which monomers are linked together chemically to form a polymer is known as polymerization [5].

Polymerization can be divided into two types: addition and condensation [6]. In addition polymers, the double bonds of monomers react to form a long chain without generating small molecules. Instead, in condensation polymers, the monomers react together losing small molecules like water or alcohol.

There are different ways to classify polymers, e.g., based on their source, chemical structure, polymer structure, method of synthesis, molecular forces, thermal response, etc. [7]. In our study, we will be particularly interested in the classification of polymers based on their behavior in presence of heat, i.e., thermoplastics and thermosets [8].

Thermoplastic raw materials soften when heated [9] and with enough heat eventually melt. It is in this state that can be shaped into multiple forms, which are kept after cooling a proper time. This process can be repeated several times (is reversible), without affecting the polymer properties.

Thermoplastics can be divided into two groups: amorphous and semicrystalline [10]. In amorphous polymers, the molecular chains are randomly ordered. Semicrystalline polymers possess highly ordered zones called spherulites, which are connected to each other with amorphous layers [11].

Thermoset raw materials are also softened by heat [12] and can be shaped too, but when cooled remain as highly cross-linked polymers that upon heating degrade instead of melt and, in consequence, cannot be thermally processed again.

Polymers have two transition temperatures [13], the glass transition temperature (T_g) and the melting temperature (T_m). Amorphous polymers only exhibit one transition (T_g); while, semicrystalline polymers exhibit both, T_g and T_m.

T_g is the temperature below which the polymer is hard and brittle, similarly to glass, and above what is flexible and soft like rubber [14]. T_m is the temperature at which the polymer crystals disappear when the polymer is heated [15].

The study of the mechanical response to an applied load is essential so as to make a good material selection. In this sense, some important mechanical properties used along this study are defined next.

The engineering stress (σ) is the applied load (F) divided by the original cross-sectional area (A_o) perpendicular to the load or

$$\sigma = \frac{F}{A_o} \qquad \text{Eq. (1.1)}$$

When a material is stressed, it is deformed. The strain (e) is a measure of deformation and is defined as,

$$e = \frac{l - l_o}{l_o} = \frac{\Delta l}{l_o} \qquad \text{Eq. (1.2)}$$

where l_o is the initial length, l is the final length after deformation, and Δl is the change in length.

The Hooke's law states that in the small displacement range (elastic deformations) σ is proportional to e as follows

$$\sigma = Ee \qquad \text{Eq. (1.3)}$$

where the constant of proportionality E is the Young's modulus and represents the material's resistance to be deformed elastically [16].

Several important properties including the Young's modulus can be identified through the tensile test. In this kind of test, a standard specimen is uniaxially loaded until failure to obtain a plot like that one shown in Figure 1.1.

The yield stress (σ_y) indicates the point at which the material starts to deform plastically [17]. The yield point is usually set at maximum load in polymers.

In several polymers, after the yield point is reached, the necking process begins. Here, a reduction in the specimen cross-sectional area manifested as a drop in load can be seen in the stress-strain curve. The process by which the neck extends along the specimen length is known as cold drawing [18].

The mechanical properties of polymers are heavily dependent on time and temperature at which are estimated (Figure 1.2), this is result of their viscoelastic nature [19].

A viscoelastic material has properties of both elastic solid (Hookean) and viscous fluid (Newtonian). In an elastic solid, the deformation is proportional to the stress, while in a viscous fluid the rate of deformation is proportional to the stress [20].

The viscoelastic behavior of polymers is revealed by modifying the testing conditions (strain rate and temperature). An increase in the strain rate causes also an increase in E and σ_y, making the polymer more rigid and brittle [21]. The same tendency is observed when the temperature is reduced.

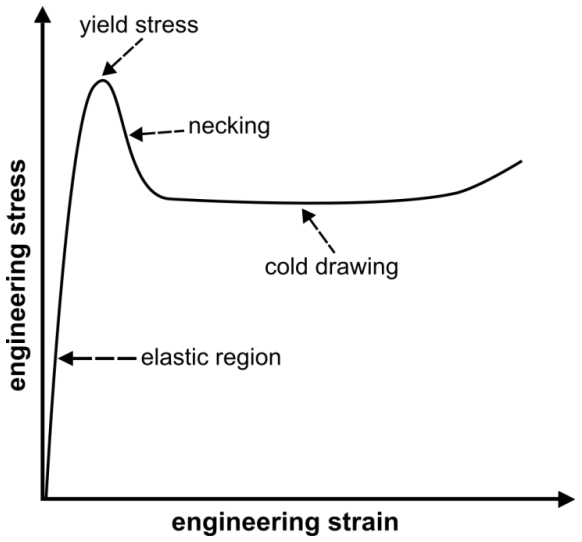

Figure 1.1 A typical engineering stress-strain curve for a ductile polymer film

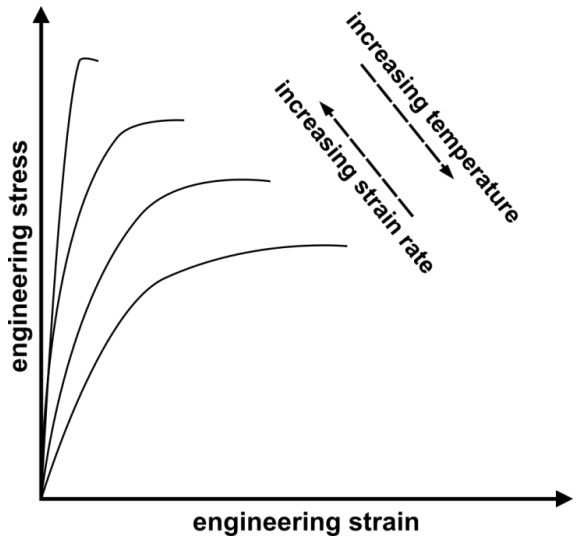

Figure 1.2 Strain rate and temperature effects on the mechanical behavior of polymers

1.2 Fracture mechanics

The strength-based design approaches [22] assume the material as a continuum without flaws [23]. However, several times, the material suffers catastrophic failures at load levels well below its yield strength [24]. This phenomenon is attributed to the presence of microscopic flaws or cracks [25], which act as stress concentrators that provoke sudden failure without prior notice. The idea of considering materials with flaws or imperfections intrinsic to their structure gave origin to the fracture mechanics concept.

Fracture mechanics characterizes the stress and strain fields near to a crack tip [26] and can be divided into three branches: Linear elastic fracture mechanics (LEFM), elastic-plastic fracture mechanics (EPFM), and post-yield fracture mechanics (PYFM). The approach chosen depends on the extension of the plastic zone in the vicinity of the crack tip.

1.2.1 Types of fracture

For the purposes of this study, a fracture can be defined as the separation into two or more parts of a component (specimen) subjected to loadings [27]. There are two types of fracture: brittle fracture and ductile fracture [28].

Brittle fracture occurs without significant plastic deformation [29] around the crack tip (small-scale yielding assumption) at the moment of crack initiation. It is characterized by unstable (instantaneous) crack growth when a critical load is reached at the crack tip.

Ductile fracture involves a large amount of plasticity at the crack tip at crack initiation. In this kind of fracture, the crack growth is stable [30], which implies the possibility that the crack stops growing on the removal of the load.

1.2.2 Linear Elastic Fracture Mechanics (LEFM)

LEFM is the basic theory of fracture [31] emerged when the concept of fracture became important to analyze the structural integrity of work components such as those used in engineering applications.

This approach is applicable to cracked elastic bodies, which response to loads is linear-elastic until final failure. However, inevitably, a small plastic zone ahead of the crack tip that does not meet this condition is generated, and LEFM includes in its analysis only if the dimensions of the plastic zone are restricted to a small region when compared to the bulk dimensions of the material (assumption of small-scale yielding) [32].

LEFM considers only cases where the fracture is brittle and uses two approaches to predict it, an energy-based approach and a stress-based approach [33].

1.2.2.1 Energy release rate (G)

Inglis [34] was the first to identify that the stress concentrations generated near to cracks decreased severely the material's strength, causing failure at lower stresses than the expected (the theoretical yield strength). However, his mathematical solution introduces a stress singularity at the crack tip that hinders its applicability to real cases.

Griffith [35] seeing the difficulties of using a strength criterion for the analysis of the crack propagation in elastically stressed bodies [36], addressed the issue from an energetic point of view.

Making an energy balance in an infinite plate similar to that one of Figure 1.3, Griffith found a relation for the stress needed to promote crack propagation, such that

$$\sigma = \sqrt{\frac{2\gamma E}{\pi a}} \qquad \text{Eq. (1.4)}$$

where σ is the remote tensile stress, γ is the specific surface energy, E is the elastic modulus, and a is the crack length.

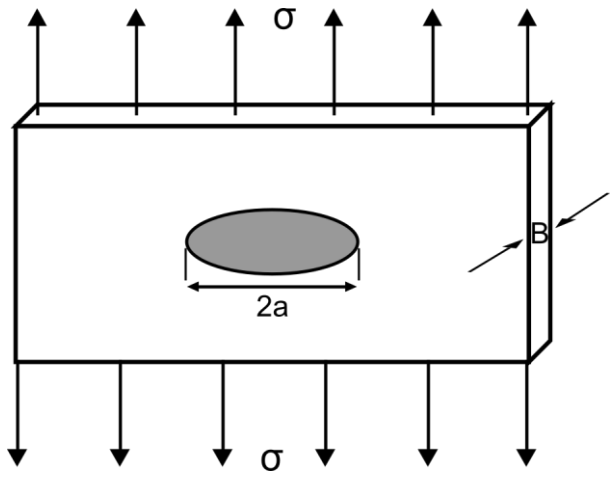

Figure 1.3 Infinite plate with a through-thickness crack subjected to a remote stress

Griffith developed its expression for determining the fracture strength of a very brittle material such as glass [37]. Nevertheless, materials like polymers and metals present localized plastic

deformation at the moment of crack propagation, causing an increase in the energy requirements. Thus, in these cases, the surface energy on its own is insufficient to quantify the energy required to promote crack growth.

With this in mind, Irwin [38] defined a new concept, the energy release rate G. It encloses the surface energy, plastic deformation, friction, micro-cracking, craze formation, void growth, and all other dissipation processes [39] related to the fracture process.

Thus, Equation (1.4) now can be rewritten as

$$\sigma = \sqrt{\frac{GE}{\pi a}} \qquad \text{Eq. (1.5)}$$

An important conclusion of this analysis is that the crack will only grow when the available energy release rate G reaches a critical value G_c (critical energy release rate). G depends on the specimen geometry, applied load, and crack length [40]. On the other hand, G_c also known as fracture energy is considered to be a material property, which represents the resistance of the material to crack propagation and can be only determined experimentally [41].

In terms of G_c, at fracture initiation, Equation (1.5) becomes

$$G_c = \frac{{\sigma_f}^2 \pi a}{E} \qquad \text{Eq. (1.6)}$$

where σ_f is the stress at the onset of fracture.

1.2.2.2 Stress intensity factor (K)

The solutions found by Inglis and Westergaard [42] to characterize fracture behavior using stress analysis lead to the conclusion that the stress at the crack tip is infinite [43], but no real material can withstand infinite stresses [44].

Irwin in 1957 [45] established that the field surrounding the crack tip can be characterized by a unique parameter [46] defined as the stress intensity factor (K). Using a uniformly stressed infinite plate (Figure 1.4), Irwin deducted the following relationship

$$\sigma_{ij} = \frac{K}{\sqrt{2\pi r}} f_{ij}(\theta) \qquad \text{Eq. (1.7)}$$

where σ_{ij} are the stress components, r is the distance from the crack tip, θ is the angle measured from the crack plane, and f (θ) is a dimensionless calibration factor. σ_{ij}, r, and θ are calculated at the point of interest.

The fracture parameter K avoids the stress singularity found at the crack tip (the term $\sigma(2\pi r)^{1/2}$ is finite) and also determines the overall stress magnitude near to the crack tip [47].

The LEFM theory states that crack propagation will occur when K reaches a critical value K_c (critical stress intensity factor). It is this value which is directly related to the strength of the material and therefore is considered as a material property under specified testing conditions [48].

While K_c is a material property, K depends on the structural integrity, crack size, and applied load [49]. The K_c value has to be determined experimentally and, with it, the critical fracture stress can be determined.

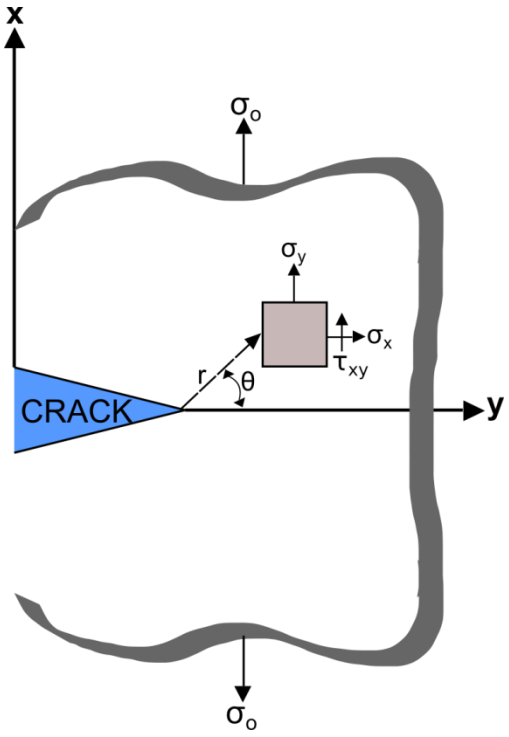

Figure 1.4 Infinite stressed plate showing a through-thickness sharp crack and the polar coordinates of an arbitrary point near to the crack tip

1.2.3 Loading modes

When loads are applied to a cracked body, the stress concentrator (crack tip) can be subjected to three different types, or any combination, of the following stresses: normal stress (σ), in-plane shear stress (τ_1), and out-of-plane shear stress (τ_2) [50] (Figure 1.5).

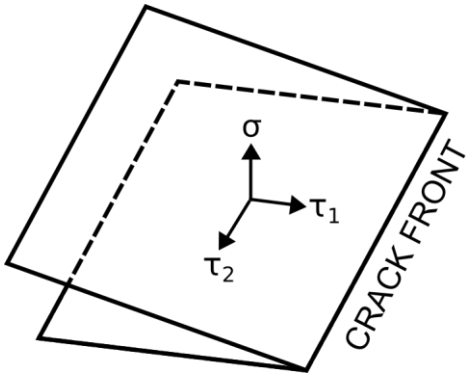

Figure 1.5 Possible types of stresses at the crack tip [50]

In fracture mechanics, these stresses are related to the crack propagation process through three different loading modes, as depicted in Figure 1.6.

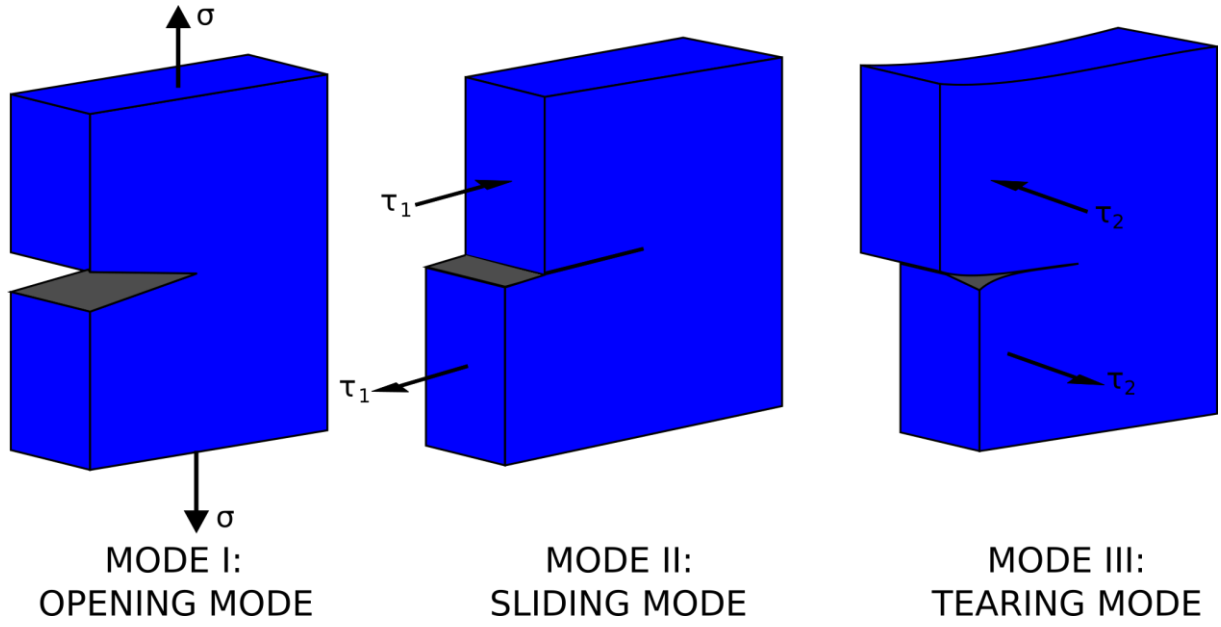

Figure 1.6 Modes of crack propagation

In mode I (opening mode), the crack tip is loaded in tension, with the tensile forces being normal to the crack plane, and the newly generated crack surfaces growing perpendicular to the crack plane.

Mode II (sliding mode) is where the crack tip experiences in-plane shear stresses that make the crack faces slide one above the other. In this way, the new crack surfaces grow on the crack plane and perpendicular to the crack front [50].

In mode III or tearing mode, the crack tip is subjected to anti-plane (out-of-plane) shear stresses that make the crack faces also slide one above the other along the crack plane, but, in this case, the crack growth is parallel to the crack front [50].

It should be clarified that can also exist situations in which the crack growth is as a combination of two or even three loading modes, this is called mixed-mode loading.

The fracture parameters K and G can adopt the subscripts I, II, or III depending on the loading mode prevailing at the crack tip. This criterion can also be extrapolated to other fracture mechanics approaches.

Since the natural crack growth is perpendicular to the maximum principal tensile stress, most failures come from crack propagation under loading mode I. Hence, the opening mode is the most used to analyze the stress fields surrounding the crack tip.

With this in mind, the LEFM fracture criteria to obtain the stress-based and energy-based fracture parameters values are established as follows

$$K \geq K_{IC} \quad \text{Eq. (1.8)}$$

$$G \geq G_{IC} \quad \text{Eq. (1.9)}$$

where K_{IC} and G_{IC} are the critical stress intensity factor in mode I and critical energy release rate in mode I, respectively.

1.2.4 State of stress

If the orientation in space of any stressed body is selected correctly, there is a unique orientation with three mutually perpendicular planes where the shear stresses are zero. These planes are called principal planes, and the normal stresses on these planes are called principal stresses [51]. The principal stresses, σ_1, σ_2, and σ_3, correspond to the x-y-z coordinates axes, respectively.

The simplest form to characterize the material's behavior to loading is the uniaxial tensile test. When a material is subjected to uniaxial tensile loading, it tries to resist to be deformed by generating

stresses in the other two orthogonal planes. Once the principal planes and their corresponding principal stresses are entirely defined under this loading condition, the material can be in plane stress, plane strain, or mixed-mode state of stress.

To illustrate these concepts, Figure 1.7 presents two plates, both stressed in the y-axis and with the z-axis being the thickness direction.

Plane stress is obtained when one of the principal stresses is zero. This condition is common in thin plates (Figure 1.7a) where the stressed component is free to deform in the thickness direction, causing a biaxial stress state.

Principal stresses are associated with principal strains [52], both acting on the same principal axes. The plane strain condition is accomplished when at least one of the principal strains is zero. This state of stress is generally observed in thick plates (Figure 1.7b) where the stressed body opposes to deformations in the thickness direction by inducing a triaxial stress state.

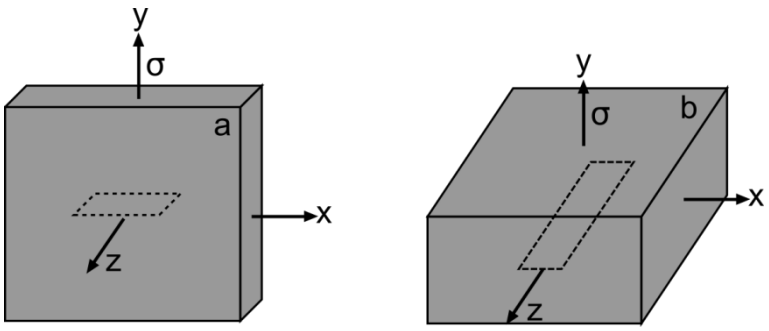

Figure 1.7 Plates with different thicknesses prone to different stress state upon loading: a) Plane stress, b) Plane strain

There are cases where the material can be at the same time in plane stress and plane strain or also called mixed-mode state of stress. In this case, when the crack initiates, plane strain conditions will prevail near to the crack tip, but at some point, near to the outer surface, plane stress will become dominant, and the crack propagation process will change from plane strain to plane stress [30].

The stress state is related directly to the amount of plastic deformation that can be generated ahead of the crack tip. Plane strain state presents maximum constraint to the plastic deformation, while the state of plane stress presents minimum constraint to it [53].

It has been experimentally proven that fracture parameters such as K and G have lower values when the material is in plane strain state than when is under plane stress conditions.

The state of plane strain reduces the ductility of the material [54], represents a more severe state of stress than plane stress [55], and is attained in thick plates containing sharp cracks.

1.2.5 Plastic zone radius

It is now clear that the immediate area to the crack tip has to be yielded to remain finite the stresses and avoid the stress singularity. In this context, the first to propose the existence of a plastic zone around the crack tip where the energy dissipation becomes possible was Irwin [56].

Knowing beforehand that the amount of material preventing the crack propagation is bigger in plane strain than in plane stress it can be inferred that the plastic zone will depend on the state of stress [57].

The definition of Irwin's plastic zone was only possible assuming the region near to the crack tip behaved as an elastic-perfectly plastic material. This means that once the yield strength of the material is exceeded in the boundary of the region near to the crack tip, the stress will no longer grow and will remain constant. It is important to clarify that this assumption is only valid for this yielded region (plastic zone), while, in the rest of the body, the stresses remain elastic as established in the elasticity theory. Figure 1.8 illustrates these concepts.

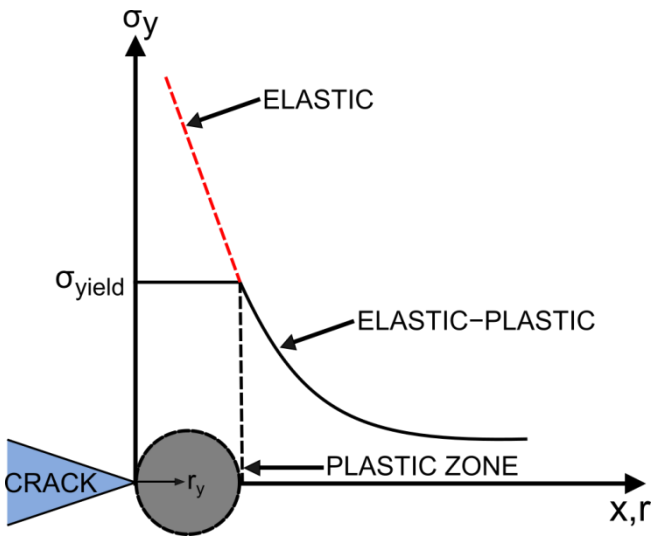

Figure 1.8 Plastic zone at the onset of crack tip growth

To measure the severity of the stresses at and near to the crack tip in Figure 1.8, Eq. (1.7) is used here with small modifications. From this equation, at an angle $\theta = 0$, and at a certain distance from the crack tip [53], it results

$$\sigma_{yield} = \frac{K_I}{\sqrt{2\pi r}} \qquad \text{Eq. (1.10)}$$

where σ_{yield} is what is known as effective yield stress and is given by the following relation

$$\sigma_{yield} = m_p * \sigma_{ys} \qquad \text{Eq. (1.11)}$$

where m_p is the plastic constraint factor [58] and σ_{ys} is the uniaxial yield stress.

m_p takes into account the restriction imposed by the material's thickness to be deformed. In plane strain state, at the crack tip, the plastic deformation is smaller and the effective yield stress necessary for yielding to occur is larger; the opposite happens when the cracked body is under plane stress conditions. Using a yield criterion (Tresca, von Mises), it results that $m_p = 1$ and $m_p = (3)^{1/2}$ for plane stress and plane strain conditions, respectively.

Solving Eq. (1.10) for the plastic zone radius ahead of the crack tip (r_y), it results

$$r_y = \frac{1}{2\pi}\left(\frac{K_I}{\sigma_{yield}}\right)^2 \qquad \text{Eq. (1.12)}$$

For plane stress conditions $\sigma_{yield} = \sigma_{ys}$ with $m_p = 1$, it is found that

$$r_y = \frac{1}{2\pi}\left(\frac{K_I}{\sigma_{ys}}\right)^2 \qquad \text{Eq. (1.13)}$$

For plane strain conditions $\sigma_{yield} = (3)^{1/2} * \sigma_{ys}$ with $m_p = (3)^{1/2}$, it is found that

$$r_y = \frac{1}{6\pi}\left(\frac{K_I}{\sigma_{ys}}\right)^2 \qquad \text{Eq. (1.14)}$$

The most important conclusions resulting from this analysis are: i) The crack tip plastic zone for a cracked body is larger when the material is under plane stress conditions than when is under plane strain conditions, i.e., the plastic zone depends on the stress state, and ii) This plastic zone is proportional to $(K_I/\sigma_{ys})^2$ [57] when following the LEFM theory.

1.2.6 Thickness effects

K_{IC} provides different values when is measured in plane stress that when is measured in plane strain, the latter affords the lowest values of this fracture parameter. In general, K_{IC} depends on the thickness parallel to the crack front [59]. Several experimental studies have done to support this argument, obtaining similar results to the ones presented in Figure 1.9.

This figure shows that as the specimen thickness increases, K_C decreases. However, when thickness reaches a certain value, K_C stops decreasing, keeping a constant value even for additional thickness increments. This K_C value is referred several times as the plane strain fracture toughness value [61,62] and represents a lower bound of material toughness [63]. In experimental studies, it is commonly used the next empirical relationship to find out the critical thickness value from which can be obtained this minimum value of fracture toughness K_{IC} [49]

$$B \geq 2.5\left(\frac{K_{IC}}{\sigma_{ys}}\right)^2 \qquad \text{Eq. (1.15)}$$

where B is the specimen thickness and the term $(K_{IC}/\sigma_{ys})^2$ is proportional to r_y.

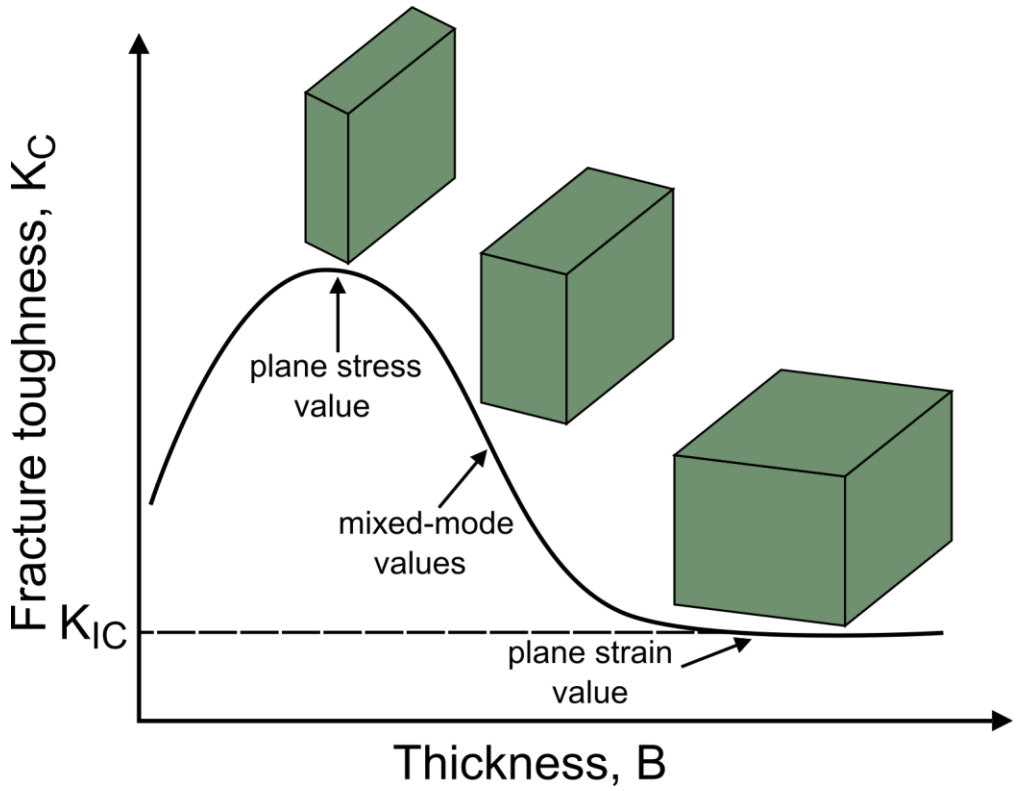

Figure 1.9 Influence of thickness on the fracture toughness values [60]

It is necessary to keep in mind that a tough material will necessary have more crack tip plasticity than a brittle one [49] and that thin plates by having minimum constraint to thickness contraction will develop crack tip plastic zones larger than thick plates where the surrounding elastic material will limit the crack tip plasticity.

Thus, for the same material, thin plates with large crack tip plastic zones will have higher fracture toughness values than thick plates with small crack tip plastic zones.

Figure 1.10 shows the appearance of the fracture surface according to the predominant state of stress and also displays again the variation of K_C with respect to the material's thickness.

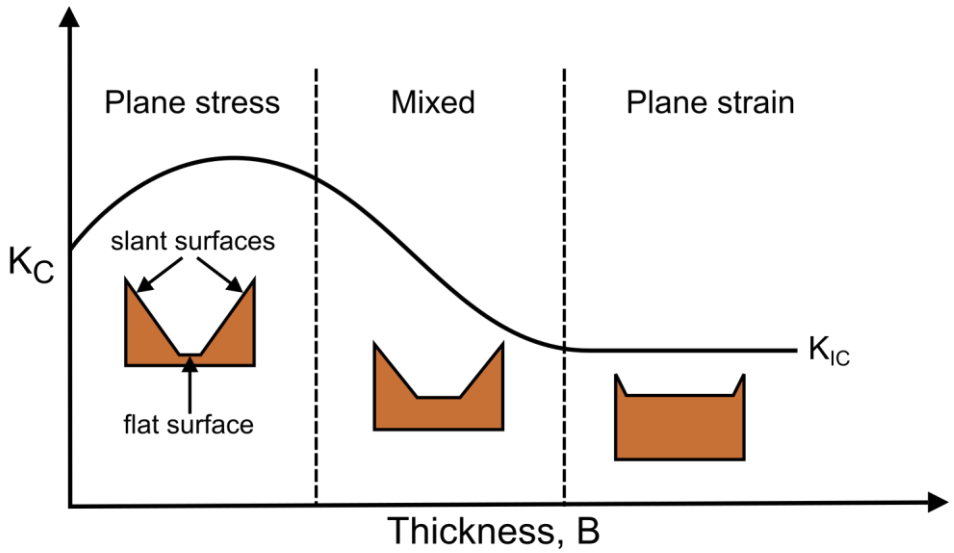

Figure 1.10 Fracture surface appearances according to the state of stress [64]

The change of K_C with thickness is directly related to the state of stress that is more dominant into the cracked body. At the crack tip in the center of a thick plate, a triaxial state of stress will develop, which at crack propagation forms flat surfaces that are characteristic of a brittle fracture. However, at the free surfaces where stresses do not exist, the state of stress will be biaxial (plane stress) and small shear lips (slanted sections) distinctive of a ductile fracture will grow at 45° with respect to the load axis [64].

For thin plates where plane stress conditions prevail, the flat fracture surfaces will be minimal, and the slanted sections will dominate on most of the material surface.

Finally, for intermediate thicknesses where different portions of flat and slanted sections compete, the state of stress will be mixed-mode [65].

1.2.7 Elastic-Plastic Fracture Mechanics (EPFM)

The LEFM theory is appropriate when applied to brittle materials. In such materials, the plasticity around the crack tip is confined to a very small zone (small-scale yielding) [66]. However, LEFM becomes inadequate when ductile cracked materials are used. These materials exhibit large amounts of plasticity ahead of the crack tip and stable crack growth prior to failure [67].

For characterizing the fracture behavior of cracked materials that can have large-scale yielding, it was necessary to extend the elastic analysis offered by LEFM, arising thus, the Elastic-Plastic Fracture Mechanics (EPFM) theory. This approach uses the J-integral and crack tip opening displacement (CTOD) concepts and although both concepts are equivalent, they utilize different methods to measure fracture toughness [68].

To distinguish between linear elastic, non-linear elastic and elastic-plastic materials, Figure 1.11 shows the response to loading for these materials.

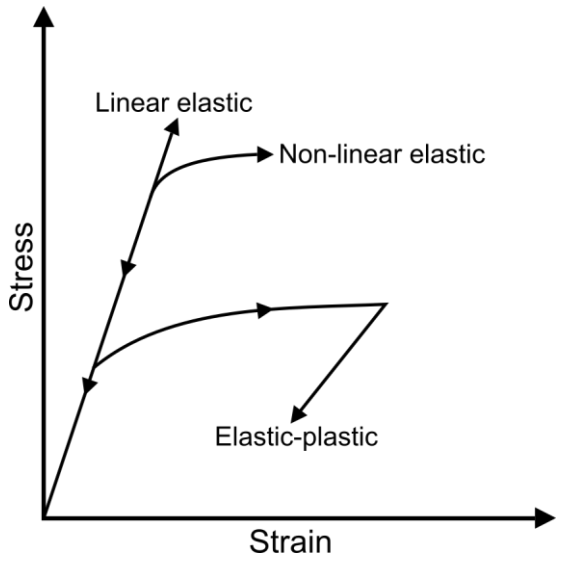

Figure 1.11 Response to stress for three different materials [69]

In a linear elastic material, the relation between stress and strain is linear until failure. In a non-linear elastic material upon loading, it appears some non-linearity but is fully recovered after the load is removed (the loading and the unloading path are the same). In an elastic-plastic material, the non-linearity is also present, but in this case, the unloading path is linear and with the slope equal to the Young's modulus [70], as a consequence, the solid remains permanently deformed after the load has been removed.

1.2.7.1 Crack tip opening displacement (CTOD)

Wells [71] was the first to use the COTD concept for characterizing fracture behavior in materials presenting large crack tip plasticity. He observed that in high-toughness and low-strength materials, the crack faces moved before crack propagation. This movement caused blunting, or, which is the same, broadening at the crack tip of the originally sharp crack [72] (Figure 1.12).

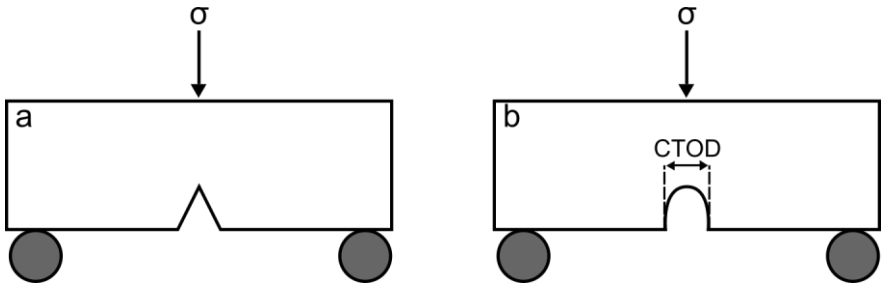

Figure 1.12 Cracked specimens: a) Sharp crack, b) Blunted crack

The opening at the crack tip by consequence of crack tip blunting was considered by Wells as a measure of fracture toughness [73] and is the main idea used in defining the CTOD as a fracture parameter.

The CTOD essentially measures the resistance of a material to the propagation of a crack. When the crack tip is totally blunted, there is a critical value (point) of the CTOD ($CTOD_c$), where the crack initiates propagation.

The LEFM states that a plastic zone develops around the crack tip that makes possible the energy dissipation. Irwin [74] argued that the crack tip plasticity leads to suppose that the crack is of somewhat larger size [75], which is called effective crack length (a_e) and is given by

$$a_e = a + r_y \qquad \text{Eq. (1.15)}$$

where r_y is the plastic zone correction and a is the crack length. These terms are depicted in Figure 1.13. Here, u_y is the crack opening and r_p is equals to $2r_y$.

After performing analysis in Figure 1.13 and using Eq. (1.10), it results

$$r_p = 2r_y = \frac{1}{\pi}\left(\frac{K_I}{\sigma_{ys}}\right)^2 \qquad \text{Eq. (1.16)}$$

The CTOD can be calculated through the Irwin plastic zone correction as follows [76]

$$CTOD = 2u_y = \frac{4\sigma}{E}\sqrt{2ar_p} = \frac{4}{\pi E}\left(\frac{K_I}{\sigma_{ys}}\right)^2 \quad \text{Eq. (1.17)}$$

where E is the Young's modulus, σ is the remote stress, and σ_{ys} is the yield stress.

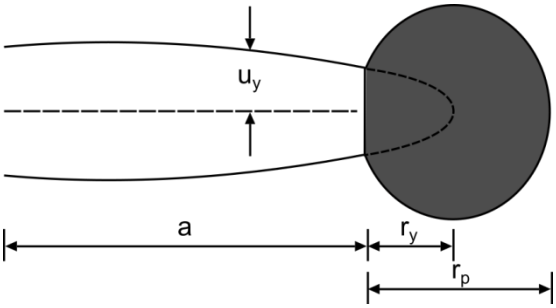

Figure 1.13 Irwin plastic zone size

1.2.7.2 J-integral

The J-integral was developed by Rice [77] as a path independent contour integral to characterize fracture behavior by measuring the rate of change of the potential energy for an elastic-plastic material [78] at or near the crack tip.

To obtain the J-integral relation as obtained by Rice, Figure 1.14 and the analysis done by Atkins and Mai [79] were mainly used here.

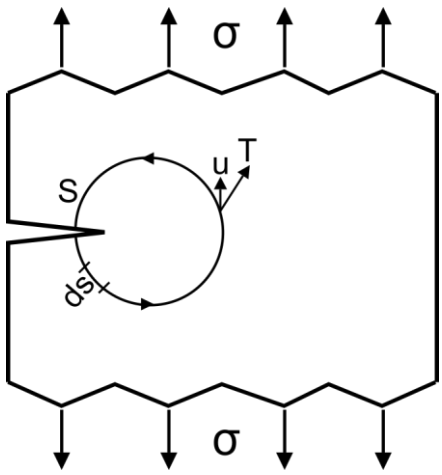

Figure 1.14 Stressed elastic-plastic body containing a crack

In Figure 1.14, S is an arbitrary contour around the crack tip, ds is an element of arc on this contour, T is the traction vector defined by the normal n along S [80], i.e., T = n.σ, and u is the displacement vector.

Carrying out an energy balance in the plate shown in Figure 1.14, it can be found that

$$U_{load} = U_{strain} + U_G \quad \text{Eq. (1.18)}$$

where U_{load} represents the potential energy due to applied loads, U_{strain} is the stored strain potential energy, and U_G is the energy required to grow a crack.

Equation (1.18) can be rewritten such that,

$$U_G = (U_{load} - U_{strain}) \quad \text{Eq. (1.19)}$$

or

$$U_G = -(U_{strain} - U_{load}) \quad \text{Eq. (1.20)}$$

The term within the parenthesis in this last relationship accounts for the potential energy of the system. According to Rice [77], Eq. (1.20) can be represented as two-dimensional line integral as follows

$$U_G = -\left(\int_V W_s \, dV - \int_S T.u ds\right) \quad \text{Eq. (1.21)}$$

where W_s is the strain energy density and V is the volume inside the contour S. In the two-dimensional case, dV is equal to dxdy for a plate with unit thickness.

Thus, the rate of change of the energy required to grow a crack (U_G) with respect to the crack length (a) for the plate showed in Figure 1.14 is given by

$$\frac{dU_G}{da} = -\frac{1}{da}\left(\int_V W_s dxdy - \int_S T.u ds\right) \quad \text{Eq. (1.22)}$$

Moreover, supposing that the curve S is fixed, it implies that da = dx, which finally leads to

$$-\frac{dU_G}{da} = \int_S \left(W_s dy - T\frac{\partial u}{\partial x} ds\right) = J \quad \text{Eq. (1.23)}$$

This is the J-integral relationship as obtained by Rice and is widely used to characterize the fracture behavior of ductile polymer films.

1.2.7.3 HRR singularity

Besides being a fracture energy parameter for elastic-plastic materials, the J-integral can also characterize the stress and strain field around the crack tip [81].

For non-linear materials, the relationship between stress and strain can be described by the Ramberg-Osgood equation law [82]

$$\frac{\varepsilon}{\varepsilon_o} = \frac{\sigma}{\sigma_o} + \alpha \left(\frac{\sigma}{\sigma_o}\right)^n \qquad \text{Eq. (1.24)}$$

where σ_o is the initial yield strength, ε_o is equal to σ_o/E, α is a material constant, n is a hardening exponent.

The first term on the right side in Eq. (1.24) represents the elastic strain, while the second term accounts for the plastic strain. In the EPFM approach, the elastic strain at the vicinity of the crack tip will be negligible when compared to the plastic strain [83]; so that, Eq. (1.24) can be reduced to a power law relation expressed by

$$\frac{\varepsilon}{\varepsilon_o} = \alpha \left(\frac{\sigma}{\sigma_o}\right)^n \qquad \text{Eq. (1.25)}$$

Based on the Ramberg-Osgood analysis, Hutchinson [84], Rice and Rosengren [85] deduced the following expressions for the stress and strain at a distance r ahead of the crack tip

$$\sigma_{ij} = \sigma_o \left(\frac{EJ}{\alpha {\sigma_o}^2 l_n r}\right)^{1/n+1} \tilde{\sigma}_{ij}(\theta, n) \qquad \text{Eq. (1.26)}$$

$$\varepsilon_{ij} = \frac{\alpha \sigma_o}{E} \left(\frac{EJ}{\alpha {\sigma_o}^2 l_n r}\right)^{n/n+1} \tilde{\varepsilon}_{ij}(\theta, n) \qquad \text{Eq. (1.27)}$$

where l_n is a integration constant for a n-range, and σ_{ij} (θ,n) and ε_{ij} (θ,n) are dimensionless functions of θ and n.

Equations (1.26) and (1.27) are known as HRR field in honor of Hutchinson, Rice, and Rosengren. In these equations, the J-integral defines the intensity of HRR singular stress and strain field [86] in a power-law hardening material and then fulfills the same role that the stress intensity factor in the case of linear elastic materials [87].

1.2.7.4 J-integral and CTOD relationship

The J-integral criterion for crack initiation is given by

$$J \geq J_C \qquad \text{Eq. (1.28)}$$

Since the mode I loading is the most common case encountered in practical cases of fracture [88], the J-integral criterion becomes in

$$J \geq J_{IC} \qquad \text{Eq. (1.29)}$$

where J_{IC} is the J-integral value at crack initiation in mode I. The Shih analysis [89] shows that there is a unique relationship between J_{IC} and $CTOD_C$. For a non-hardening material in plane stress, assuming that the stress in the plastic zone ahead of the crack tip is σ_y (yield stress) then

$$J_{IC} = \sigma_y * CTOD_C \qquad \text{Eq. (1.30)}$$

1.2.7.5 The Begley and Landes method

There are different methods to experimentally measure J_{IC}. Specifically, the Begley and Landes [90], the resistance curve [91], and the single-specimen [92] methods are among the most used. The Begley and Landes method was used in this thesis work to obtain the J-integral values and will be explained next.

In this method, the first step is to obtain the load-displacement curves for a set of test specimens with the same size but different crack lengths. Figure 1.15 shows the load-displacement curves for a polyethylene terephthalate glycol-modified (PETG).

Then, a series of displacements (d_1, d_2, d_3, d_4,…) are carefully selected and the area under the curve (A_1, A_2, A_3, A_4,…) corresponding to each displacement is calculated (Figure 1.16). This is done for all curves, using the same displacements [93].

The area under the load-displacement curve represents the energy absorbed during fracture (U). Here, the J-integral as defined in Eq. (1.23) is used to obtain the J-integral values. The energy measurement is performed at constant displacement; therefore, the second term on the right side of Eq. (1.23) becomes zero and gives rise to the alternative definition of J-integral that was also established by Rice [77] where,

$$J = \int_S W_s dy = -\frac{1}{t}\left(\frac{dU}{da}\right)_{cte} \qquad \text{Eq. (1.31)}$$

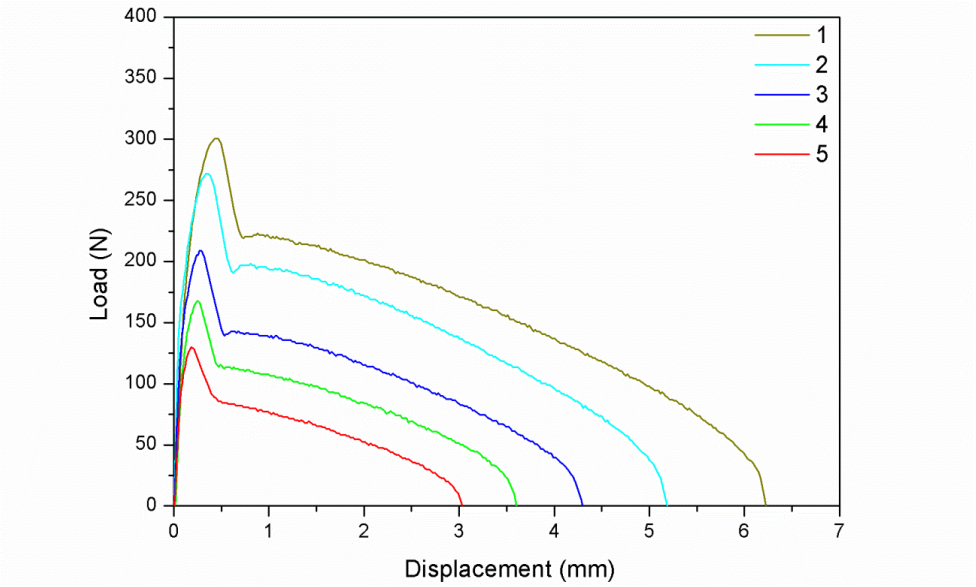

Figure 1.15 Load response for a PETG polymer material

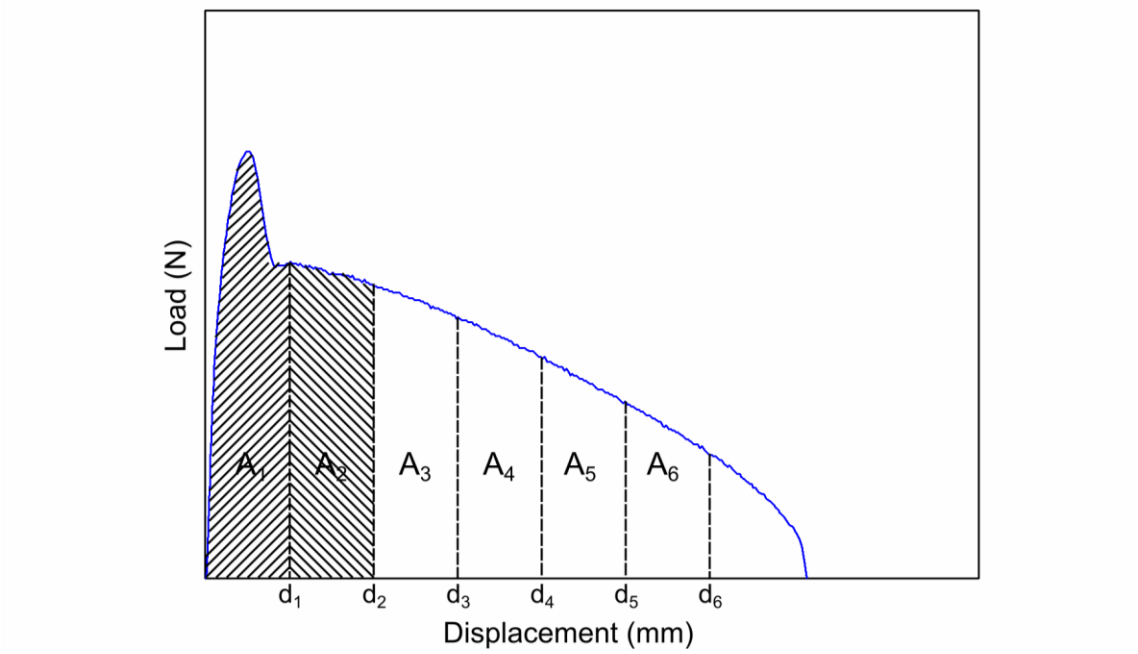

Figure 1.16 Energy measurement at constant displacement under the load-displacement curve

To evaluating the J-integral as defined in Eq. (1.31), the energy divided by the specimen thickness (t) as a function of the crack length when the displacement is fixed is represented in Figure 1.17. The points belonging to the same displacement show linearity and can be adjusted by a straight line, where the slopes of the regression lines are the J-values.

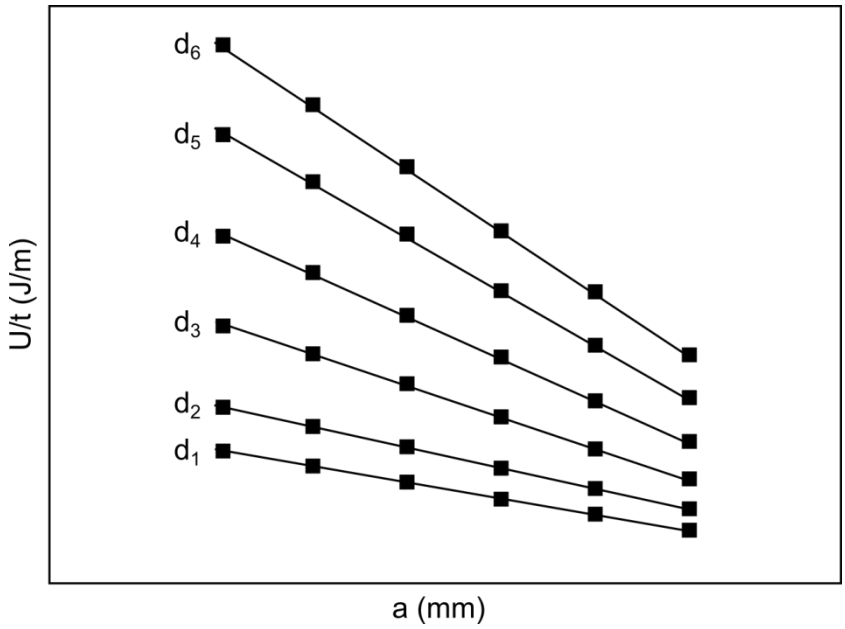

Figure 1.17 Specific energy absorbed versus crack length at constant displacement

Finally, the J-values of each slope in Figure 1.17 are plotted as a function of their respective constant displacements to obtain the J-integral plot as shown in Figure 1.18. J_{IC} is obtained by introducing the $CTOD_C$ value in Figure 1.18.

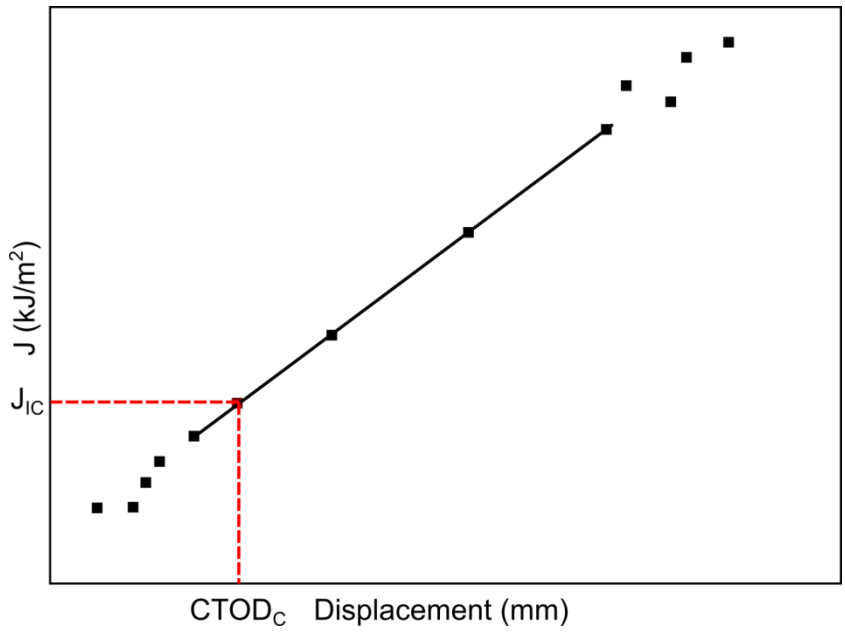

Figure 1.18 J-integral plot

1.2.8 Post-Yield Fracture Mechanics (PYFM)

The PYFM approach emerged for characterizing failure in tough materials after significant plastic deformation had taken place [94]. The Essential Work of Fracture (EWF) is the most used method for this type of fracture characterization.

1.2.8.1 Essential Work of Fracture (EWF) method

The EWF approach was first proposed by Cotterell and Reddell [95] after Broberg's work on stable crack growth [96-98] was published. It is based on the hypothesis that the total energy involved on the ductile fracture of a pre-cracked specimen (W_f) can be separated into two terms.

$$W_f = W_e + W_p \qquad \text{Eq. (1.32)}$$

where W_e, the essential work of fracture, represents the energy required for the creation of two new surfaces during the crack propagation, whereas the second term, W_p, is called the plastic work or the non-essential work of fracture and collects all other sources of energy produced throughout the fracture process (plastic deformation around the crack tip, heat dissipation, etc.).

The term W_e is considered to be proportional to the area of the Fracture Process Zone (FPZ), while W_p is proportional to the volume of the Outer Plastic Zone (OPZ). These zones are schematized in Figure 1.19 for a double edge notched tension (DENT) specimen.

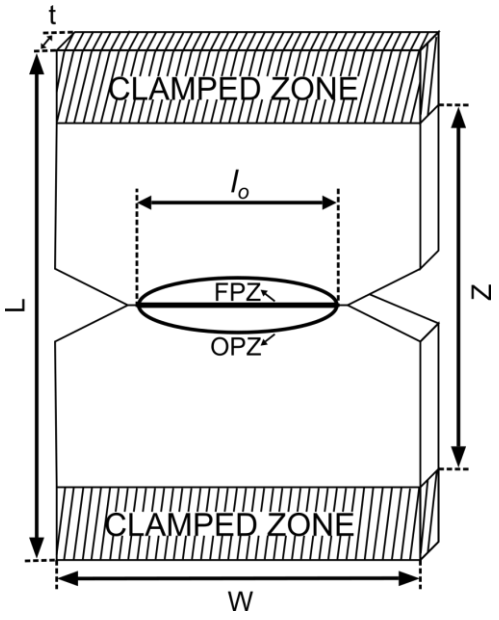

Figure 1.19 DENT specimen geometry

In this figure, l_o is the initial ligament length, t is the specimen thickness, W is the specimen width, L is the specimen length, and Z is the real specimen area tested. The DENT specimen geometry showed in Figure 1.19 is the most appropriate for mode I testing because the transverse stresses between the notches are tensile and therefore buckling problems are avoided [99].

Rewriting Eq. (1.32) using specific terms, i.e., dividing all terms by the area of the ligament cross-section, the following expression can be obtained:

$$w_f = \frac{W_f}{l_o.t} = w_e + \beta w_p.l_o \qquad \text{Eq. (1.33)}$$

where β is a factor that depends on the shape of the OPZ.

It is possible to assess Eq. (1.33) by performing a series of tests on specimens with different ligament lengths, and subsequently plotting the specific total work of fracture (w_f) as a function of their ligament lengths. A simple regression analysis of this plot (Figure 1.20) shows that the specific essential work of fracture (w_e) and the specific non-essential work of fracture (βw_p) are the intercept for a zero ligament length and the slope of the linear regression line, respectively.

For a specific material, w_e and βw_p account for the resistance to crack initiation and the resistance to crack propagation, respectively.

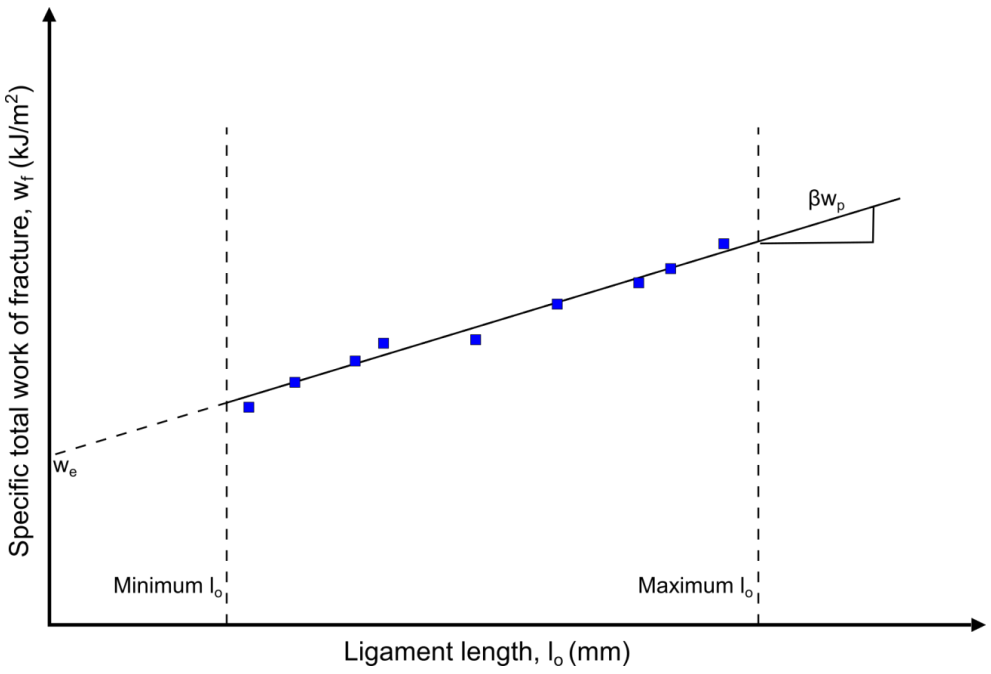

Figure 1.20 Schematic EWF plot

The EWF technique was originally developed for metals [100] and later extended to polymers by Mai [101].

1.2.8.1.1 Key requirements

In the EWF analysis, the following three basic key assumptions are made:

a) The ligament length is fully yielded prior to the onset of crack propagation.

This key assumption is rarely accomplished, and in some polymers this theoretical requirement is not fulfilled, and thus w_e becomes an apparent toughness only useful for comparison purposes.

In a DENT specimen, the ligament length will be completely yielded prior to the onset of crack propagation if it is less than twice the size of the plastic zone radius, r_p. Under plane stress conditions:

for a linear plastic zone

$$2r_p = \frac{\pi}{8}\left(\frac{Ew_e}{{\sigma_y}^2}\right) \qquad \text{Eq. (1.34)}$$

and for a circular plastic zone

$$2r_p = \frac{Ew_e}{\pi{\sigma_y}^2} \qquad \text{Eq. (1.35)}$$

where E is the Young's modulus and σ_y is the yield stress.

Although having a ligament length that is less than twice the radius of the plastic zone is a reasonable size criterion, it appears to be too restrictive considering the evidence encountered in amorphous copolyesters [102, 103].

b) Fracture occurs under plane stress conditions.

There are constraints on the ligament length to assure a pure plane stress state in the specimens.

The polymer films have a thickness of less than 1 mm. A practical lower limit of 5 mm in the ligament length has been accepted when preparing DENT specimens. The upper limit in the ligament requires full-ligament yielding before crack initiation. Hence, the ligament length has to be less than twice the plastic zone radius in DENT specimens.

Another upper limit is given by the relationship:

$$l_o \leq \frac{W}{3}$$ Eq. (1.36)

where W is the specimen width. This last condition is necessary to prevent edge effects.

c) Good quality notches

Good quality means identical and repetitive sharp notches without plastic deformation in front of the notch tip. This requirement guarantees self-similar load-displacement and ligament length-displacement curves for the tested specimens [103,104].

The notch sharpening is of critical importance in obtaining good results. There is evidence [105,106] that the larger the notch tip radius, the higher the w_e values. Thus, the notches should be sharpened as much as possible without significantly lowering the value of w_e.

It is also demonstrated [107,108] that the larger the plastic deformation in front of the notch tip, the higher the w_e values.

1.2.8.1.2 Other considerations

The EWF parameters, as well as the other mechanical properties, can be affected by the microstructure, degree of crystallinity, chain orientations, molecular weight, and additives such as lubricants or plasticizers, among others. The viscoelastic nature of polymers affects the mechanical properties, and the EWF parameters will be also affected by the temperature and the strain rate.

Hill has demonstrated [109,110] that in the DENT geometry under plane stress conditions, no stress can exceed the value of $1.15*\sigma_y$. Thus, the maximum stress (σ_{max}) registered during the DENT test has to be between σ_y and $1.15*\sigma_y$ (Figure 1.21), where σ_y is the yield stress. Theoretically, at small values of l_o, the specimen can be in a mixed state of stress, which increases σ_{max}. Therefore, this Hill criterion could be useful to determine the lower limit of the ligament length. In practice, the experimental variability in the σ_{max} values creates difficulties for the application of this criterion.

Clutton [105] has suggested another criterion, which utilizes the mean of the maximum stresses ($\sigma_{max,av}$), where

$$0.9\sigma_{max,av} < \sigma_{max,av} < 1.1\sigma_{max,av}$$ Eq. (1.37)

This criterion is represented in Figure 1.22 and is used to remove data where an error in dimensional measurement or in load exists.

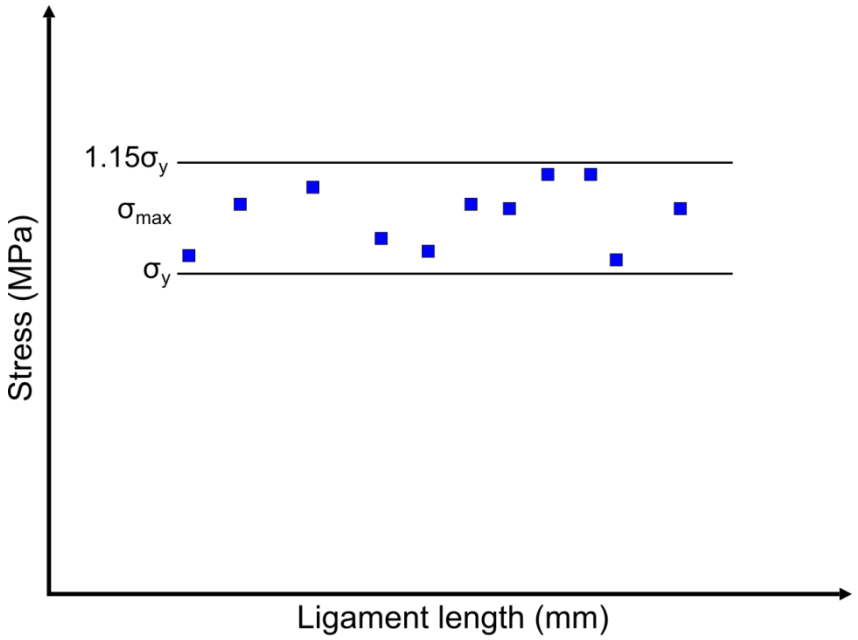

Figure 1.21 Hill's criterion

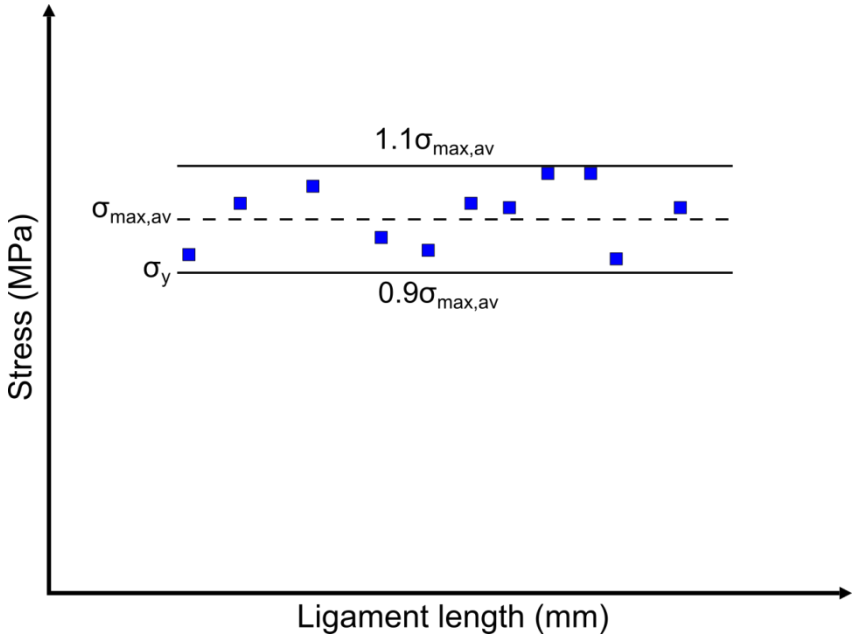

Figure 1.22 Clutton's criterion

1.3 Microdeformation mechanisms

Fracture toughness is a material property controlled by the local plasticity settled ahead of the crack tip [111]. In polymers, the main mechanisms that can lead to plastic deformation are shear yielding and crazing [112].

Ductile polymers, thin films, cracked materials with blunted notches, or some combination thereof deform naturally by shear yielding. In this microdeformation mechanism that takes place at constant volume, the polymer chains slide past each other leading to a large change in the specimen shape [112]. Macroscopically, shear bands appear at 45° to the direction of the maximum principal tensile stress (Figure 1.23).

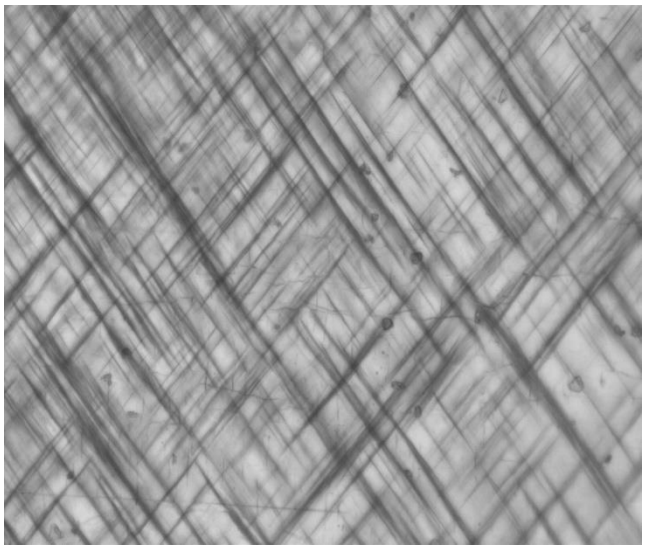

Figure 1.23 Shear bands generated in a polymer tensile test specimen during loading

Shear yielding and crazing are localized deformation mechanisms [113], but meanwhile, shear yielding takes place at constant volume, crazing is a cavitation process that causes a volume increase in the polymer matrix [114].

Essentially, crazes are microvoids bridged with highly oriented polymeric material named microfibrils [115]. Upon loading, these microfibrils are stretched and oriented in the principal stress direction. At the same time, the craze grows perpendicularly to the applied load. Figure 1.24 shows a craze with its main characteristics.

Due to the fibrillar structure that supports the craze's integrity, these microvoids are capable of transmitting loads and hence do not qualify as cracks [58]. However, at some point, the craze will lead to a microcrack in a craze-crack transition process [116], and the material will fail precisely at the craze tip.

Thick specimens, notched materials containing sharp cracks, high strain rates, and low temperatures are conditions where crazing is dominant. The same applies to materials that undergo brittle fracture; therefore, crazing is normally associated with brittle failure [113].

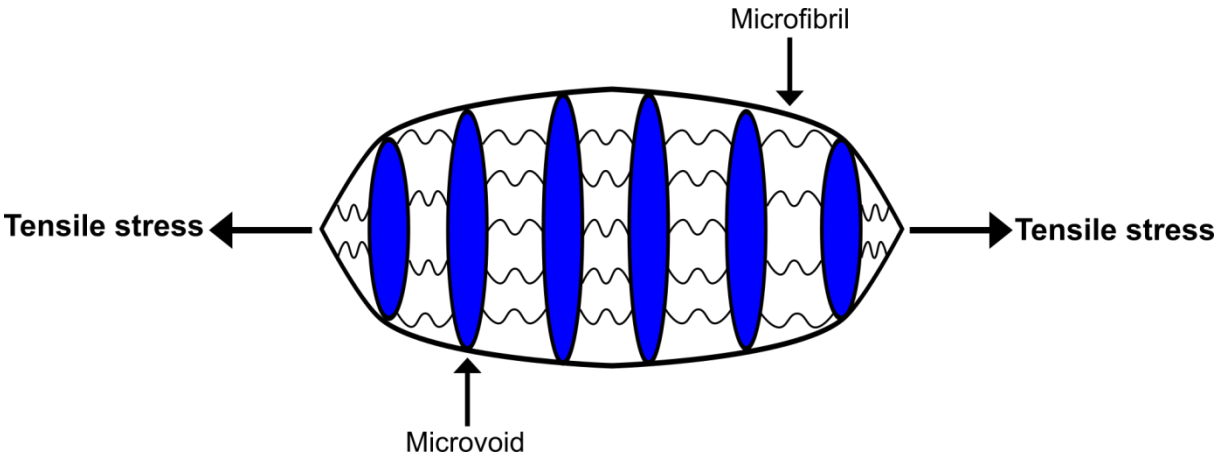

Figure 1.24 Schematic diagram of a craze [117]

1.4 References

[1] Chanda M. Introduction to Polymer Science and Chemistry: A Problem-Solving Approach. 2nd ed. London: CRC Press; 2013.

[2] Nicholls L, Gadd K. Chemistry AQA A-level year 1 and AS. London: HarperCollins; 2015.

[3] Ducheyne P, Healy KE, Hutmacher DW, Grainger DW, Kirkpatrick CJ. Comprehensive biomaterials, Volume 1: metallic, ceramic and polymeric biomaterials. Boston: Newnes; 2011.

[4] Fried JR. Polymer Science and Technology. 3rd ed. New York: Prentice Hall; 2014.

[5] Tan KH. Humic Matter in Soil and the Environment: Principles and Controversies. 2nd ed. New York: Marcel Dekker; 2003.

[6] Saunders KJ. Organic Polymer Chemistry: An introduction to the organic chemistry of adhesives, fibres, paints, plastic, and rubbers. Netherlands: Springer Science and Business Media; 1973.

[7] Karak N. Fundamentals of polymers: Raw materials to finish products. New Delhi: PHI learning; 2009.

[8] Kumar A, Gupta RK. Fundamentals of polymer engineering, revised and expanded. New York: Marcel Dekker; 2003.

[9] Callister WD, Retwisch DG. Fundamentals of materials science and engineering: An integrated approach. 4th ed. New Jersey: John Wiley and Sons; 2012.

[10] Wise RJ. Thermal welding of polymers. Woodhead publishing; 1999.

[11] Ralston BE. Soy protein plastics: Material formulation, processing and properties. Proquest; 2008.

[12] Salmon ER. Encapsulation of electronic devices and components. New York: Marcel Dekker; 1986.

[13] Park HD, Chang IS, Lee KJ. Principles of membrane bioreactors for wastewater treatment. New York: CRC Press; 2015.

[14] Lampman S. Characterization and failure analysis of plastics. Ohio: ASM International; 2003.

[15] Robertson GL. Food packaging: Principles and practice. 2nd ed. New York: Marcel Dekker; 2005.

[16] Poitout DG. Biomechanics and biomaterials in orthopedics. London: Springer-Verlag; 2004.

[17] Stokes RJ, Evans DF. Fundamentals of interfacial engineering. New York: John Wiley and Sons; 1997.

[18] Young RJ, Lovell PA. Introduction to polymers. 3rd ed. Boca Raton: CRC Press; 2011.

[19] Landel RF, Nielsen LE. Mechanical properties of polymers and composites. 2nd ed. New York: CRC Press; 1993.

[20] Guyon E, Hulin JP, Petit L, Mitescu C. Physical hydrodynamics. 2nd ed. New York: Oxford University Press; 2015.

[21] Rudin A. The elements of polymer science and engineering. San Diego: Academic Press; 1999.

[22] Dillard D. Advances in structural adhesive bonding. Cambridge: Woodhead Publishing; 2010.

[23] Brinson HF, Brinson LC. Advances in structural. New York: Springer; 2015.

[24] Chen Q, Thouas G. Biomaterials: A basic introduction. Boca Raton: CRC Press; 2014.

[25] Lalena JN, Cleary DA. Principles of inorganic materials design. New Jersey: John Wiley and Sons; 2005.

[26] Milne I, Ritchie O, Karihaloo BL. Comprehensive structural integrity. Elsevier; 2003.

[27] Saxena A. Fracture mechanics for engineers. Boca Raton: CRC Press; 1998.

[28] Mouritz AP. Introduction to aerospace materials. Cambridge: Woodhead Publishing; 2012.

[29] Mittemeijer EJ. Fundamentals of materials science: The microstructure-property relationship using metals as model systems. New York: Springer; 2011.

[30] Liu AF. Mechanics and mechanisms of fracture: An introduction. Ohio: ASM International; 2005.

[31] Bazant ZP, Cedolin L. Stability of structures: Elastic, inelastic, fracture and damage theories. New York: Oxford University Press; 1991.

[32] Prawoto Y. Solids mechanics for materials engineers: Principles and applications of meso mechanics. London: Lulu.com; 2013.

[33] Viswanathan R. Damage mechanisms and life assessment of high temperature components. Ohio: ASM International; 1989.

[34] Inglis CE. Stresses in plate due to presence of crack and sharp corners. Transactions of the Institute of Naval Architects 1913; 55: 219-241.

[35] Griffith AA. The phenomena of rupture and flow in solids. Philosophical Transactions of the Royal Society of London 1921; 221; 163-198.

[36] Bains AS, Singh B, Aulakh TS. Towards to fracture mechanics framework. International Journal of Technology and Engineering 2016; 1: 14-18.

[37] Stavrogin AN, Tarasov BG. Experimental physics and rock mechanics. New York: CRC Press; 2001.

[38] Irwin GR. Relation of stresses near a crack to the extension force. Ninth International Congress of Applied Mechanics. Brussels: 1956, p.245-251.

[39] Zehnder AT. Fracture mechanics. London: Springer; 2012.

[40] Talreja R, varna J. Modeling damage, fatigue and failure of composite materials. Cambridge: Woodhead Publishing; 2015.

[41] Freund LB. Dynamic fracture mechanics. New York: Cambridge University Press; 1998.

[42] Westergaard HM. Bearing pressures and cracks. Journal of Applied Mechanics 1939; 6: A49-53.

[43] Richard HA, Sander M. Fatigue crack growth: Detect-assess-avoid. Switzerland: Springer; 2016.

[44] Packham DE. Handbook of adhesion. 2nd ed. Chichester: John Wiley and Sons; 2005.

[45] Irwin GR. Analysis of stresses and strains near the end of a crack traversing a plate. Journal of Applied Mechanics 1957; 24: 361-364.

[46] Halford GR, Gallagher JP. Fatigue and fracture mechanics. ASTM International; 2001.

[47] Rusell A, Lee KL. Structure-property relations in nonferrous metals. New jersey: John Wiley and Sons; 2005.

[48] Ragab AA, Bayoumi SEA. Engineering solid mechanics: Fundamentals and applications. Boca Raton: CRC Press; 1998.

[49] Grandt AF. Fundamentals of structural integrity: Damage tolerant design and nondestructive evaluation. New Jersey: John Wiley and Sons; 2003.

[50] Shen B, Stephansson O, Rinne M. Modelling rock fracturing processes: A fracture mechanics approach using FRACOD. Netherlands: Springer; 2013.

[51] Collins JA, Busby HR, Staab GH. Mechanical design of machine elements and machines: a failure prevention perspective. New Jersey: John Wiley and Sons; 2010.

[52] Norton RL. Cam design and manufacturing handbook, volume 1. New York: Industrial Press; 2002.

[53] Grossman G, Zardini C. The ELFNET book on failure mechanism, testing methods, and quality issues of lead-free solder interconnects. London: Springer; 2011.

[54] Farag MM. Materials and process selection for engineering design. 3rd ed. Boca Raton: CRC Press; 2014.

[55] Brantley WA, Eliades T. Orthodontic materials: Scientific and clinical aspects. Stuttgart: Thieme; 2001.

[56] Irwin GR. Handbook of physics, Vol.6. Berlin: Springer; 1958, p. 551-590.

[57] Wei RP. Fracture mechanics: Integration of mechanics, materials science and chemistry. New York: Cambridge University Press; 2010.

[58] Kinloch AJ, Young RJ. Fracture behavior of polymer. New York: Elsevier Science Publishing; 1983.

[59] Blair M, Stevens TL. Steel casting handbook. 6th ed. Ohio: ASM International; 1995.

[60] Research Center NDT. Fracture toughness 2016. https://www.nde-ed.org/EducationResources/CommunityCollege/Materials/Mechanical/FractureToughness.htm (accessed December 28, 2016).

[61] Brown WF Jr, Srawley JE. Plane strain crack toughness testing of high strength metallic materials. ASTM STP 410, American Society for Testing and Materials, Philadelphia, PA: 1966.

[62] E 399-90. Standard test method for plane-strain fracture toughness of metallic materials. American Society for Testing and Materials, Philadelphia, PA: 1990.

[63] Szycher M. High performance biomaterials: A complete guide to medical and pharmaceutical applications. Pennsylvania: Technomic Publishing Company; 1991.

[64] Farahmand B, Bockrath G, Glassco J. Fatigue and fracture mechanics of high risk parts: Application of LEFM and FMDM theory. New York: Chapman and Hall; 1997.

[65] Lan W, Deng X, Sutton MA, Cheng CS. Study of slant fracture in ductile materials. International Journal of Fracture 2006; 141: 469-496.

[66] Gdoutos EE. Fracture mechanics: An introduction. 2nd ed. Dordrecht: Springer; 2006.

[67] Newman JC. Elastic-plastic fracture mechanics technology. Philadelphia: ASTM International; 1985.

[68] Schwalbe KH. The crack tip opening displacement in elastic-plastic fracture mechanics: Proceedings of the workshop on the CTOD methodology. Geesthacht: Springer; 1986.

[69] Prawoto Y. Application of linear elastic fracture mechanics in materials science and engineering: Easy and simple guide to use fracture mechanics outside the mechanics world. North Carolina: Lulu.com; 2011.

[70] Anderson TL. Fracture mechanics: Fundamentals and applications. Boca Raton: Taylor and Francis; 2005.

[71] Wells AA. Application of fracture mechanics at and beyond general yielding. British Welding Journal 1963; 10: 563-570.

[72] Soratur SH. Essentials of dental materials. New Delhi: Jaypee Brothers Medical Publishers; 2002.

[73] Czichos H, Saito T, Smith LE, editors. Springer handbook of metrology and testing, Heidelberg: Springer; 2011, p. 339-656.

[74] Irwin GR. Plastic zone near a crack and fracture toughness. Proceedings of 7th Sagamore Conference 1960, p. IV-63.

[75] de Wit R. A review of generalized failure criteria based on the plastic yield strip model. ASTM STP 791, American Society for Testing and Materials, Philadelphia: 1982, p. 124-150.

[76] Broek D. Elementary engineering fracture mechanics. 4th ed. Dordrecht: Martinus Nijhoff Publishers; 1986.

[77] Rice JR. A path independent integral and the approximate analysis of strain concentration by notches and cracks. Journal of Applied Mechanics 1968; 35: 379-386.

[78] Mohammadi S. Extended finite element method for fracture analysis of structures. Oxford: Blackwell Publishing Ltd; 2008.

[79] Atkins AG, Mai YW. Elastic and plastic fracture: metals, polymers, ceramics, composites, biological materials. 2nd ed. Chichester: Ellis Horwood Limited; 1988.

[80] Landes JD, Begley JA. "Recent developments in J_{IC} testing", Developments in fracture mechanics test methods standardization, ASTM STP 632. In: Brown WF, Kaufman JG (editors), 1977, p. 57-81.

[81] Farahmand B. Predictive modeling: For fatigue and fracture mechanics allowables. New York: Springer; 2009.

[82] Ramberg W, Osgood WR. Description of stress-strain curves by three parameters. National Advisory Committee on Aeronautics, Technical Note, 902; 1943.

[83] Khoei AR. Extended finite element method: Theory and applications. West Sussex: John Wiley and Sons; 2015.

[84] Hutchinson JW. Singular behavior at the end of a tensile crack tip in a hardening material. Journal of Mechanics and Physics of Solids 1968; 16: 13-31.

[85] Rice JR, Rosengren GF. Plane strain deformation near a crack tip in a power-law hardening material. Journal of Mechanics and Physics of Solids 1968; 16: 1-12.

[86] Murakami Y. Correlation between strain singularity at the crack tip under overall plastic deformation and the exponent of the Coffin – Manson law. In: Solomon HD, Halford GR, Kaisand LR (editors). Low cycle fatigue, ASTM STP 942, Philadelphia: American Society for Testing and Materials; 1988, p.1048-1065.

[87] May IL. Structural integrity and petrochemical industry. Energy Materials – Materials Science and engineering for Energy Systems 2008; 3: 208-219.

[88] Zhuang Z, Liu Z, Cheng B, Liao J. Extended finite element method. Oxford: Academic Press; 2014.

[89] Shih CF. Relationships between the J-integral and the crack tip opening displacement for stationary and extending cracks. Journal of Mechanics and Physics of Solids 1981; 29: 305-326.

[90] Begley JA, Landes JD. The J integral as a fracture criterion. In: Fracture toughness ASTM STP 514. Philadelphia: American Society for Testing and Materials; 1972, p. 1-20.

[91] Hale GE, Ramsteiner F. J-fracture toughness of polymers at slow speed. In: Moore DR, Pavan A, Williams JG (editors). Fracture mechanics testing methods for polymers, adhesives and composites. Oxford: Elsevier Science, LTD.; 2001, p. 123-157.

[92] Hashemi S, Williams JG. Single and multi-specimen methods for J_{IC} determination of toughened nylons. Journal of Materials Science 1991; 26: 621-630.

[93] Zhou Y, Yang L, Huang Y. Micro and macromechanical properties of Materials. Boca Raton: CRC Press; 2013.

[94] Heald PT, Spink GM, Worthington PJ. Post Yield Fracture Mechanics. Materials Science and Engineering 1972; 10: 129-138.

[95] Cotterell B, Reddell JK. The essential work of plane stress ductile fracture. International Journal of Fracture 1977; 13: 267-277.

[96] Broberg KB. Critical review of some theories in fracture mechanics 1968; 4: 11-19.

[97] Borberg KB. Crack-growth criteria and non-linear fracture mechanics. Journal of the Mechanics and Physics of Solids 1971; 19: 407-418.

[98] Broberg KB. On stable crack growth. Joutnal of the Mechanics and Physics of Solids 1975; 23: 215-237.

[99] Cotterell B, Pardoen T, Atkins AG. Measuring toughness and the cohesive stress-displacement relationship by the essential work of fracture concept. Engineering Fracture Mechanics 2005; 72: 827-848.

[100] Mai YW, Cotterell B. The essential work of fracture for tearing of ductile metals. International Journal of Fracture 1984; 24: 229-236.

[101] Mai YW, Cotterell B. On the essential work of ductile fracture in polymers. International Journal of Fracture 1986; 32: 105-125.

[102] Karger-Kocsis J. For what kind of polymer is the toughness assessment by the essential work concept straightforward? Polymer Bulletin 1996; 37: 119-126.

[103] Martínez AB, León N, Arencón D, Sánchez-Soto M. Essential work of fracture, crack tip opening displacement, and J-integral relationship for a ductile polymer film. Polymer Testing 2016; 55: 247-256.

[104] Martínez AB, León N, Arencón D, Sánchez-Soto M. The post-yield fracture of a ductile polymer film: Notch quality, essential work of fracture, crack tip opening displacement, and J-integral. Engineering Fracture Mechanics 2017; 173: 21-31.

[105] Clutton E. Essential work of fracture. In: Moore DR, Pavan A, Williams JG (editors). Fracture mechanics testing methods for polymers, adhesives and composites. Oxford: Elsevier Science, LTD.; 2001, p. 177-195.

[106] Williams JG, Rink M. The standardisation of the EWF test. Engineering Fracture Mechanics 2007; 74: 1009-1017.

[107] Martínez AB, Segovia A, Gamez-Perez J, Maspoch ML. Influence of femtolaser notch sharpening technique in the determination of essential work of fracture (EWF) parameters. Engineering Fracture Mechanics 2009; 76: 1247-1254.

[108] Pegoretti A, Castellani L, Franchini L, Mariani P, Penati A. On the essential work of fracture of linear low-density-polyethylene. I. Precision of the testing method. EFM 2009; 76: 2788-2798.

[109] Hill R. On discontinuous plastic plates, with special reference to localized necking in thin sheets. Journal of the Mechanics and Physics of Solids 1952; 1: 19-30.

[110] Hill R. The mathematical theory of plasticity. New York: Oxford University Press; 1998.

[111] Deblieck RAC, van Beek DJM, Remiere K, Ward IM. Failure mechanisms in polyolefines: The role of crazing, shear yielding and the entanglement network. Polymer 2011; 52: 2979-2990.

[112] Riande E, Díaz-Calleja R, Prolongo MG, Masegosa RM, Salom C. Polymer viscoelasticity: stress and strain in practice. New York: Marcel Dekker; 1999.

[113] Estevez R, Tijssens MGA, Van der Giessen E. Modeling of the competition between shear yielding and crazing in glassy polymers. Journal of the Mechanics and Physics of Solids 2000; 48: 2585-2617.

[114] Kausch HH. Polymer fracture. Berlin: Springer-Verlag; 1987.

[115] Friedrich K. Crazes and shear bands in semi-crystalline thermoplastics. In: Kausch HH (editor). Crazing in polymers. Advances in Polymer Science, Vol. 52-53. Berlin: Springer; 1983, p. 225-274.

[116] Brown HR. A molecular interpretation of the toughness of glassy polymers. Macromolecules 1991; 24: 2752-2756.

[117] Sokkar T, El-Farahaty K, Seisa E, Omar E, Agour M. Online investigation of optical properties and craze propagation of drawn polypropylene fiber by using interferometric image analysis. Optics and Photonics Journal 2014; 4: 165-181.

Chapter 2

State of the art and aims of the work

2.1 Introduction

Polymers materials being cheaper, more versatile and durable, and easier to process than other materials, they are often the natural choice for many applications. According to the data collected by PlasticsEurope (the Association of Plastics Manufacturers in Europe) and EPRO (the European Association of Plastics Recycling and Recovery Organisations), the plastic demand in Europe for main market sectors during the year 2015 was as that one shown in Figure 2.1.

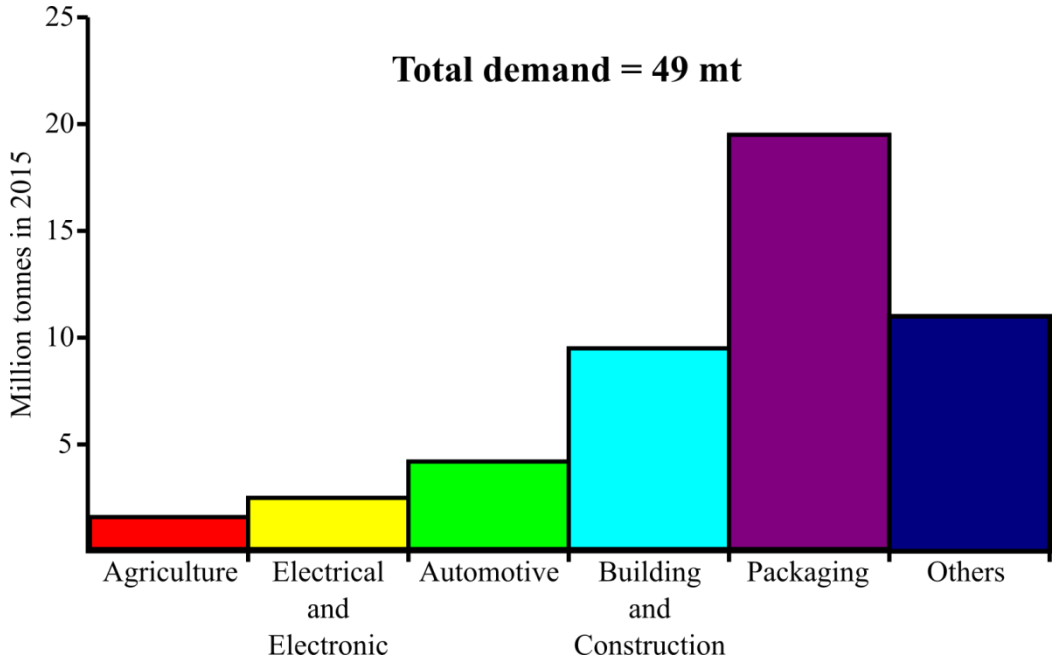

Figure 2.1 European plastics demand by market segment in 2015 [1]

The polymer films were originally developed for being used as packaging materials for food products, consumer goods, and liquid and bulk chemical and petrochemical products, as well as for household purposes [2]. These materials display remarkable properties. As an example, in Figure 2.2, a scheme with the required properties of polymer films for food packaging is depicted.

The traditional mechanical properties for ductile polymer films, such as Young's modulus (E), uniaxial tensile yield stress (σ_y), and Poisson's ratio (ν), among others, are well-defined and studied, but this is not the case for the properties to fracture, where fracture toughness, which is one of the most important mechanical properties of any material [4], receives special attention.

Toughness is a mechanical property that represents the ability of a material to absorb energy during deformation up to fracture [5]. Fracture toughness refers to the ability of a material containing a pre-

existing crack to resist fracture [6,7] or can also be seen as the amount of energy needed to propagate a crack [8].

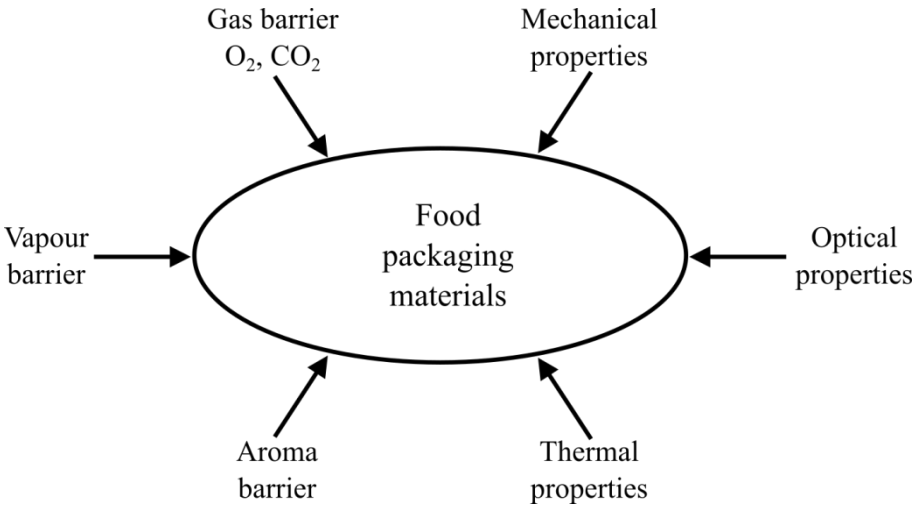

Figure 2.2 Properties of polymer films for food packaging applications [3]

The polymer films have been used for applications considered normal, such as those mentioned above, where the traditional mechanical properties were enough to describe their mechanical behavior. However, as the polymer films are being increasingly used for engineering applications, the fracture toughness characterization becomes of crucial importance [9].

The discipline in charge of characterizing the fracture behavior of materials is the Fracture Mechanics. Depending on the amount of plastic deformation concentrated ahead of the crack tip, Fracture Mechanics utilizes different approaches to characterize fracture toughness.

The Linear Elastic Fracture Mechanics (LEFM) is used when the plastic yielding is confined to a small zone near to the crack tip (assumption of small-scale yielding), and the fracture is brittle. When the plasticity in front of the crack tip becomes large, the Elastic Plastic Fracture Mechanics (EPFM) applies, and the J-integral and Crack Tip Opening Displacement (CTOD) are the approaches to be used. Finally, when the crack propagates through a highly deformed and yielded material the Post-Yield Fracture Mechanics (PYFM) through the Essential Work of Fracture (EWF) can be used.

The materials studied in this work are ductile polymer films, with different micro-deformation mechanisms, and where a large plastic zone surrounds the crack tip. Thus, the concepts expressed by the LEFM are not applicable, and the J-integral, the CTOD, and the EWF are the correct approaches to describe their fracture behavior.

Ductile fracture is accompanied by extensive necking before complete failure occurs. This kind of fracture takes place under plane stress conditions and consequently provides a plane stress fracture toughness value that is thickness-dependent.

In this regard, this chapter is mainly focused on presenting the current research made for characterizing the fracture toughness of ductile polymer films.

2.2 Essential Work of Fracture

Broberg [10-12] suggested that the non-elastic region at the crack tip should be divided into an inner region where the fracture process takes place and an outer region where plastic deformation occurs [13].

Cotterell and Reddel [14] based on Broberg's idea developed the essential work of fracture concept. They labeled the work done in the inner region as the essential work of fracture (w_e) and the work done in the outer region as the non-essential work of fracture (βw_p).

The EWF technique was originally developed to characterize the ductile fracture of thin metal sheets [15] in out-of-plane (mode III) tearing fracture using two-leg trouser specimens (Figure 2.3). Mai [16] later extended the EWF analysis to cover ductile tearing of polymer materials that undergo necking before failure. A more detailed description of the procedure can be found elsewhere [17,18].

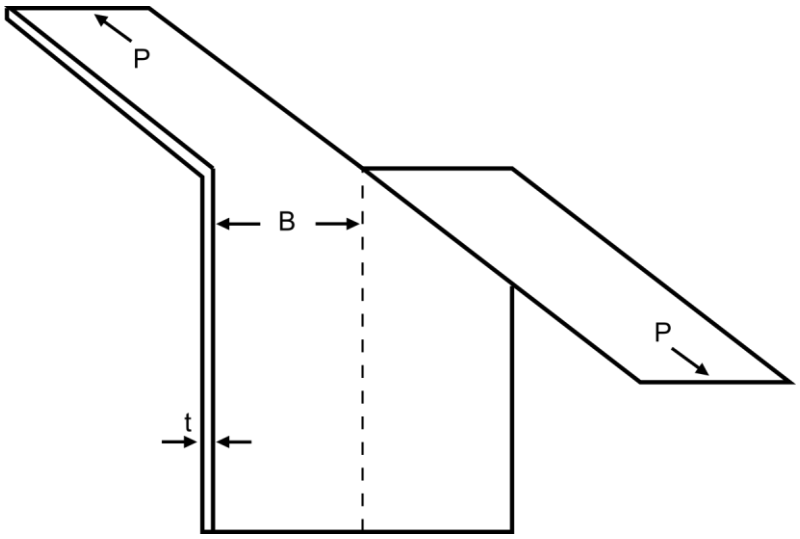

Figure 2.3 Two-leg trouser test specimen

In Figure 2.3, P is the load applied, t is the specimen thickness, and B is the width of the legs. In our study, the fracture assessment was entirely obtained for in-plane (mode I) stress fracture.

The EWF approach is gaining importance over other traditional approaches (the J-integral and the CTOD) to characterize the plane stress toughness of ductile polymer films. This is mainly due to the apparent ease with which the specimens may be prepared and tested.

The specific essential work of fracture (w_e) becomes an inherent material parameter only when the ligament is fully yielded before crack initiation and is independent of the specimen geometry, as first verified by Mai and Cotterell [19]. When this happens, w_e accounts for the material's resistance to crack initiation. However, the complete ligament yielding before crack initiation is difficult to accomplish and w_e becomes an apparent fracture toughness that is only valid for comparison purposes.

There is a European Structural Integrity Society (ESIS) test protocol [13] for the EWF method, and several round-robin exercises [13,20] have been performed under the guidance of the ESIS technical committee 4 (TC4).

In spite of the apparent simplicity of the test, some aspects of the validity of this technique remain controversial; there are intricate details that seem to play an important role in the repeatability and reproducibility of the EWF test. This problem has been, and still is, a topic of much debate and these concerns indicate that the EWF procedure is not yet sufficiently defined to be considered as a standard.

To quantify fracture toughness, the EWF approach is based on the energy partitioning method and two different criteria has been traditionally used to do this: the yielding work and the initiation work.

In the yielding work, the energy partition is applied to the load-displacement curve at maximum load [21] (Figure 2.4). Here, the total work of fracture (W_f) is divided into two components: the work needed for yielding the ligament area (W_y) and the work of fracture for subsequent necking and tearing (W_n) [18].

The initiation work also partitions W_f into two components, but, in this case, the partition criterion takes place after necking of the ligament area: W_I (irreversible initiation process involving yielding, necking, and crack tip blunting) and W_{II} (crack propagation and extended necking in the plastic zone) [18,22] (Figure 2.5).

However, these energy partition methods [21,22] resulted to be inaccurate. In this thesis work, we demonstrated that the energy partition must be performed in the stress-displacement curve at the crack initiation displacement (d_i) (Figure 2.6). In this way, the specific total work of fracture (w_f) is separated into two components: w_e (the energy just up to crack initiation) and βw_p (the propagation energy).

A new approach [23] partitions W_f into three components, the work associated with necking and crack propagation (W_e), the work consumed during plastic deformation (W_p), and a new term, the work related to recoverable viscoelastic deformation (W_v). For the moment, this attempt to modify the EWF approach has only be proved in metallocene linear low-density polyethylene (m-LLDPE) copolymers, more research is needed to secure its applicability for the plane stress fracture toughness characterization of ductile polymer films.

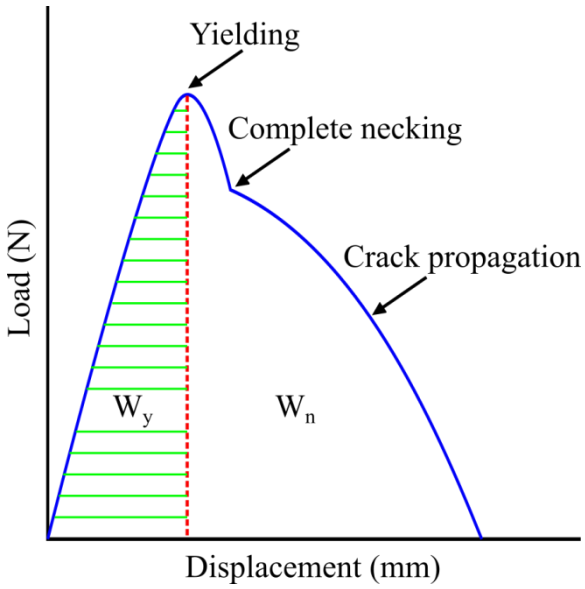

Figure 2.4 Yielding work energy partitioning method

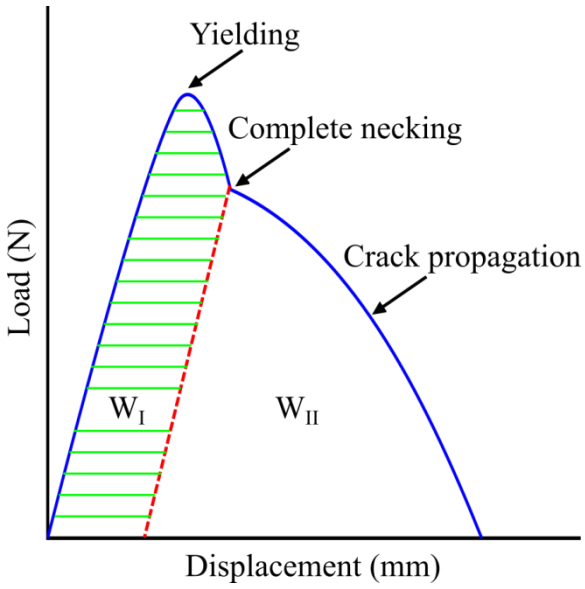

Figure 2.5 Initiation work energy partitioning method

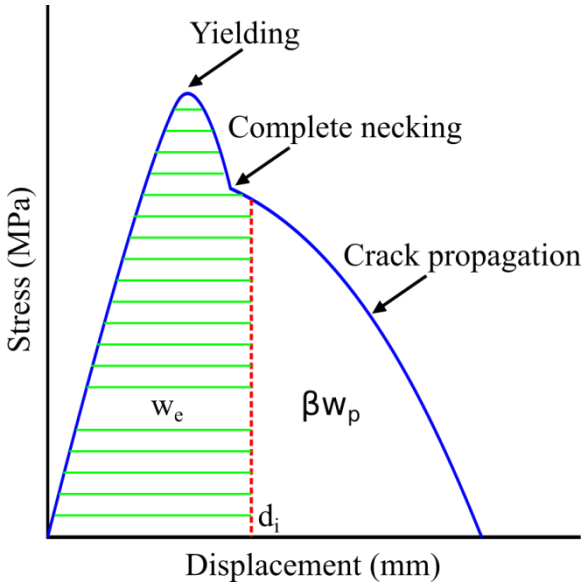

Figure 2.6 New energy partitioning method

2.2.1 Specimen geometry

When w_e is an inherent material parameter, it should be independent of the specimen geometry. Most published research has been performed using the DENT specimen geometry.

There is experimental evidence that when the specimen width (W) and the distance between clamps (Z) (Figure 1.19) are more than twice the largest ligament value, the w_e values do not change [24, 25]. However, when Z is more than twice W, the specimens can become wavy in their own plane during the test [24] and thus modify the stress distribution in the ligament zone. Values of Z that are smaller than W seem to be far from the infinite plate case, with the result probably influenced by the close proximity of the cross-heads to the fracture region.

2.2.2 Specimen thickness

For a given thickness, w_e is a material parameter, which is independent of the geometry of the test specimen [26]. However, in non-oriented amorphous polymers with thicknesses lower than 1 mm, it seems that w_e and βw_p remain nearly constant as the thickness changes [27]. For semicrystalline thermoplastics, there are variations but attributed to the polymer's crystallinity [24].

Applying the EWF analysis to specimens with very small thicknesses (less than 0.1 mm) can be difficult. Besides the required careful handling, buckling problems can be generated in the ligament zone during testing.

Recently, to improve the stability under tensile loading of polymer thin films with thicknesses very reduced, a custom-built film fixture was designed and used in DENT specimens for the EWF analysis [28]. Using this device, the out-of-plane buckling was minimized and thus the stress distribution in the ligament zone remained unaffected [29].

2.2.3 Test speed and temperature

On most of the research made on EWF, the selection of the strain rate is somewhat arbitrary. However, it must be taking into account that as a result of the viscoelastic behavior of the polymers, the mechanical properties change by modifying the testing conditions (strain rate and temperature).

An increase in the test speed causes an increase in the yield strength and elastic modulus but the ductility decreases. All this implies that the area below the stress-displacement curve will be smaller, which contribute to obtaining lower values of w_e and βw_p, but this drop is slight at conventional testing speeds [24,25,30]. The opposite effect is observed when the temperature is increased [31,32].

2.3 J-integral and CTOD

The J-integral represents an energy contour path integral that is independent of the path around the crack. Rice showed [33] that the J-integral is essentially equal to the energy release rate of work done on a non-linear elastic body containing a crack per unit surface area of crack growth.

In a preceding study, Martínez et al. [34] found that w_e represented the energy per unit ligament area at crack initiation. This leads to the question of whether w_e is equivalent to J_{IC} in plane stress conditions because both parameters have the same physical meaning and good numerical agreement. Other authors [35-36] have proposed the equivalence between these fracture parameters.

Another important concept, first proposed by Wells in 1963 [37] is the crack tip opening displacement (CTOD). This concept is used to determine a fracture parameter for ductile materials. It essentially measures the resistance of the material to the propagation of a crack. A direct relationship between the J-integral and CTOD concepts exists [Eq. (1.30)].

2.4 Displacement measurement

The measured parameters by a classical testing machine include load and displacement. The force is provided by a force transducer (load cell) and the displacement by mechanical devices that in some way have contact with the test specimen. Such devices include specimen grips and strain gauges.

The strain obtained in this way encompasses the relative movement between two points, without being possible to directly obtain the global strain field [38].

Optical full-field measurement techniques like holography, speckle interferometry, photoelasticity, moiré, and Digital Image Correlation (DIC) are becoming more increasingly used to measure full-field strain measurements on standard specimens [39].

The DIC technique was developed in the early 1980s [40-42] and is widely used in the field of experimental mechanics to measure deformations on the surface of an object [43-45].

In general, DIC is based on the principle of comparing speckle patterns on the surface of the undeformed (reference) and deformed specimens, or between any two deformation states. Surfaces with high contrast are required to avoid image distortion and therefore inaccurate data. Hence, before testing, one surface of each DENT specimen must be covered with a thin white coating before being spray-painted with a random array of black points, as required by the DIC system.

By applying this optical technique, it is possible to measure the deformation (displacement) and the ligament length on the DENT specimens, allowing the EWF, CTOD, and J-integral analyses to be performed on a unique set of DENT specimens [46-49].

The DIC system permits measuring the displacement very close to the crack tip, in this way the CTOD is quantified. There is experimental evidence that w_e is insensitive to changes in the gauge length chosen for displacement measurements. However, βw_p and the measured displacement increase slightly with increasing gauge length [50].

2.5 Notch quality

For the same material, variations in the w_e values provided by different laboratories can be found [17]. These variations have been attributed to differences in the notch quality [34,50].

To perform the notch sharpening in ductile films, two different procedures are available: femtosecond pulsed laser ablation and razor blade sliding.

Laser ablation removes material from a surface by irradiating it with a laser beam. Depending on the equipment used, the emitted laser pulses can be obtained at different time scales, e.g., microsecond, nanosecond, picosecond, and femtosecond laser pulses. In our work, with the aim of micromachining a sharp crack, high-density femtosecond laser pulses equipment was used to irradiate the pre-notch tip of the DENT specimens.

It is important to emphasize that when the laser beam interacts with the polymer's surface, and the phase change (solid-vapor/plasma) takes place, the heat conduction is negligible. This avoids melted and deformed material at the crack tip.

The reliance on the operator by using the femtosecond pulsed laser ablation as notch sharpening procedure is minimal. Thus, high-quality notches are obtained with similar dimensions to each other in both sharpening depths and crack tip radii.

Razor blade sliding is a sharpening procedure in which a fresh razor blade is passed across the pre-notch tip in a single pass in order to follow the same track and thus avoiding bifurcations. Sharpening by razor blade sliding is an operator-dependent technique and is the generalized way to sharpening pre-notches in polymer films.

The notch sharpening is crucial to obtain good results. There is evidence [51] that razor blade sharpened specimens with damage ahead of the notch tip provide high w_e values. The larger the plastic deformation in front of the notch tip, the higher the w_e values.

Also, the larger the notch tip radius, the higher the w_e values. Thus, the notches should be sharpened as much as possible without significantly lowering w_e. Williams and Rink [20] recommend a notch tip radius equal or less than 15 μm. However, it seems that decreasing the notch tip radius leads to lower w_e values [51].

The femtolaser ablation technique produces sharp, high-quality notches without plastic deformation in front of the crack tip.

Martínez et al. [50] found that the razor blade sliding technique delivered much higher w_e values than the femtolaser ablation. The reason for this behavior was explained by the negligible plastic deformation at the crack tip in the femtolaser specimens and the elevated plastic deformation ahead of the notch tip in the razor blade sharpened specimens.

Freezing the specimens using liquid nitrogen before applying the razor blade sharpening can be an option if the plastic deformation ahead of the notch tip wants to be reduced.

Other procedures for generating notches have been tried unsuccessfully, which include cuts made by scissors or die-punch and scalpel cuts generated starting from the notch tip. These techniques generate greater plastic deformation ahead of the notch tip and result in higher w_e values than does the razor blade sliding method [13] or scalpel sliding [51].

2.6 Materials

All polymers that meet the EWF key assumptions can be successfully tested. However, differences can arise from one another during testing.

In single-phase homopolymers and copolymers, full ligament yielding must show a load-stress drop (necking) in the related load-displacement and stress-displacement curves, but this is not the case for multiphasic polymers, such as the rubber-toughened ones, where micro-deformation mechanisms such as multiple shear yielding or multiple crazing can take place [27].

Below is a brief summary of the materials used in this work. All of them fulfill entirely the key requirements established by the EWF approach.

2.6.1 PET

Polyethylene terephthalate (PET) is considered the most common polyester among the thermoplastic polymers. PET can be formed through the combination of two monomers, ethylene glycol and terephthalic acid, which results in the monomer ethylene terephthalate. After polymerization, this monomer finally forms the characteristic repeat unit of this polymer (Figure 2.7).

PET is a crystallizable thermoplastic polymer that can exist in amorphous or semicrystalline state. One way to obtain one or another is by modifying the processing conditions. If during processing the polymer is cooled quickly, it will result in an amorphous PET (transparent), but with controlled slow cooling, a semicrystalline PET (opaque and white) will be obtained.

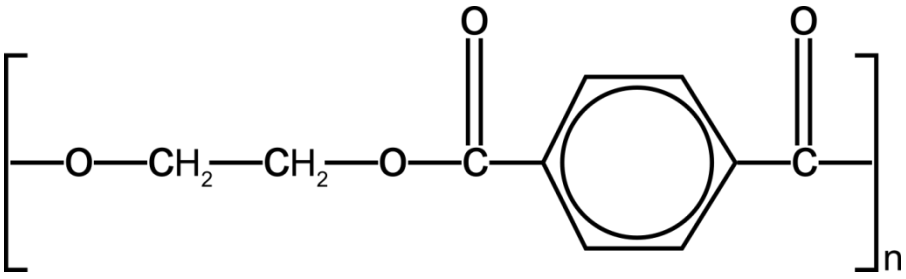

Figure 2.7 Repeating unit of PET [52]

Besides the differences in optical properties, the amorphous PET will be more flexible and with lower mechanical strength that the semicrystalline PET. Thus, to obtain one of these polymers depends

on the particular application in which will be used. Some applications include liquid containers, auto parts, and fibers used in shirts and carpets.

2.6.2 PETG

Polyethylene terephthalate glycol-modified (PETG) is a modified version of PET. The addition of a second glycol (1.4-cyclohexanedimethanol-CHDM) during the polymerization breaks the ethylene-glycol chain giving rise to an irregular molecular structure. The entire process inhibits the material's capacity for crystallization and leads to a new polymer (Figure 2.8).

When an amorphous PET is exposed to heat, it is possible that T_g is exceeded, provoking an undesired crystallization that can make the polymer to go from ductile to brittle. The inclusion of CHDM hinders the crystallization and makes the polymer walls softer, increasing its impact strength.

Between the possible disadvantages of this polymer are: the susceptibility to scratch and that can easily be weakened by UV light. Some applications include electronic devices, visual merchandising, and medical braces.

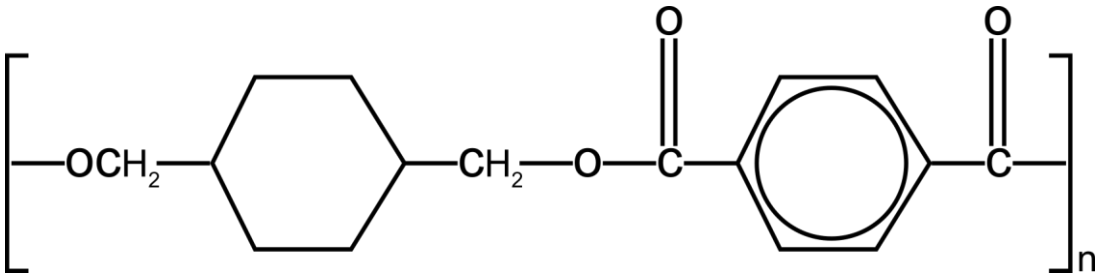

Figure 2.8 Repeating unit of PETG [52]

2.6.3 ECOZEN

Bio-based polymers are defined as materials where at least a portion of the polymer structure comes from renewable resources [53]. These polymers reduce the CO_2 emissions (carbon footprint) by switching from the fossil to bio-carbon [54]. Examples of renewable carbon resources include wheat, vegetable oil, potatoes, soy, corn, and rice.

A bio-based amorphous copolyester (ECOZEN), developed by SKYGREEN chemicals (Korea), was chosen to be studied. This copolyester is produced by the polymerization of terephthalic acid, ethylene glycol, 1.4-cyclohexanedimethanol, and a bio-based monomer that is derived from renewable resources [55].

ECOZEN provides an increased performance over conventional polyesters such as PET and PETG, particularly in relation to the glass transition temperature, chemical resistance, and oxygen barrier properties. It is also Bisphenol A-free; thus, it might be an excellent choice for food contact applications. Further, notched Izod impact specimens made of ECOZEN tested using ASTM D256 do not break.

Applications of this copolyester include food containers, sheet/film for optical uses, outdoor signboards, and bottles (water, juice, sports).

2.6.4 EPBC

The commodity plastics or commercial plastics include polyvinyl chloride (PVC), polypropylene (PP), polyethylene (PE), polystyrene (PS), and polyethylene terephthalate (PET). These polymers are the most used in terms of volume and number of applications [56].

Polypropylene (PP) is one of the most used commodity thermoplastics due mainly to its low cost and other attractive properties [57]. However, PP has the disadvantage of becoming brittle at low temperatures ($T_{g,PP} \approx 0°C$), which decreases its impact resistance.

One way to improve the poor impact behavior at low temperatures of PP is blending it with an elastomeric phase that decreases its T_g. Ethylene satisfies this purpose and, in addition, the ethylene-propylene particles obtained possess a good interfacial adhesion with the matrix [57].

The mechanism responsible for the toughness reinforcement is the formation of shear bands (multiple shear yielding) around the elastomeric particles, which absorbs most of the deformation energy. This mechanism may be accompanied by cavitation of the elastomeric particles.

Heterophasic ethylene-propylene block polymers (EPBC) with different ethylene contents can be obtained. The molecular weight and ethylene content have a great impact on the fracture toughness parameters. There is evidence [57] that when comparing EPBCs with similar molecular weight, the higher the ethylene content, the higher the impact fracture toughness, whereas, at similar ethylene content, the higher the molecular weight, the higher the impact fracture toughness.

2.7 Aims of the work

The overall aim of the present work is to analyze in full-detail the fracture behavior of ductile polymer films that have different deformation micromechanisms by applying the appropriate fracture mechanics approaches and methods.

Specific objectives include:

- Provide a better understanding of the factors that have a strong influence on the repeatability and reproducibility of the EWF test
- Analyze the effect of different notch sharpening techniques on the fracture parameters values
- Clarify the aspects that make the specific essential work of fracture (w_e) an inherent material property and with the same conceptual meaning and quantitative value that the J-integral at crack initiation (J_{IC})
- Investigate in detail the effect of the notch quality on the shape and size of the registered stress-displacement curves and on the crack growth range

To reach these goals the following strategy was defined and followed:

1. Material characterization

To investigate the applicability of the EWF test method, materials with different microdeformation mechanisms were chosen. Specifically, three materials that undergo necking before failure (PET, PETG, and ECOZEN) and two different grades of an EPBC that deform via multiple shear bands were studied. A physical, chemical, and thermal characterization were performed on the starting materials to determine, when applicable, the glass transition temperature, the percent crystallinity, the ethylene content, the molecular weight, among others.

2. Specimen manufacture

Two kinds of specimens were prepared: dumbbell shaped and DENT specimens. The deformation behavior was determined by performing tensile tests on the dumbbell shaped specimens, and DENT specimens were used to perform the fracture tests.

3. Notch sharpening procedure

As the notch sharpening procedure has a great influence on the fracture parameters values, different techniques were used to sharpening the DENT specimens. When the DIC system was used, after sharpening and before testing, one surface of each specimen was adequately sprayed with a speckle pattern, as required by the DIC system.

4. EWF test

The key requirements that affect the repeatability and reproducibility of the EWF test method were completely analyzed for all studied materials and for two notch sharpening procedures (femtosecond laser ablation and razor blade sliding). A new plot (stress-displacement plot) can help to discard non-valid specimens and to define w_e as an initiation value, that is, an inherent material parameter.

5. CTOD

The DIC system allows measuring the displacement very close to the crack tip. Then, the CTOD is measured, and the $CTOD_C$ value can be obtained. This value can be compared to the displacement at crack initiation (d_i) as found in the new stress-displacement plot.

6. Propagation range analysis

For the EWF test method to be applicable, the ligament length must be fully yielded prior to the onset of crack initiation. In this way, the propagation region is independent of the notch sharpening procedure, and thus the crack growth and propagation energy must be the same for the femtolaser and razor blade sharpened specimens. To prove this, two new plots were developed, the normalized crack growth-displacement and the load-crack length plots. These plots can also be used to discard anomalous specimens.

7. J analysis

The Begley and Landes experimental method was used to determining the J-values looking for evidence that w_e is equal to J_{IC} in plane stress.

8. Shape of the stress-displacement curves

The EWF behavior of notches sharpened in different ways can be analyzed. To do this, several notch sharpening procedures were used, including razor blade sliding on specimens frozen by liquid nitrogen, saw cutting, plastically deformed saw cutting, scalpel sliding, and drilled holes used as notches. The results were compared with the femtolaser and razor blade sharpened specimens.

As different notch sharpening procedures provide different levels of plastic deformation at the crack tip, differences would also be expected in the shape and size of the stress-displacement curves. These differences will lead to different w_e values. For all notch sharpening procedures, identical βw_p values can be obtained. This is a consequence of the identical crack propagation behavior, which is independent of the plastic deformation in front of the notch root.

With this in mind, the shape and size of the stress-displacement curves that were notched in different ways were analyzed to clarify their EWF behavior. In the propagation region, it is also identified the parabolic shape of the stress-displacement curves, which modeled relates the specific non-essential work of fracture with the stress at crack initiation and the extension ratio during the crack growth.

2.8 References

[1] PlasticsEurope (Association of Plastics Manufacturers). Plastics-the Facts 2016. https://www.plasticseurope.org (accessed July 24, 2017).

[2] Park ES. Antimicrobial polymeric materials for packaging applications. The Battle Against Microbial Pathogens: Basic Science, Technological Advances and Educational Programs, Vol. 1 2015: 500-511.

[3] Balakrishnan P, Thomas MS, Pothen LA, Thomas S, Sreekala MS. Polymer Films for Packaging. Encyclopedia of Polymeric Nanomaterials 2014: 1878-1884.

[4] Zhang P, Ma L, Fan F, Zeng Z, Peng C, Loya PE, Liu Z, Gong Y, Zhang J, Zhang X, Ajayan PM, Zhu T, Lou J. Fracture toughness of graphene. Nature communications 2014; 5: 3782.

[5] Zhang X, Beake BD, Zhang S. Toughness Evaluation of Thin Hard Coatings Films. In: Zhang S, editor. Thin Films and Coatings: toughening and Toughness Characterization, 2015, p. 47-122.

[6] Griffith AA. The Phenomena of Rupture and Flow in Solids. Philosophical Transactions of the Royal Society of London 1921; 221: 163-198.

[7] Lawn B. Fracture of Brittle Solids. 2nd ed. New York: Cambridge University Press; 1993.

[8] Lindeburg MR. FE Mechanical Review Manual. California: Professional Publications Inc.; 2014.

[9] Zhang S, Deen S, Fu Y, Du H. Toughness measurement of thin films: a critical review. Surface and Coatings Technology 2005; 198: 74-84.

[10] Broberg KB. Critical review of some theories in fracture mechanics. International Journal of Fracture 1968; 4: 11-19.

[11] Broberg KB. Crack-growth criteria and non-linear fracture mechanics. Journal of the Mechanics and Physics of Solids 1971; 19: 407-418.

[12] Broberg KB. On stable crack growth. Journal of the Mechanics and Physics of Solids 1975; 23: 215-237.

[13] Clutton E. Essential work of fracture. In: Moore DR, Pavan A, Williams JG, editors. Fracture mechanics testing methods for polymers, adhesives and composites. Oxford: Elsevier Science, Ltd.; 2001, p. 177-195.

[14] Cotterell B, Reddel JK. The essential work of plane stress ductile fracture. International Journal of Fracture 1977; 13: 267-277.

[15] Mai YW, Cotterell B. The essential work of fracture for tearing of ductile metals. International Journal of Fracture 1984; 24: 229-236.

[16] Mai YW, Cotterell B. On the essential work of ductile fracture in polymers. International Journal of Fracture 1986; 32: 105-125.

[17] Bárány T, Czigány T, Karger-Kocsis J. Application of the essential work of fracture (EWF) concept for polymers, related blends and composites. Progress in Polymer science 2010; 35: 1257-1287.

[18] Martínez AB, Gamez-Perez J, Sanchez-Soto M, Velasco JI, Santana OO, Maspoch ML. The essential work of fracture (EWF) method. Analyzing the post-yielding fracture mechanics of polymers. Engineering Failure Analysis 2009; 16: 2604-2617.

[19] Mai YW, Cotterell B. Effect of specimen geometry on the essential work of plane stress ductile fracture. Engineering Fracture Mechanics 1985; 21: 123-128.

[20] Williams JG, Rink M. The standardisation of the EWF test. Engineering Fracture Mechanics 2007; 74: 1009-1017.

[21] Karger-Kocsis J, Czigany T, Moskala EJ. Thickness dependence of work of fracture parameters of an amorphous copolyester. Polymer 1997; 38: 4587-4593.

[22] Ferrer-Balas D, Maspoch ML, Martínez AB, Santana OO. On the essential work of fracture method: energy partitioning of the fracture process in iPP films. Polymer Bulletin 1999; 42: 101-108.

[23] Hossain MM, Lee CF, Fiscus DM, Sue HJ. Physical assessment of essential work of fracture parameters based on m-LLDPE blown films. Polymer; 2016; 96: 104-111.

[24] Maspoch ML, Ferrer D, Gordillo A, Santana OO, Martínez AB. Effect of the specimen dimensions and the test speed on the fracture toughness of iPP by the essential work of fracture (EWF) method. Journal of Applied Polymer Science 1999; 73: 177-187.

[25] Arkhireyeva A, Hashemi S, O'Brien M. Factors affecting work of fracture of uPVC. Journal of Materials Science 1999; 34: 5961-5974.

[26] Arkhireyeva A, Hashemi S. Combined effect of temperature and thickness on work of fracture parameters of unplasticized PVC film. Polymer Engineering and Science 2002; 42: 504-518.

[27] Martínez AB, León N, Segovia A, Cailloux J, Martínez PP. Effect of specimen notch quality on the essential work of fracture of ductile polymer films. Engineering Fracture Mechanics 2017; 180: 296-314.

[28] Lee CF, Sue HJ, Fiscus DM. Refined fixture design for effective essential work of fracture toughness characterization of m-LLDPE thin films. Polymer Testing 2013; 32: 256-264.

[29] Cotterell B, Pardoen T, Atkins AG. Measuring toughness and the cohesive stress-displacement relationship by the essential work of fracture concept. Engineering Fracture Mechanics 2005; 72: 827-848.

[30] Maspoch ML, Gamez-Perez J, Karger-Kocsis J. Effects of thickness, deformation rate and energy partitioning on the work of fracture parameters of uPVC films. Polymer Bulletin 2003; 50: 279-286.

[31] Arkhireyeva A, Hashemi S. Influence of temperature on plane stress ductile fracture of poly (ethylene terephthalate) film. Plastic, Rubber and Composites 2001; 30: 125-131.

[32] Hashemi S, Arkhireyeva A. Influence of temperature on work of fracture parameters in semi-crystalline polyester films. Journal of Macromolecular Science Part B-Physics 2002; 41: 863-880.

[33] Rice JR. A path independent integral and the approximate analysis of strain concentration by notches and cracks. Journal of Applied Mechanics 1968; 35: 379-386.

[34] Martínez AB, Segovia A, Gamez-Perez J, Maspoch ML. Essential work of fracture analysis of the tearing of a ductile polymer film. Engineering Fracture Mechanics 2010; 14: 2654-2661.

[35] Mai YW, Powell P. Essential work of fracture and j-integral measurements for ductile polymers. Journal of Polymer Science-Part B: Polymer Physics 1991; 29: 785-793.

[36] Rink M, Andena L, Marano C. The essential work of fracture in relation to J-integral. Engineering Fracture Mechanics 2014; 127: 46-55.

[37] Wells AA. Application of fracture mechanics at and beyond general yielding. British Welding Journal 1963; 10: 563-570.

[38] Tung SH, Sui CH. Application of digital-image-correlation techniques in analyzing crack cilindrical pipes. Sadhana 2010; 35: 557-567.

[39] Grédiac M. The use of full-field measurement methods in composite material characterization: interest and limitations. Composites Part A: Applied Science and Manufacturing 2004; 35: 751-761.

[40] Peters WH, Ranson WF. Digital imaging techniques in experimental stress analysis. Optical Engineering 1982; 21: 427-431.

[41] Peters WH, Ranson WF, Sutton MA Chu TC, Anderson J. Application of digital correlation methods to rigid body mechanics. Optical Engineering 1983; 22: 738-742.

[42] Sutton MA, Wolters WJ, Peters WH, Ranson WF, McNeill SR. Determination of displacements using an improved digital image correlation method. Image vision computing 1983; 1: 133-139.

[43] Vacher P, Dumoulin S, Morestin F, Mguil-Touchal S. Bidimensional strain measurement using digital images. Journal of Mechanical Engineering Science 1999; 213: 811-817.

[44] Wattrise B, Chysochoos A, Muracciole JM, Némoz-Gaillard M. Analysis of strain localization during tensile tests by digital image correlation. Experimental Mechanics 2001; 41: 29-39.

[45] Chavalier L, Calloch S, Hild F, Marco Y. Digital image correlation used to analyze the multiaxial behavior of rubber-like materials. European Journal of Mechanics – A/Solids 2001;20: 169-187.

[46] Martínez AB, León N, Arencón D, Sánchez-Soto M. Essential work of fracture, crack tip opening displacement, and J-integral relationship for a ductile polymer film. Polymer Testing 2016; 55: 247-256.

[47] Martínez AB, León N, Arencón D, Sánchez-Soto M. The post-yield fracture of a ductile polymer film: Notch quality, essential work of fracture, crack tip opening displacement, and J-integral. Engineering Fracture Mechanics 2017; 173: 21-31.

[48] León N, Martínez AB, Castejón P, Arencón D, Martínez PP. The fracture testing of ductile polymer films: Effect of the specimen notching. Polymer Testing 2017; 63: 180-193.

[49] León N, Martínez AB, Castejón P, Martínez PP, Arencón D. Notch effect on the fracture of a polymeric film. Theoretical and Applied Fracture Mechanics

[50] Martínez AB, Segovia A, Gamez-Perez J, Maspoch ML. Influence of femtolaser notch sharpening technique in the determination of essential work of fracture (EWF) parameters. Engineering Fracture Mechanics 2009; 76: 1247-1254.

[51] Pegoretti A, Castellani L, Franchini L, Mariani P, Penati A. On the essential work of fracture of linear low-density-polyethylene. I. Precision of the testing method. Engineering Fracture Mechanics 2009; 76: 2788-2798.

[52] Baranowski M, Wozniak-Braszak A, Jurga K, Jurga J, Holderna-Natkaniec K. Molecular dynamics in poly (ethylene terephthalate) (PET) and poly (ethylene terephthalate)-glycol (PETG). High Pressure Physics Division, Institute of Physics, Adam Mickiewicz University 2005.

[53] Bell SL. Bio-based polymers. IHS Chemical Process Economic Program - Report 26SA; 2013.

[54] Narayan R. Biobased and biodegradable plastics: rationale, drivers, and technology exemplars. In: Khermani K, Scholz C (editors). 2nd ed. Alabama: American Chemical Society; 2012, p. 13-31.

[55] SK chemicals. https://www.skchemicals.com (accessed November 11, 2017).

[56] Subramanian MN. The basics of troubleshooting in plastics processing: an introductory practical guide. New Jersey: John Wiley and sons; 2011.

[57] Martínez AB, Arencón D, Rodríguez J, Salazar A. Influence of the notch sharpening on the impact fracture toughness of ethylene-propylene block copolymers. Polymer Testing 2014; 36: 75-81.

Chapter 3

Results

3.1 EWF, J-integral, and CTOD relationships

In this first section, the relationships among the specific essential work of fracture (w_e), the J-integral at crack initiation (J_{IC}), and the critical crack tip opening displacement ($CTOD_C$) are mainly discussed.

A polyethylene terephthalate (PET) (Section 3.1.1) and a polyethylene terephthalate glycol-modified (PETG) films (Section 3.1.2) were used to investigate these relationships.

To do this, a Digital Image Correlation (DIC) system was used to measure the deformation and the ligament length on double edge notched tension (DENT) specimens. This technique allowed the essential work of fracture (EWF), the J-integral, and the crack tip opening displacement (CTOD) analyses to be performed on a unique set of DENT specimens.

The main aim of this part of the thesis was to find evidence that w_e is an initiation value and equal in quantity and meaning to J_{IC} in a state of plane stress.

Section 3.1.1 – Reference:

Martínez AB, León N, Arencón D, Sánchez-Soto M. Essential work of fracture, crack tip opening displacement, and J-integral relationship for a ductile polymer film. Polymer Testing 2016; 55: 247-256. DOI: 10.1016/j.polymertesting.2016.09.004.

Section 3.1.2 – Reference:

Martínez AB, León N, Arencón D, Sánchez-Soto M. The post-yield fracture of a ductile polymer film: Notch quality, essential work of fracture, crack tip opening displacement, and J-integral. Engineering Fracture Mechanics 2017; 173: 21-31. DOI: 10.1016/j.engfracmech.2017.01.019.

3.1.1 Essential work of fracture, crack tip opening displacement, and J-integral relationship for a ductile polymer film

ATTENTION ¡
Pages 67 to 75 of the thesis, containing the text mentioned above, are available at the editor's web
https://www.sciencedirect.com/science/article/pii/S0142941816306262

Polymer Testing 55 (2016) 240–246

Contents lists available at ScienceDirect

Polymer Testing

journal homepage: www.elsevier.com/locate/polytest

Test Method

Essential work of fracture, crack tip opening displacement, and J-integral relationship for a ductile polymer film

A.B. Martínez, N. León*, D. Arencón, M. Sánchez-Soto

Centre Català del Plàstic, Departament de Ciència dels Materials i Enginyeria Metal·lúrgica, Universitat Politècnica de Catalunya-BarcelonaTech, C/Colom 114, 08222, Terrassa, Spain

ARTICLE INFO

Article history:
Received 29 June 2016
Received in revised form
18 August 2016
Accepted 4 September 2016
Available online 7 September 2016

Keywords:
Essential work of fracture
J-integral
Polymer film

ABSTRACT

A unique set of double-edge notched tension specimens of a Polyethylene Terephthalate Glycol-modified film was tested in mode I, plane stress. The load was registered on a universal testing machine. The displacements, ligament lengths, and video frames were recorded by a Digital Image Correlation system. With these registered data, the essential work of fracture, J-integral, and crack tip opening displacement (CTOD) fracture concepts have been applied. The onset of crack initiation was through a completely yielded ligament. The analysis showed that the intrinsic specific work of fracture, w_e, is the specific energy just up to crack initiation, which is an initiation value. w_e has both a coincident value and the same conceptual meaning as J_0, the J-integral at the onset of crack initiation. The relationship between J_0 and CTOD is also determined. The influence on the notch quality when the specimens were sharpened by two different procedures, femtosecond laser ablation and razor blade sliding, was analyzed in detail.

1. Introduction

One of the most important characteristics that make polymers such useful materials, especially in the packaging industry, is their ability to be manufactured into ductile films and thin sheets. When characterizing these materials, the tests for determining the mechanical properties are well established, but this is not the case for fracture properties.

The linear elastic fracture mechanics (LEFM) approach is used to study fractures occurring at nominal stresses well below the material yield stress. The main hypothesis of LEFM considers that the dissipated energy is confined in a small area near the crack tip (small-scale yielding) and the fracture is brittle, without extensive deformation.

LEFM is not applicable in cases where the crack propagation occurs through a highly deformed and yielded material. Instead, the J-integral, the crack tip opening displacement (CTOD), and the essential work of fracture (EWF) can be used to quantify fracture toughness. Although the J-integral method has been traditionally employed in materials with large plastic deformation surrounding the crack tip, the EWF approach is gaining popularity to characterize the plane stress toughness of ductile polymer films, basically using the double-edge notched tension (DENT) configuration, mainly due to the apparently simple preparation and easy testing of the DENT specimen. The extensive use of the EWF technique has been reviewed [1,2].

The intrinsic specific work of fracture, w_e, becomes an inherent material parameter only when the complete ligament yielding of the polymer sample precedes the onset of crack initiation. However, this condition is rarely met; in most articles it is not satisfied and w_e is an apparent toughness that is only valid for comparison purposes. Nevertheless, it is known [2] that amorphous copolyesters such as PETG meet this condition, and it is certainly an excellent material for the EWF analysis.

To perform the notch sharpening in ductile polymer films, two different procedures are available: femtosecond laser ablation and razor blade sliding. In an earlier work on an ethylene-propylene block copolymer (EPBC) film, Martínez et al. [3] observed significant differences in the intrinsic essential work of fracture values when the femtolaser ablation and razor blade sliding techniques were applied, with the latter providing much higher values than the former one. The reason for this behaviour was associated with the accumulation of plastically deformed material at the tip of the razor blade sharpened notch and the almost negligible plastic deformation when the sharpening was realized by femtolaser ablation.

* Corresponding author. Tel.: +34 93 783 70 22.
E-mail address: noel.leon@estudiant.upc.edu (N. León).

http://dx.doi.org/10.1016/j.polymertesting.2016.09.004
0142-9418/

3.1.2 The post-yield fracture of a ductile polymer film: Notch quality, essential work of fracture, crack tip opening displacement, and J-integral

ATTENTION ¡
Pages 77 to 86 of the thesis, containing the text mentioned above, are available at the editor's web
https://www.sciencedirect.com/science/article/pii/S0013794416303897

Engineering Fracture Mechanics 173 (2017) 21–31

Contents lists available at ScienceDirect

Engineering Fracture Mechanics

journal homepage: www.elsevier.com/locate/engfracmech

The post-yield fracture of a ductile polymer film: Notch quality, essential work of fracture, crack tip opening displacement, and J-integral

A.B. Martínez, N. León *, D. Arencón, M. Sánchez-Soto

Centre Català del Plàstic, Departament de Ciència dels Materials i Enginyeria Metal·lúrgica, Universitat Politècnica de Catalunya-Barcelona TECH, C/Colom 114, 08222 Terrassa, Spain

ARTICLE INFO

Article history:
Received 14 September 2016
Received in revised form 20 January 2017
Accepted 30 January 2017
Available online 23 January 2017

Keywords:
Essential work of fracture
Crack tip opening displacement
J-integral
Polymer film
Remolaser

ABSTRACT

Double edge notched tension (DENT) specimens of a polyethylene terephthalate (PET) film were tested in an universal testing machine, measuring the displacement and the ligament lengths with a digital image correlation (DIC) system. With these data the essential work of fracture (EWF), crack tip opening displacement (CTOD), and the J-integral fracture methods were compared. The specimens were tested in mode I under plane stress conditions, verifying that the crack always propagated through a fully yielded ligament. It has been proved that w_e, the specific essential work of fracture was the specific energy just up to crack initiation and has the same value that J- integral at crack initiation, J_i. The relationship of these parameters with the CTOD was also shown. The influence of the notch quality on the fracture behaviour when the specimens were sharpened by two different methods, femtosecond laser ablation or by razor blade sliding, has also been analysed in detail.

1. Introduction

The ability of polymers to be shaped in practically any form makes possible to obtain films which are mainly used in the packaging and agriculture market segments that accounts for a 39.8% and 4.3% of the plastic global demand, respectively.

The classical tests for determining the mechanical properties of polymer films are well established and standardized, but this is not the case for the fracture properties.

The linear elastic fracture mechanics (LEFM) approach is used to study fractures occurring at nominal stresses well below the material yield stress. The main hypothesis of LEFM considers that the dissipated energy is confined in a small area near the crack tip (small scale yielding), and the fracture is brittle, without extensive deformation.

The LEFM approach is not applicable when the plasticity around the crack tip becomes too large; in those cases the elastic plastic fracture mechanics (EPFM) apply and CTOD and J-integral are appropriate methods to characterize fracture. When the crack propagation occurs through a highly deformed and yielded material then the post-yield fracture mechanics (PYFM) can also be applied and the EWF is the most suitable method. For ductile polymers where crack propagation occurs through a fully yielded ligament, the EWF, the CTOD, and the J-integral are commonly used.

The EWF is gaining acceptance to characterize the plane stress toughness of ductile polymer films in mode I, basically using the double edge notched tension (DENT) configuration. The widespread use of the EWF technique is due to the apparent simple DENT specimen preparation and the simple testing.

The specific work of fracture, w_e, becomes an inherent material parameter only if the ligament fully yields before the crack initiation.

In a previous work [1] carried out on an EPBC (ethylene-propylene block copolymer) material where the ligament was completely yielded before the onset of crack initiation, it was concluded that the specific work of fracture was the energy per unit of ligament area just up to crack initiation, that is, an initiation value. This conclusion drives to the question of whether this value is equivalent to J_i in plane stress conditions, because both parameters have the same physical meaning. According to Mai et al. [2] the essential work of fracture is equivalent to the J-integral at initiation, J_i. Although good numerical agreement

* Corresponding author.
E-mail address: noel.leon@estudiant.upc.edu (N. León).

http://dx.doi.org/10.1016/j.engfracmech.2017.01.019
0013-7944/

3.2 Essential work of fracture, notch effect, and fracture testing of ductile polymer films

The EWF approach has become very popular to characterize the fracture of polymer films and is increasingly used due to its apparent simple preparation and easy testing.

In spite of the apparent simplicity of the EWF test, some aspects of the validity of this technique remain controversial. These aspects are mainly related to the specimen manufacture, particularly the quality of the notches, and were studied more in depth here.

The shape and size of the stress-displacement curve affect the w_e and βw_p values. In Sections 3.2.1 and 3.2.2, the effect of different quality notches on the shape of the stress-displacement curves for two different grades of a rubber-toughened ethylene-propylene block copolymer (EPBC) was analyzed in detail. The effect on the stress-displacement curves of specimens with non-collinear notches, and specimens having misalignment with the load axis have been also studied.

In Section 3.2.2 and Annex, the EWF, J-integral, and CTOD fracture characterization methods are again used in an attempt to provide a better understanding of the EWF approach for characterizing the fracture toughness of thin ductile polymer films.

The parabolic shape of the stress-displacement curve in the propagation range is identified and quantified in the Annex for a bio-based thermoplastic copolyester (ECOZEN) and for all other materials studied in this research work.

The main aim of this part of the thesis was to contribute to a better understanding and to clarify some of the controversial factors involved in the EWF test.

In general, there is a limited understanding of the polymers to which the EWF approach can be applied. Three polymers that neck before failure (PET, PETG, and ECOZEN) and two different grades of EPBC which deform by the formation and propagation of multiple shear bands were used to evaluate the validity of the EWF approach to polymers with distinct micro-mechanisms of deformation.

Section 3.2.1 – Reference:

Martínez AB, León N, Segovia A, Cailloux J, Martínez PP. Effect of specimen notch quality on the essential work of fracture of ductile polymer films. Engineering Fracture Mechanics 2017; 180: 296-314. DOI: 10.1016/j.engfracmech.2017.06.007.

Section 3.2.2 – Reference:

León N, Martínez AB, Castejón P, Arencón D, Martínez PP. The fracture testing of ductile polymer films: Effect of the specimen notching. Polymer Testing 2017; 63: 180-193. DOI: 10.1016/j.polymertesting.2017.08.022.

Annex – Reference:

León N, Martínez AB, Castejón P, Martínez PP, Arencón D. Notch effect on the fracture of a polymeric film **(Under review**). Theoretical and Applied Fracture Mechanics 2018.

3.2.1 Effect of specimen notch quality on the essential work of fracture of ductile polymer films

ATTENTION ¡

Pages 90 to 107 of the thesis, containing the text mentioned above, are available at the editor's web
https://www.sciencedirect.com/science/article/pii/S0013794417303405

Engineering Fracture Mechanics 180 (2017) 296–314

Contents lists available at ScienceDirect

Engineering Fracture Mechanics

journal homepage: www.elsevier.com/locate/engfracmech

Effect of specimen notch quality on the essential work of fracture of ductile polymer films

A.B. Martínez [a], N. León [a,*], A. Segovia [a], J. Cailloux [a], P.P. Martínez [b]

[a] Centre Català del Plàstic, Departament de Ciència dels Materials i Enginyeria Metal·lúrgica, Universitat Politècnica de Catalunya, BarcelonaTech, C/Colom 114, 08222 Terrassa, Spain
[b] NUDEC SA, C/ Pintor Vila Cinca, 24-28, Pol. Ind. Can Humet de Dalt, 08213 Polinyà, Spain

ARTICLE INFO

Article history:
Received 31 March 2017
Received in revised form 7 June 2017
Accepted 7 June 2017
Available online 9 June 2017

Keywords:
Notch sharpening
Notch quality
Essential work of fracture
Polymer film

ABSTRACT

The essential work of fracture approach has been employed to analyse the effect of notch sharpening on the fracture toughness of a semicrystalline multiphase ethylene-propylene block copolymer. Double edge notched tension specimens were sharpened using different techniques: femtolaser ablation, razor blade sliding at room and liquid nitrogen temperatures, saw cutting, plastically deformed saw cutting, and scalpel sliding. The notch sharpening techniques provide notches of different quality in relation to both the notch tip radius and the plastic deformation in front of the crack tip. The best quality notches were produced by the femtolaser ablation technique, which provides very sharp notches without plastic deformation ahead of the crack tip. The effects of the non-collinearity of the notches and tilted specimens on the testing machine grips were also analysed. The shape of the registered stress–displacement curves shows differences, but only in the range comprised between the displacements corresponding to the maximum stress and the onset of crack initiation. A larger crack tip radius and/or larger extent of plastic deformation in front of the notch root leads to larger values of the displacement at the onset of crack initiation, resulting in higher values for the specific essential work of fracture. Yet on the other hand, the values of the slope of the essential work of fracture plot remain unchanged. A lower value for the specific essential work of fracture was obtained for the specimens sharpened using the femtolaser ablation technique.

1. Introduction

Films and thin sheets of polymers, polymer blends, and polymer composites are used in a wide variety of applications such as packaging, agriculture, coating, paint, among others. Their toughness is often a basic requisite to meet some industry needs.

The Linear Elastic Fracture Mechanics (LEFM) approach is used to study fractures occurring at nominal stresses well below the material yield stress. The dissipated energy is confined in a small area near the crack tip and the fracture is brittle. The LEFM approach is not applicable when the plasticity around the crack tip becomes too large; in those cases the Elastic Plastic Fracture Mechanics (EPFM) approach applies. When the crack propagation occurs through a highly deformed and

* Corresponding author.
E-mail address: noel.leon@estudiant.upc.edu (N. León).

http://dx.doi.org/10.1016/j.engfracmech.2017.06.007
0013-7944/

3.2.2 The fracture testing of ductile polymer films: Effect of the specimen notching

ATTENTION ¡

Pages 109 to 121 of the thesis, containing the text mentioned above, are available at the editor's web
https://www.sciencedirect.com/science/article/pii/S0142941817308036

Polymer Testing 63 (2017) 180–193

Contents lists available at ScienceDirect

Polymer Testing

journal homepage: www.elsevier.com/locate/polytest

Test Method

The fracture testing of ductile polymer films: Effect of the specimen notching

N. León [a, *], A.B. Martínez [a], P. Castejón [a], D. Arencón [a], P.P. Martínez [b]

[a] Centre Català del Plastic, Departament de Ciència dels Materials i Enginyeria Metal·lúrgica, Universitat Politècnica de Catalunya, BarcelonaTech, C/Colom 114, 08222 Terrassa, Spain
[b] NUDEC SA, C/ Pintor Vila Cinca, 24-28, Pol. Ind. Can Humet de Dalt, 08213 Polinyà, Spain

ARTICLE INFO

Article history:
Received 16 June 2017
Received in revised form
14 August 2017
Accepted 17 August 2017
Available online 19 August 2017

Keywords:
Fracture
Essential work of fracture
J-integral
Polymer film

ABSTRACT

The fracture of a ductile polymer film, a heterophase ethylene-propylene block copolymer, has been studied, combining a range of characterisation methods in an attempt to provide a better understanding of the intricate details that play an important role in the repeatability and reproducibility of the essential work of fracture test. The experimental factors that have a strong influence on the resulting parameters are clearly explained, with particular attention to the effect of the quality of the notches, the non-collinearity of the two edge notches in double edge notched tension specimens, and the lack of alignment of the specimen with the load axis once it is mounted on the load train. Furthermore, the influence of these experimental factors on the registered stress-displacement curves is also studied, and a criterion and the method for separating non-valid specimens are established.

1. Introduction

Polymer films are used in a wide variety of applications. Their toughness is often a basic requisite to meet some industry needs.

The Linear Elastic Fracture Mechanics (LEFM) approach is used to study fractures occurring at nominal stresses well below the material yield stress. The dissipated energy is confined in a small area near the crack tip, and the fracture is brittle. The LEFM approach is not applicable when the plasticity around the crack tip becomes large; in those cases the Elastic Plastic Fracture Mechanics (EPFM) is applied. When the crack propagation occurs through a highly deformed and yielded material then Post-Yield Fracture Mechanics can also be applied and the Essential Work of Fracture (EWF) is a suitable methodology.

The EWF approach has become very popular to characterise fracture of polymer films and is increasingly used due to its apparent simple preparation and easy testing. The EWF characterises the plane stress toughness in mode I, generally using the double edge notched tension (DENT) configuration for the specimens.

In spite of the apparent simplicity of the EWF test, some aspects of the validity of this technique remain controversial; there are intricate details that seem to play an important role in the repeatability and reproducibility of the test. This problem has been and still is a topic of much debate, and these questions indicate that the EWF procedure is not yet sufficiently well-defined to be standardised. Some of the aspects of the test validity are related to the specimen manufacture, particularly the quality of the notches.

Two sets of specimens have been prepared, the first one sharpened by the femtosecond laser ablation technique, and the second one sharpened by the classical razor blade sliding technique. These two sets of specimens have been characterised by combining the EWF, J-integral, and crack tip opening displacement (CTOD) methods in an attempt to provide a better understanding of the EWF fracture approach for characterising the fracture toughness of a ductile polymer film. The connection between the quality of the notches and the shape and size of the registered stress-displacement curves has been established. This was done in order to find a criterion and a method to eliminate non-valid specimens. Furthermore, it has been studied in detail how the size and shape of the stress-displacement curves are related to the EWF fracture parameters.

The effect on the stress-displacement curves of specimens with non-collinear notches, specimens with different quality between the two edge notches, and specimens having a lack of alignment with the load axis once mounted on the testing machine grips have

* Corresponding author.
E-mail address: noel.leon@estudiant.upc.edu (N. León).

http://dx.doi.org/10.1016/j.polymertesting.2017.08.022
0142-9418/

Chapter 4
Global discussion

4.1 Introduction

One of the key requirements to apply the EWF technique is that the ligament length must be fully yielded before crack initiation. This ensures that the fracture mechanism is the same irrespective of the ligament length. All the polymer film materials used in this thesis work accomplished this key requirement.

The materials studied were a polyethylene terephthalate (PET), a polyethylene terephthalate glycol-modified (PETG), a bio-based thermoplastic copolyester (ECOZEN) and two different commercial grades of a rubber-toughened ethylene-propylene block copolymer (EPBC1 and EPBC2).

The deformation behavior was carried out on standard dumbbell-shaped specimens following the ISO standard 527 (PET, PETG, EPBC2, and ECOZEN) and the ASTM standard D 638 (EPBC1). The cross-head speeds used were 1 mm/min for the PET, PETG, and ECOZEN specimens and 2 mm/min for the EPBCs specimens. Figure 4.1 shows the dumbbell-shaped geometry and dimensions corresponding to the ISO standard 527; the ASTM D 638 specimen is very much alike to this geometry.

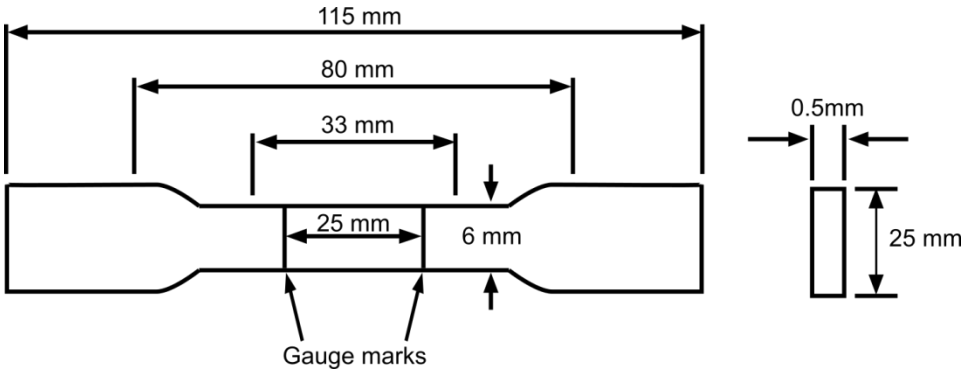

Figure 4.1 Dumbbell-shaped geometry

In-plane (mode I) fracture tests were performed to obtain the plane stress fracture toughness values for all materials. All the EWF tests were carried out in DENT specimens.

The DENT specimen configuration is the most appropriate for mode I testing of polymer films because the transverse stresses between the notches are tensile and bucking problems are avoided. Figure 4.2 shows the DENT specimen geometry used for all the materials.

All the DENT specimens were prepared in the machine direction (MD) orientation and, except when indicated, tested with the tensile direction perpendicular to the collinear notches.

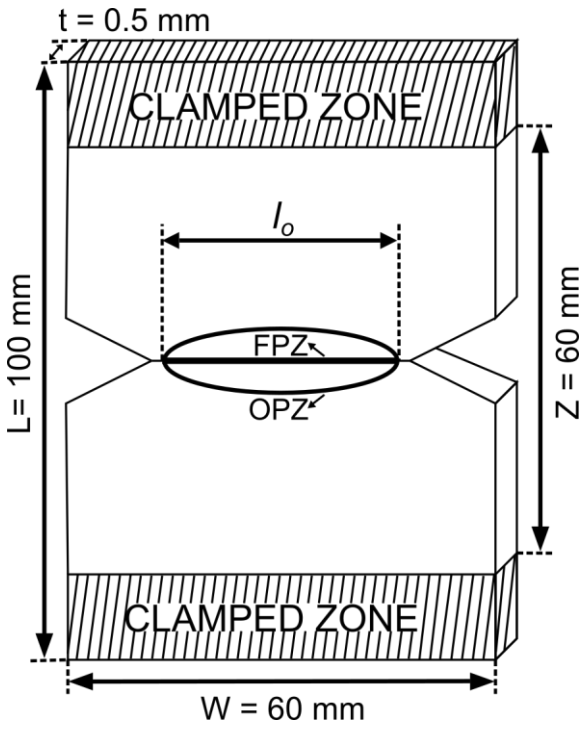

Figure 4.2 DENT specimen geometry and dimensions

For the PET, PETG, ECOZEN, and EPBC2, the load was measured in a Zwick servo-hydraulic testing machine and, at the same time, the displacements were measured by the DIC system and Aramis software (GOM, Germany). In the EPBC1, the load was measured in a universal testing machine (Galdabini Sun 2500, Italy) and the displacement was measured by a one-camera video extensometer (Mintron OS-65D, Taiwan). The cross-head speeds used were 1 mm/min for the PET, PETG, and ECOZEN specimens and 2 mm/min for the EPBCs specimens.

In the PET, PETG, ECOZEN, and EPBC2, DIC system images obtained during the tests were recorded for all specimens. These images were analyzed after with the Aramis software to measure the displacement and ligament length evolution throughout the test. With these data, the load-displacement, the stress-displacement, and the ligament length-displacement plots were obtained to perform EWF, CTOD, and J-integral analyses in a unique set of DENT specimens.

The razor blade sliding and the femtosecond pulsed laser ablation techniques were mainly used as notch sharpening procedures. For the EPBC1 and EPBC2, razor blade sliding applied to specimens frozen in liquid nitrogen was also used. In addition, for EPBC1, saw cutting, plastically deformed saw cutting, and scalpel sliding were used to analyze the effect of different notches on the shapes of the stress-displacement curves. The non-collinearity of the two edge notches and the lack of alignment of the specimen with the load axis once it is mounted on the load train were also studied.

4.2 Deformation behavior

In the PET, PETG, and ECOZEN specimens, the tensile stress-strain curves showed a yield point at maximum load where necking started, followed by a sudden load drop where neck developed. Afterwards, there was a drawing of the necked region (cold drawing), during which the tensile deformation continued at a constant stress (engineering flow stress, σ_{fs}), followed by a stress drop when the specimen ruptured. The EPBCs ruptured specimens showed a whitening zone in the deformed area, which is characteristic of the heterophase polymers that have multiple shear yielding as a deformation mechanism. Figure 4.3 shows examples of curves obtained after tensile tests were carried out for all the materials.

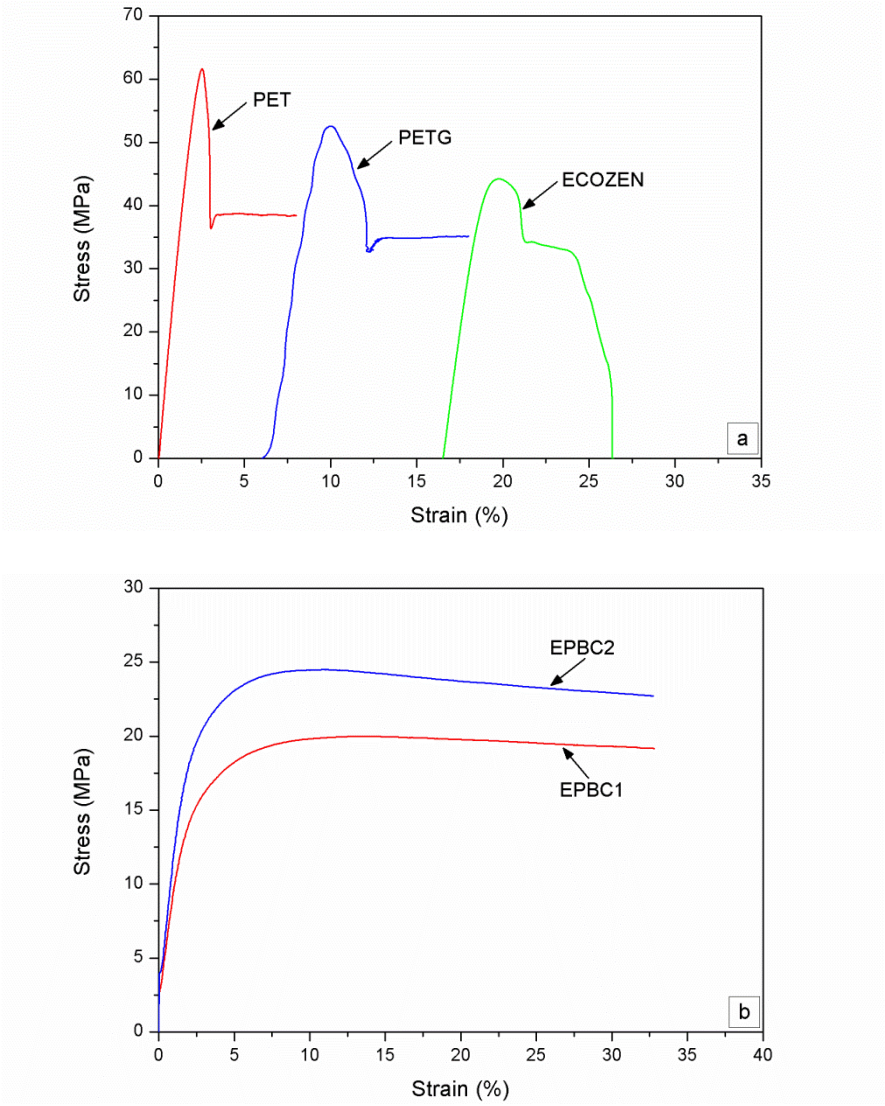

Figure 4.3 Tensile stress-strain curves to characterize deformation behavior: a) Materials that neck before failure, b) Materials that deform via the formation of multiple shear bands

Table 4.1 shows the results obtained from tensile testing. For the materials that undergo necking, PET was the material that could be more stretched before yielding. For the EPBC1 [M_z ($.10^3$) = 878] and EPBC2 [M_z ($.10^3$) = 1026], the greater the Z-average molecular weight (M_z), the higher the yield stress (σ_y) and the elastic modulus (E) at similar ethylene content.

Table 4.1 Classical mechanical properties values by performing uniaxial tensile tests

Property	Material				
	PET	PETG	ECOZEN	EPBC1	EPBC2
Yield stress (σ_y) MPa	58.61±2.05	51.00±1.50	44.48±0.42	20.60±0.20	25.00±0.20
Elastic modulus (E) GPa	2.64±0.02	1.89±0.50	1.91±0.42	1.03±0.01	1.24±0.10
Poisson's ratio (υ)	0.40±0.01	0.42±0.01	0.44±0.01	----	----
Engineering flow stress (σ_{fs})	37.37±1.48	34.40±1.20	33.77±0.44	----	----

4.3 Notch quality

The notch sharpening is of critical importance in obtaining good results. Several methods are found in the literature that can be used for sharpening notches in polymer films. Further, it appears that the notch quality is dependent on the technique used and on the skill of the operator performing the notch sharpening procedure.

In a set of DENT specimens, it is possible to have three different specimen populations that show distinct behaviors to each other, which are responsible for the non-similarity and crossing of the curves in the load-displacement, stress-displacement, and ligament length-displacement plots. These include specimens with two different notches, specimens with two equal notches and negligible plastic deformation, and specimens with two equal notches both of which have noticeable plastic deformation.

When the specimen has two different edge notches, crack initiation does not begin at the same time. Conversely, when the two edge notches are equal, the crack initiation happens at the same time.

Some of the femtolaser and razor blade sharpened specimens were observed by scanning electron microscopy (SEM) and/or optical microscopy (OM). Independently of the material, the femtolaser specimens turned out to be virtually identical, with no plastic deformation and negligible thermal damage ahead of the notch tip (Figure 4.4a). The razor blade sliding technique being operator-

dependent can deliver notches with differences in the sharpening depth, crack tip radius, and plastic deformation at the crack tip (Figure 4.4b).

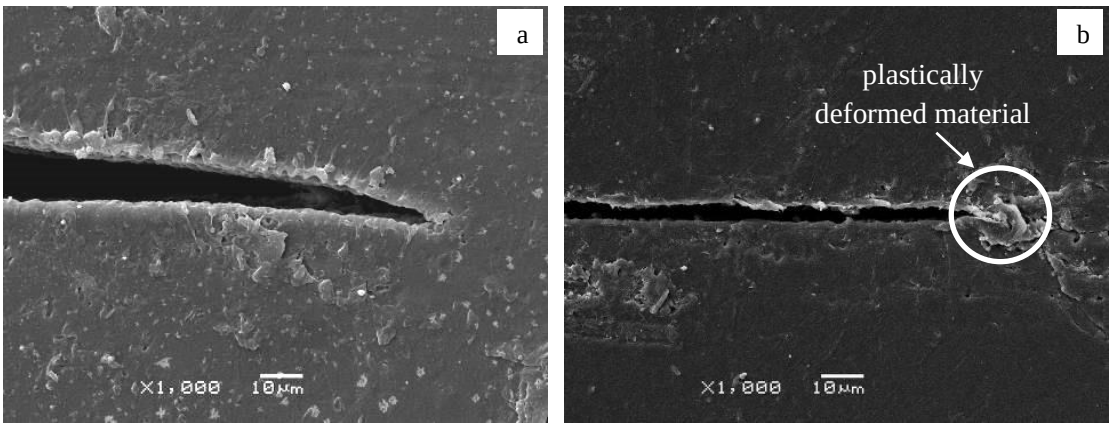

Figure 4.4 SEM micrographs of an EPBC2 specimen: a) Femtolaser notch, b) Razor blade notch

For PET, PETG, and ECOZEN, it was possible to obtain specimens with and without plastic deformation at the notch tip when razor blade sliding was applied.

In the EPBCs, the razor blade sharpened specimens revealed volume accumulation of plastically deformed material at the notch tip (Figure 4.4b), which was induced by the compressive component of the sideways sliding force. In addition, the DENT specimens presented some stress whitening ahead of the notch tip, indicating that plastic deformation had taken place. This was not present in the femtolaser sharpened specimens (Figure 4.5).

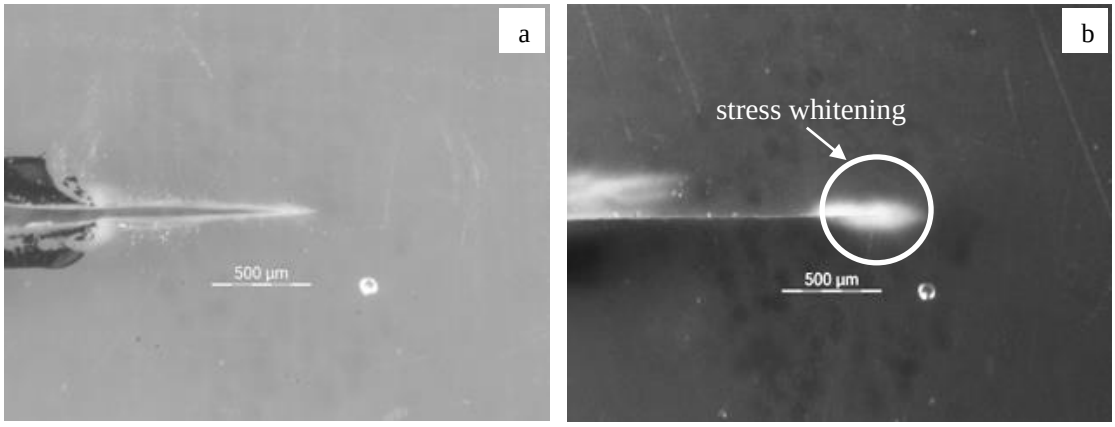

Figure 4.5 Optical micrographs of an EPBC2 specimen: a) Femtolaser notch, b) Razor blade notch

The second phase of the EPBC act as stress concentrator, and so only a small compressive component of the sliding force is needed to produce plastic deformation, which is visualized as whitening.

Both notch sharpening techniques produced similar notch tip radius. The differences arise in the plastic deformation in front of the notch tip and in the sharpening depth.

For the razor blade sharpened specimens, the plastic deformation can be present in different levels ahead of the notch tip, while for the femtolaser sharpened specimens is absent.

Table 4.2 shows the notch tip radius and the sharpening depth accomplished for the different materials and notch sharpening procedures used.

Table 4.2 Notch parameters values for all tested materials

Material	Notch tip radius (μm)		Sharpening depth (μm)	
	Femtolaser	Razor blade	Femtolaser	Razor blade
PET	1	1	300	400-600
PETG	0.8	<1	300	300-500
ECOZEN	1	1	1000	100-250
EPBC1	1	1	480	500-550
EPBC2	<1	<1	750	900-1300

4.4 The EWF and CTOD analyses

The DIC system allows obtaining the load-displacement and ligament length-displacement plots, from which the EWF, CTOD and J-integral analyses can be performed.

In the EWF analysis, the following three basic key assumptions are made: the ligament length is fully yielded prior to the onset of crack initiation, fracture occurs under plane stress conditions, and good quality notches are required.

The last key requirement guarantees the self-similarity of the load-displacement, stress-displacement, and ligament length-displacement curves for specimens having different ligament lengths.

Self-similarity of the load-displacement and ligament length-displacement plots is the first criterion to elucidate the validity of a tested specimen, helping to eliminate specimens with poor quality notches.

A careful observation of the frames stored by the DIC system showed that in the femtolaser sharpened specimens both notches propagated simultaneously; further, all the registered load-displacement and ligament length-displacement plots had self-similarity.

Instead, for the razor blade sharpened specimens, the DIC images revealed that in some specimens the two notches did not propagate simultaneously. This effect was attributed to differences between the two notches.

In other razor blade sharpened specimens, the load-displacement and ligament length-displacement graphs showed crossing curves (did not accomplish self-similarity) and were discarded.

The EWF parameters were obtained by performing a series of tests on the specimens with different ligament lengths and plotting the specific total work of fracture (w_f) (the area under the stress-displacement plot) as a function of their ligament lengths.

A regression analysis on this plot provided the specific essential work of fracture (w_e) as the intercept at zero ligament length, and the specific non-essential work of fracture (βw_p) as the slope of the linear regression line [1]. Figure 4.6 shows the EWF plots obtained for PET, PETG, and ECOZEN materials.

For the low tough polymers (PET, PETG, and ECOZEN) selecting razor blade sharpened specimens without plastic deformation at the notch tip, it leads to the same w_e values as for the femtolaser sharpened specimens.

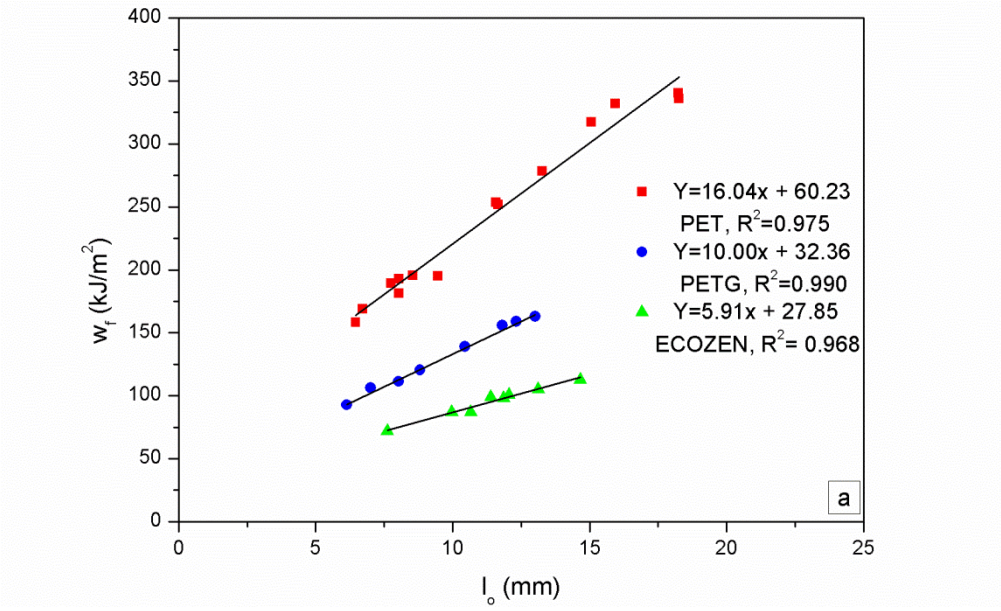

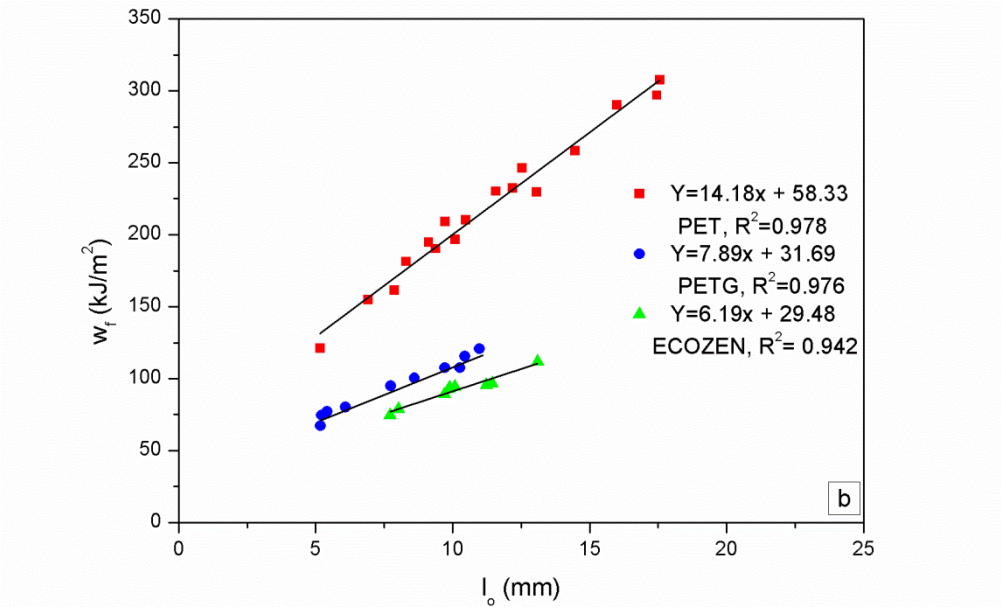

Figure 4.6 EWF plots for materials that undergo necking: a) Femtolaser, b) Razor blade

Instead, for the toughest polymers (EPBCs) where a small compressive component of the sideways sliding force induces a large plastic deformation ahead of the notch tip, it results in higher values of w_e compared with the femtolaser sharpened specimens. Figure 4.7 shows the EWF plots obtained for the EPBCs materials.

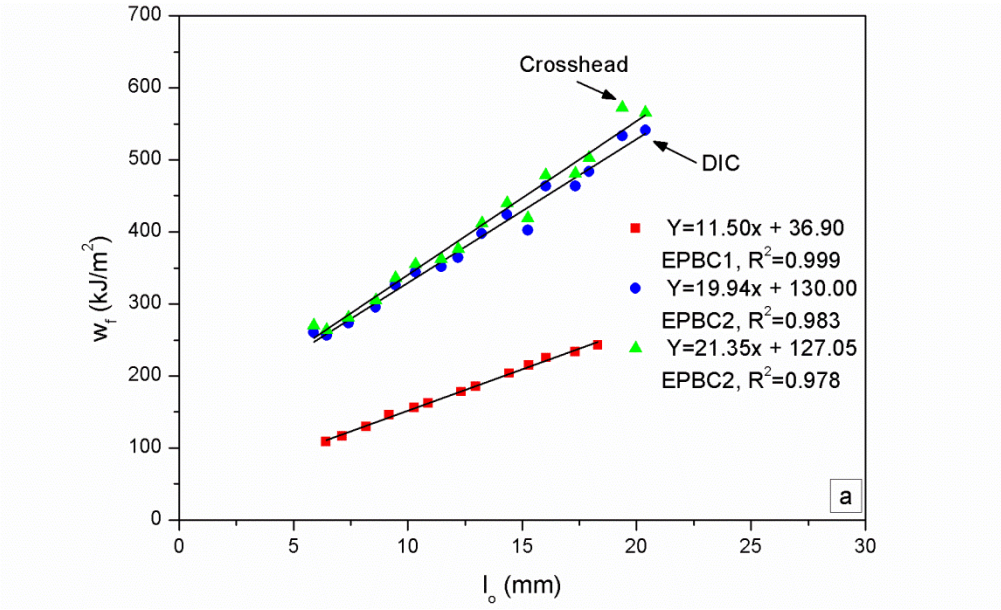

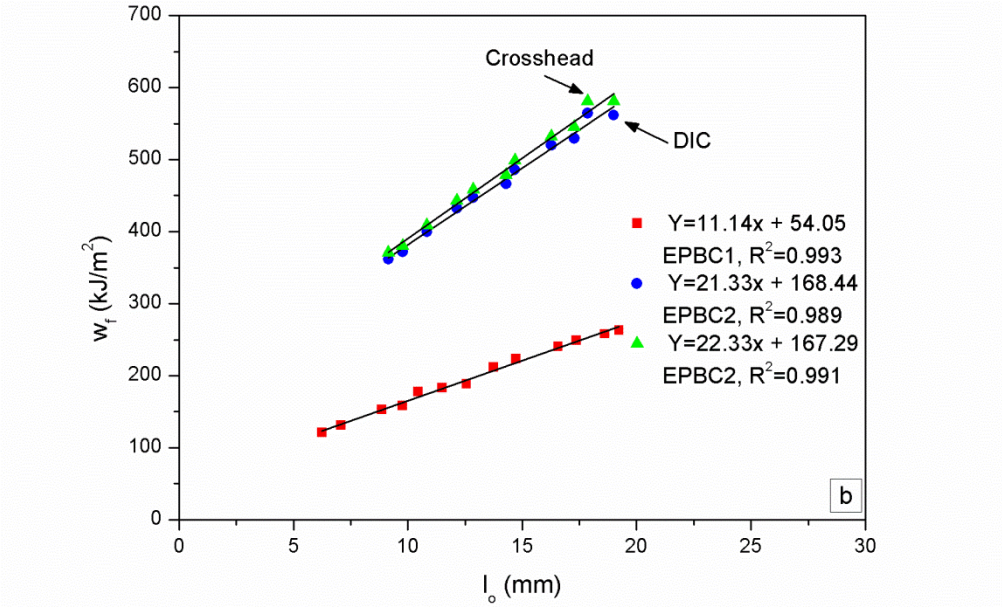

Figure 4.7 EWF plots for materials that deform via multiple shear yielding: a) Femtolaser, b) Razor blade

The EWF parameters obtained from the w_f – l_o plots for the femtolaser and razor blade sliding techniques using the DIC system (PET, PETG, ECOZEN, and EPBC2) and the video-extensometer (EPBC1) are presented in Table 4.3.

Table 4.3 Essential work of fracture parameters for all tested materials

Sharpening procedure	EWF parameters	PET	PETG	ECOZEN	EPBC1	EPBC2
Femtolaser	w_e (kJ/m^2)	60.23	32.36	27.85	36.90	130.00
	βw_p (MJ/m^3)	16.04	10.00	5.91	11.50	19.94
Razor blade	w_e (kJ/m^2)	58.33	31.69	29.48	54.05	168.44
	βw_p (MJ/m^3)	14.18	7.89	6.19	11.14	21.33

It can be concluded from Table 4.3 that for the polymers that undergo necking used in this work, PET possesses the highest resistance against crack initiation and crack propagation. The w_e value for the ECOZEN is slightly lower than the value of PETG, as can be expected, due to its chemical structure as a modified PETG.

In the case of the EPBCs, it has been proved that at similar ethylene content the fracture toughness increases with increasing the molecular weight [2,3]. The greater the molecular weight, the greater the entanglements [3]. Therefore, EPBC2 with greater molecular weight will have higher w_e and βw_p values than EPBC1.

For the EPBC2, the displacements were measured in two different forms: DIC system and testing machine cross-head. The w_e values as measured from both ways were practically coincident, but the slopes changed slightly (Table 4.4 and Figure 4.7). The same behavior has been previously observed [4,5].

Table 4.4 EWF parameters for the EPBC2 using the DIC system and cross-head displacement

Material	Notch sharpening procedure	EWF parameters			
		DIC system		Cross-head displacement	
		w_e	βw_p	w_e	βw_p
EPBC2	Femtolaser	130.00	19.94	127.05	21.35
	Razor blade	168.44	21.33	167.29	22.33

The DIC displacements were measured using as a reference two points located close to the initial sharpened notch, and such that OPZ was contained between the points. The distance between these reference points was taken to be constant for all specimens. In this way, the elastic and viscoelastic contributions due to the bulk polymer located outside OPZ were negligible. This explains the variations in the value of the slope when the displacements were measured using the DIC system or the testing machine cross-head.

A new plot was used to clarify the EWF analysis [5]. If the registered loads are divided by the area of their initial ligament and graphed in a single graph for each sharpening procedure, the stress-displacement plot is achieved. For all materials, a set of overlapping stress-displacement curves (heads) can be observed in the low displacement range up to a displacement value (d_i), from which the curves (tails) start to diverge. The hatched area accounts for w_e and the displacement at the end of this area is the crack initiation displacement (d_i). The stress corresponding to d_i is the crack initiation stress (σ_i). The average of the maximum stresses (σ_{max}) can also be identified.

Figure 4.8 shows the stress-displacement plots for the femtolaser sharpened specimens of two different materials.

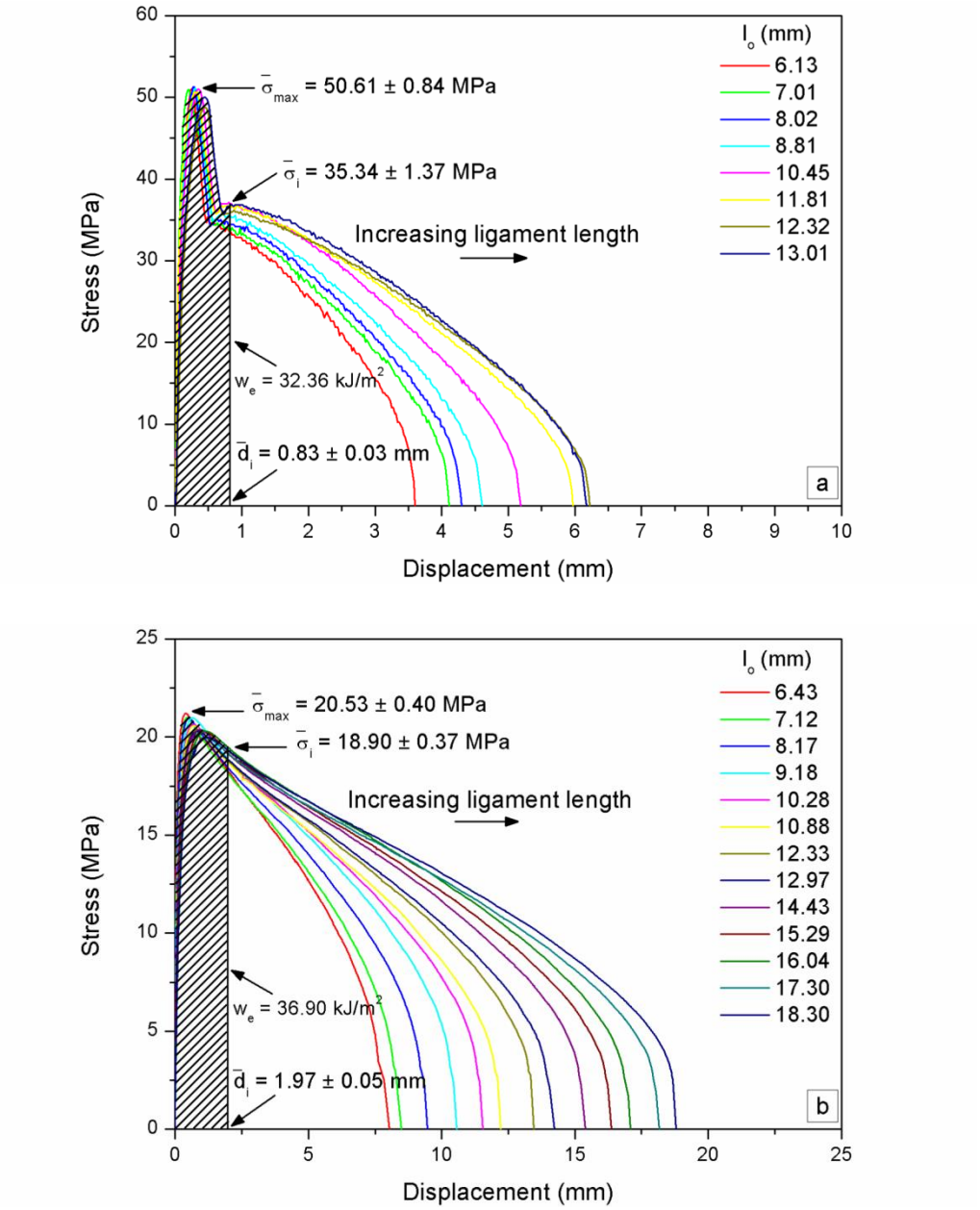

Figure 4.8 Stress-displacement plots for femtolaser sharpened specimens: a) PETG, b) EPBC1

It is important to clarify that the heads of the stress-displacement curves for the PET, PETG, and ECOZEN closely resemble those of the uniaxial tensile tests, including the stress drop characteristic of the necking before d_i. For the femtolaser and razor blade sharpened specimens, the σ_{max} values are comparable to σ_y (uniaxial tensile yield stress), and the σ_i values might be σ_{fs} (engineering flow stress) if the experimental variability is taking into account. In the EPBCs, no resemblance was found between the stress-strain curves from the tensile tests and the stress-displacement curves.

The parameters obtained from the overlapping stress-displacement curves are presented in Table 4.5 for all materials.

Table 4.5 Stress-displacement parameters for all tested materials

Sharpening procedure	Average parameters	PET	PETG	ECOZEN	EPBC1	EPBC2
Femtolaser	σ_{max} (MPa)	54.20±1.40	50.61±0.84	42.48±0.46	20.63±0.40	28.75±0.74
	σ_i (MPa)	35.56±1.89	35.34±1.37	34.82±1.18	18.90±0.37	25.89±0.46
	d_i (mm)	1.52±0.05	0.83±0.03	0.80±0.01	1.97±0.05	4.94±0.11
Razor blade	σ_{max} (MPa)	55.03±1.27	47.01±2.69	44.22±0.94	20.57±0.39	28.26±0.25
	σ_i (MPa)	35.96±1.89	31.45±0.83	35.69±0.68	18.82±0.26	25.35±0.15
	d_i (mm)	1.49±0.07	0.92±0.02	0.83±0.02	2.84±0.06	6.54±0.04

In all materials, for the entire sets of femtolaser sharpened specimens, the overlapping stress-displacement curves (heads) presented a unique population. Instead, differences were found in some materials for the razor blade sharpened specimens.

In the EPBC2, 16 razor blade sharpened specimens were tested. The stress-displacement plot with the overlapping curves showed 5 anomalous specimens (Figure 4.9a), four specimens corresponding to the shorter ligament lengths and the fifth one to the largest ligament length. The Clutton [1] and Hill [6] criteria were used to discard the 5 anomalous specimens. The work was entirely recalculated with the remaining 11 valid specimens (Figure 4.9b).

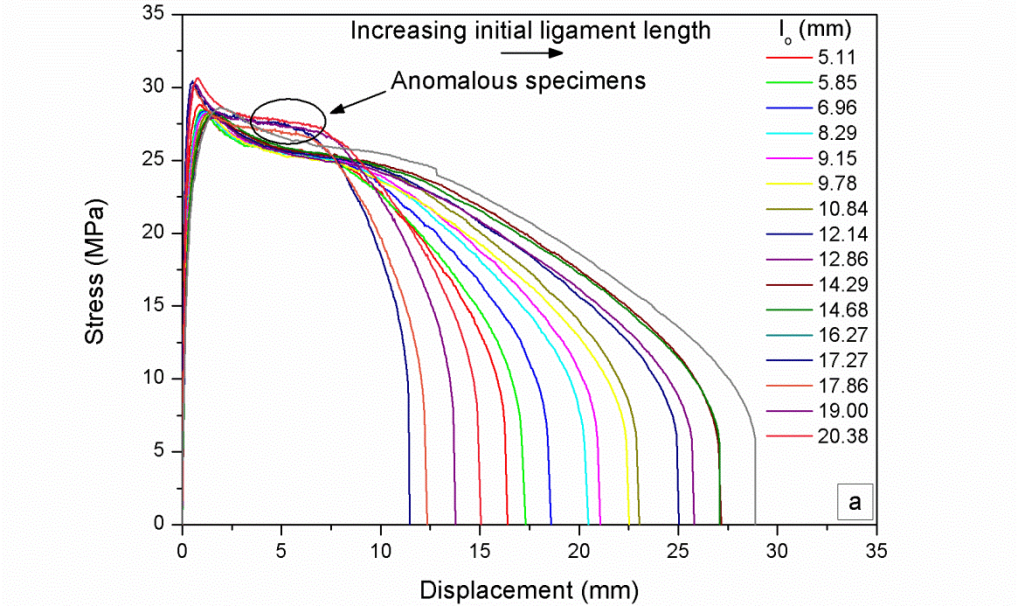

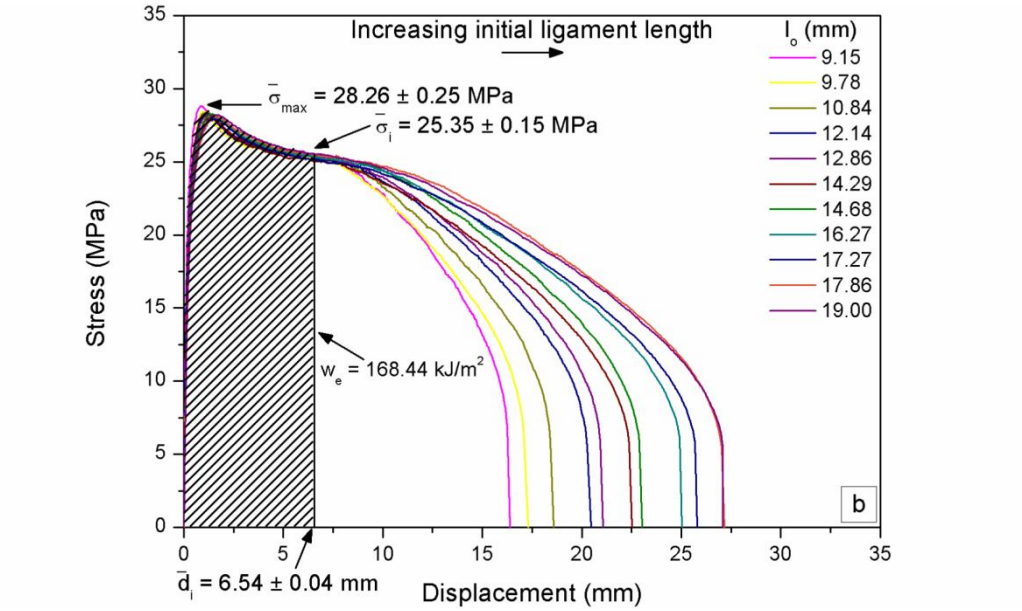

Figure 4.9 Stress-displacement plots for the EPBC2: a) Graph showing the anomalous specimens, b) Graph showing only the valid specimens

In the ECOZEN, 13 specimens were tested using the razor blade sliding technique as notch sharpening procedure. The stress-displacement plot revealed 2 different populations. In the first one (9 specimens), the heads overlapped, and d_i occurred after the necking of the ligament length. In the second one (4 specimens), the heads did not completely overlap, and d_i occurred before the complete necking of the ligament length, resulting in a large standard deviation for σ_i (Figure 4.10a).

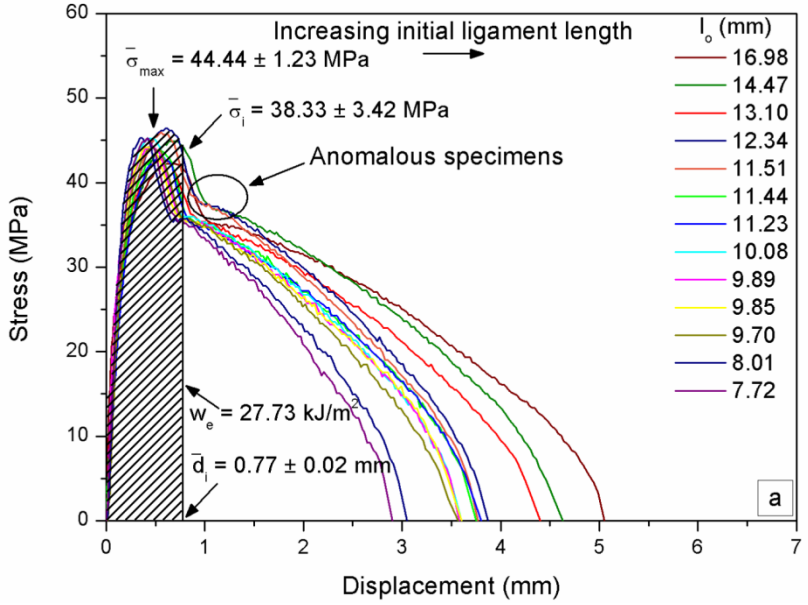

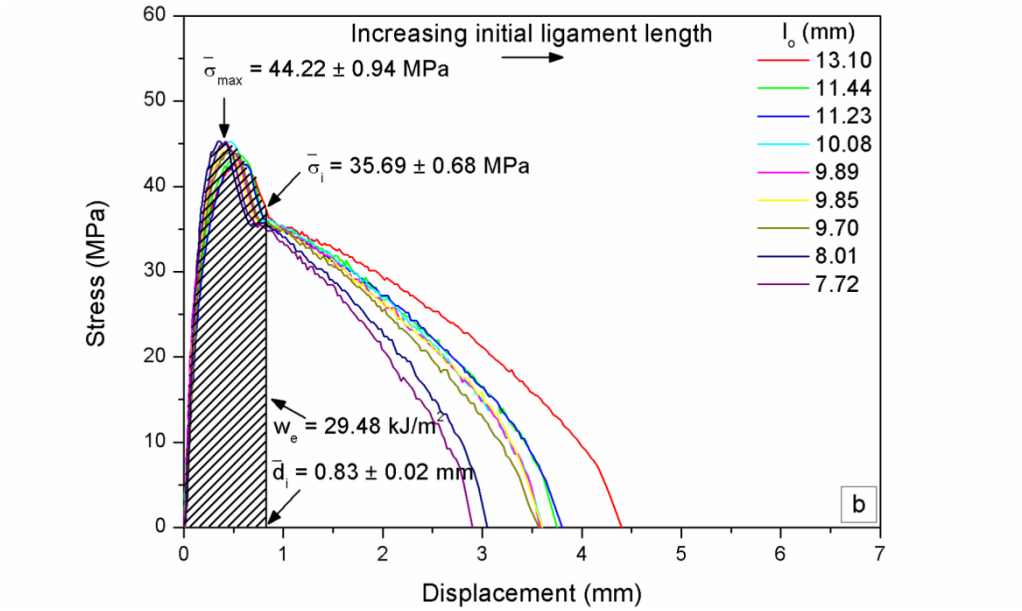

Figure 4.10 Stress-displacement plots for the ECOZEN: a) Graph showing the anomalous specimens, b) Graph showing only the valid specimens

These two sets of curves can be explained by differences between the two populations in the plastic deformation ahead of the notch tip. Once the population of the specimens with excessive plastic deformation was separated, the remaining 9 specimens were in a plane stress state, completely yielded, and necked before crack initiation (Figure 4.10b). The Hill and Clutton criteria were also satisfied.

Once w_e, σ_y, and E were obtained, the plastic zone radius ($2r_p$) was calculated for all materials.

In the PET, the specimens with initial ligament length greater than $2r_p$ were eliminated from the analysis for both notch sharpening procedures. In the EPBCs, all valid specimens were lower than $2r_p$ for both notch sharpening procedures.

In the PETG and ECOZEN, ligament lengths larger than the theoretical maximum ligament length obtained using the plastic zone radius equation were used. Although this equation is a reasonable size criterion, it appears to be too restrictive considering the evidence found in the DIC images and that indicated by the stress drop before d_i was reached, which indicates that for all valid specimens the ligament was fully yielded before the onset of crack initiation.

The alternative criterion for the upper ligament length [$l_o \leq (W/3)$] was satisfied with all the materials.

Hashemi and O'Brien [7] have shown that for plane stress DENT specimens there is a linear relationship between the displacement at rupture (d_r) and the initial ligament length (l_o). When d_r is

represented as a function of l_o, the intercept at zero ligament length represents the CTOD at crack initiation $CTOD_C$ (critical crack tip opening displacement).

Figure 4.11 shows the $d_r - l_o$ plots for the PET, PETG, and ECOZEN materials, while Figure 4.12 presents the $d_r - l_o$ plots for the EPBCs materials.

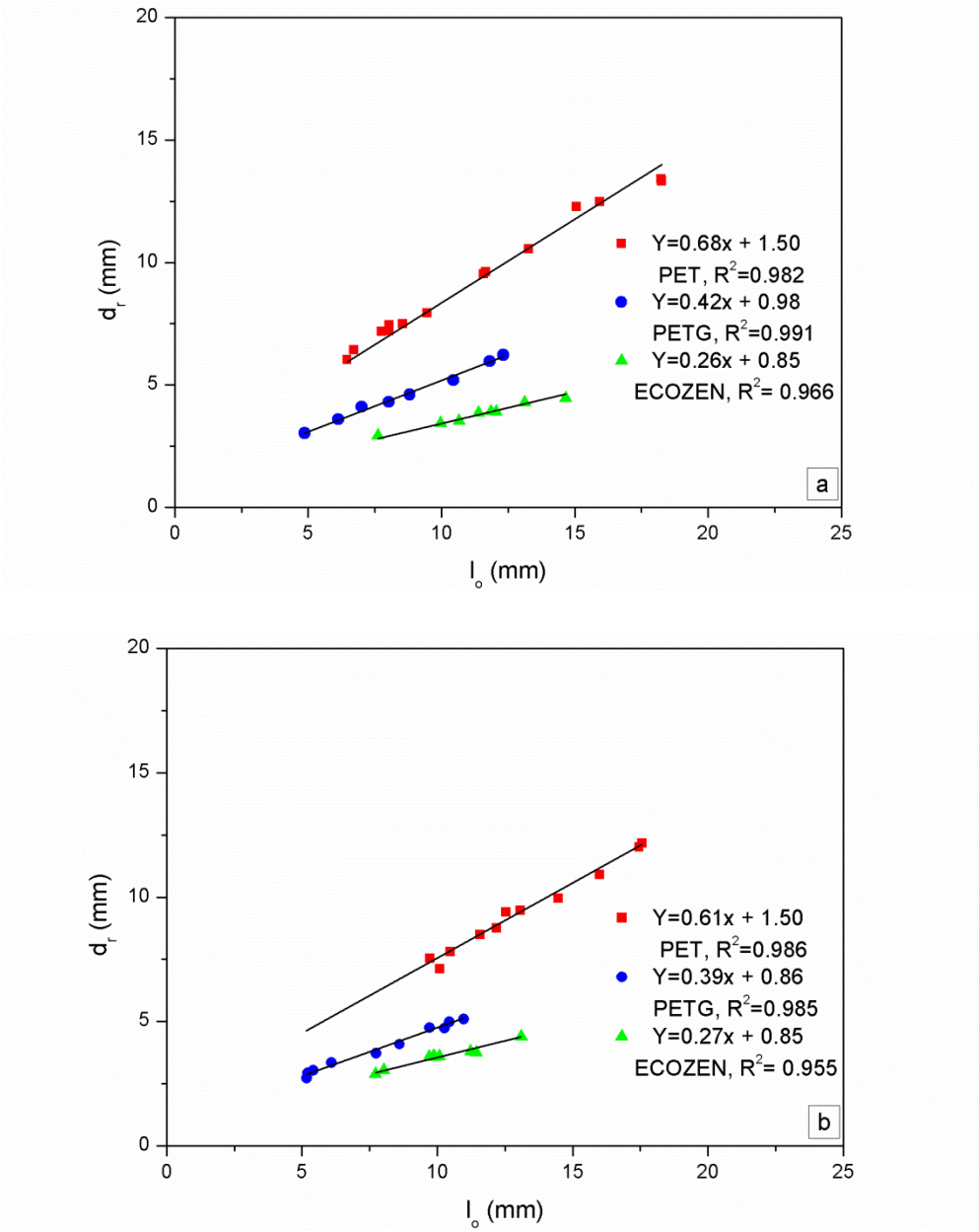

Figure 4.11 $d_r - l_o$ plots for materials that undergo necking: a) Femtolaser, b) Razor blade

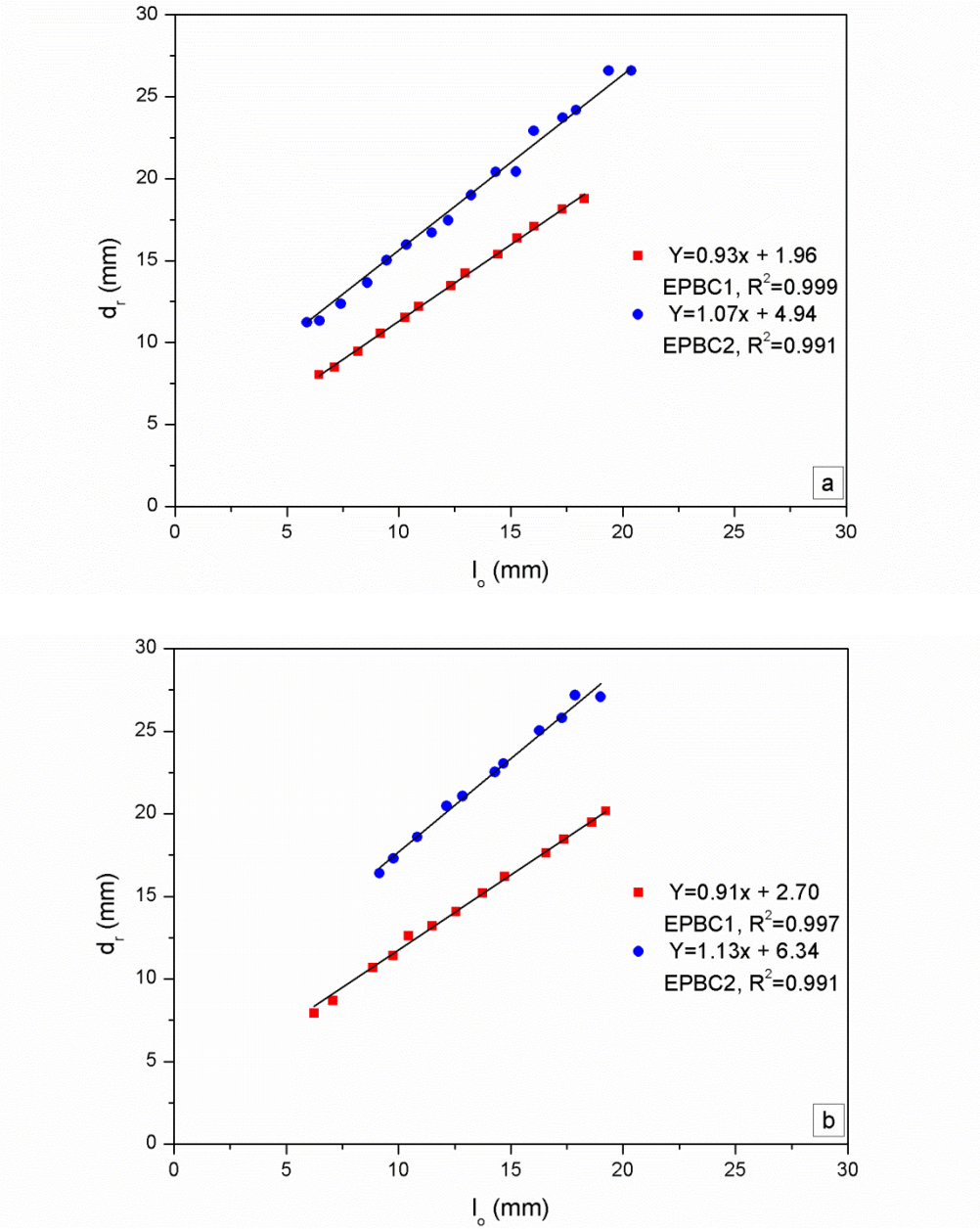

Figure 4.12 $d_r - l_o$ plots for materials that deform via the formation of multiple shear bands: a) Femtolaser, b) Razor blade

Table 4.6 shows the $CTOD_C$ values for all the materials tested. These values agree well with their corresponding d_i values as identified in the stress-displacement plots.

In the PET, PETG, and ECOZEN, the $CTOD_C$ values coincide for both notch sharpening procedures. However, this is not the case for the EPBCs. The reason for this lays in the larger plastic deformation at the crack tip for the razor blade sharpened specimens. This will be explained in detail later.

Table 4.6 $CTOD_C$ values for all tested materials

Sharpening procedure	$CTOD_C$ (mm)				
	PET	PETG	ECOZEN	EPBC1	EPBC2
Femtolaser	1.50	0.98	0.85	1.96	4.94
Razor blade	1.50	0.86	0.85	2.70	6.34

The sequence of events leading to the fracture of a DENT specimen encompasses the opening and blunting of the notch tip with the yielding and necking of the ligament area (heads), followed by crack initiation and propagation until complete fracture (tails). This fracture process is represented in Figure 4.13, where l_i is the ligament length at d_i, l is the measured ligament length during the test, and Δa_b is the crack length increment due to blunting.

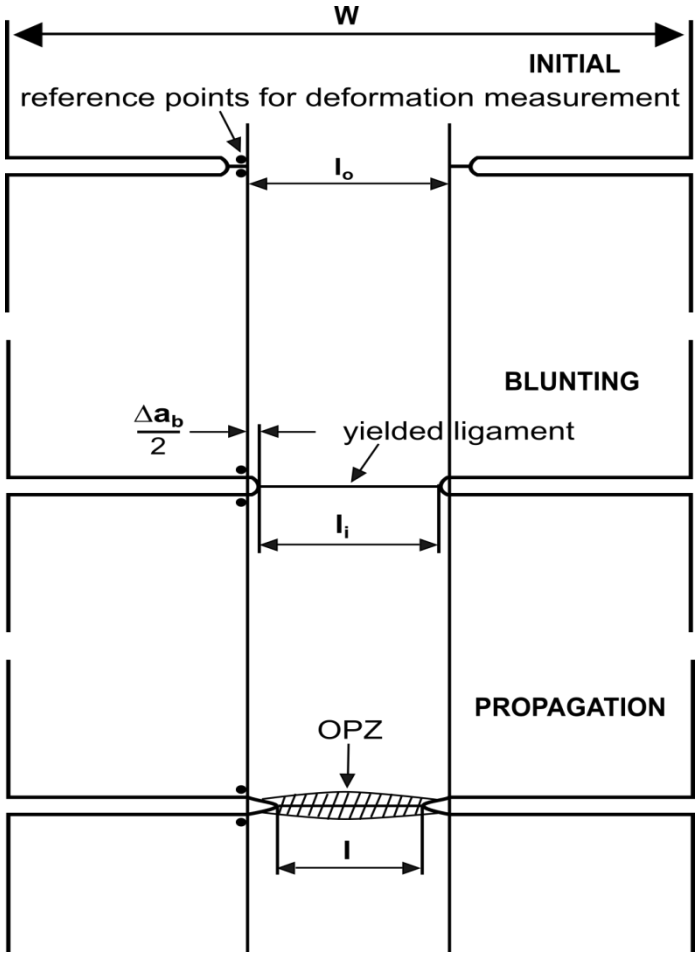

Figure 4.13 Schematic DENT test evolution

When l_i is represented as a function of l_o, a linear dependence between the two variables exists. Δa_b is the intercept at zero ligament length on this plot. Figures 4.14 and 4.15 show the $l_i - l_o$ plots, and Table 4.7 contains the Δa_b values for all the materials tested.

Even following a careful observation of the frames stored by the DIC system, we were not able to distinguish the exact frame, in which blunting finishes and crack initiation begins, but the DIC images indicated that prior to d_i there is no crack propagation and afterwards, the crack growth has already begun.

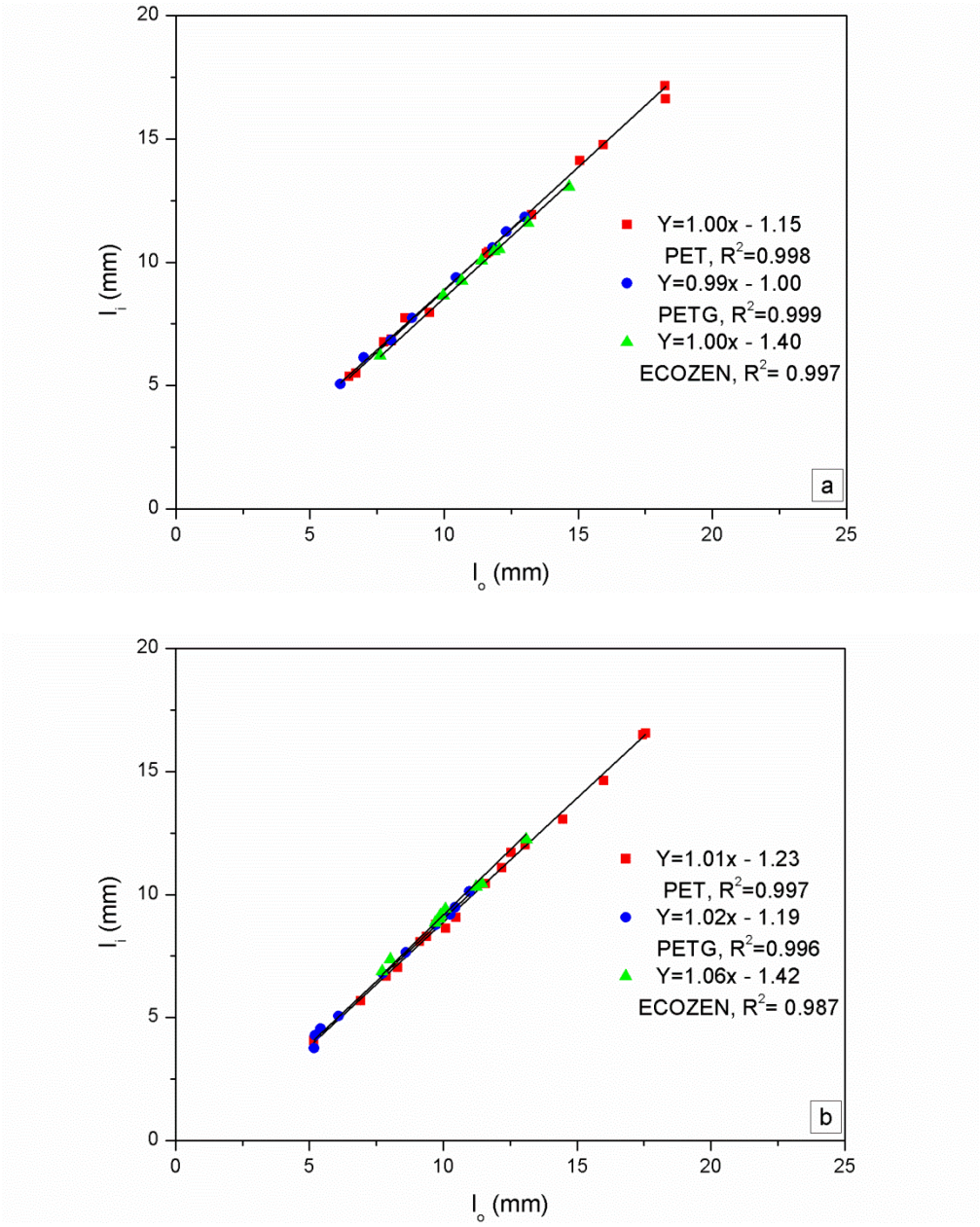

Figure 4.14 $l_i - l_o$ relationship for materials that undergo necking: a) Femtolaser, b) Razor blade

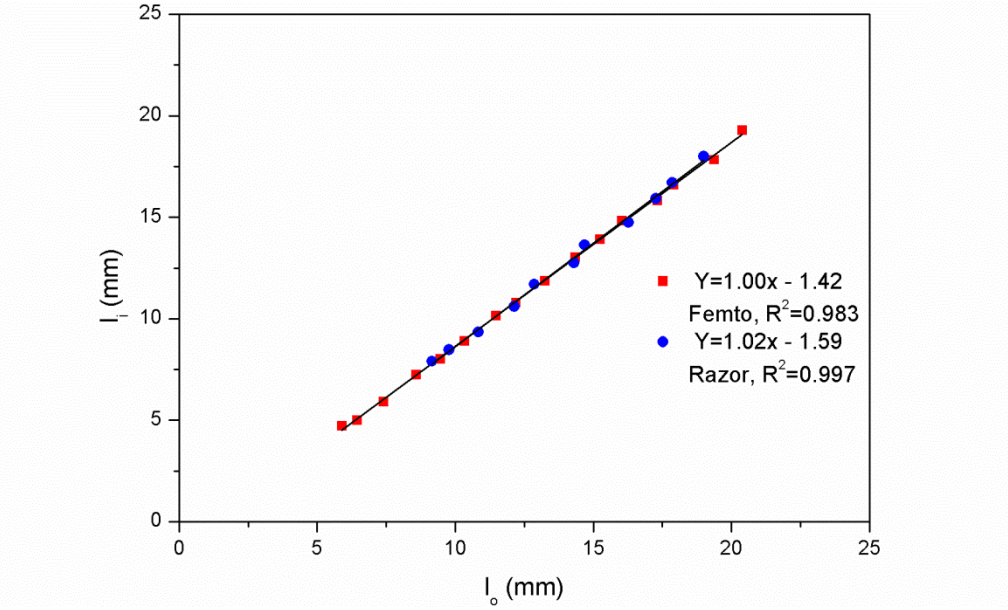

Figure 4.15 l_i – l_o relationship in the EPBC2 specimens

Table 4.7 Crack tip blunting values for all tested materials

Sharpening procedure	Δa_b (mm)				
	PET	PETG	ECOZEN	EPBC1	EPBC2
Femtolaser	1.15	1.00	1.40	----	1.42
Razor blade	1.23	1.19	1.42	----	1.59

4.4.1 Propagation range analysis.

In our work, two new plots that help to separate non-valid specimens were introduced. Specifically, the normalized crack growth-displacement and the load-crack length were plotted. The normalized crack growth-displacement plot was obtained for the EPBC2 and ECOZEN materials, while the load-crack length plot was obtained for the PET, PETG, ECOZEN, and EPBC2 materials.

To ensure that the fracture mechanism is the same irrespective of the ligament length, the specimens must show a common and steady fracture phenomenology during crack growth. In the ligament length-displacement plot, the crack growth is comprised between $CTOD_C$ and d_r values. This crack growth range can be normalized using the Δa_b and $CTOD_C$ values. The normalized crack growth-displacement plot was helpful to discard specimens showed variations in the propagation region.

For the EPBC2 (femtolaser), specimens that did not overlap in the normalized crack growth-displacement plot had to be separated and the entire work recalculated (2 of 16 specimens were discarded) (Figure 4.16a). In the case of the razor blade sharpened specimens, this plot (Figure 4.16b) revealed the same 5 anomalous specimens that the stress-displacement plot (Figure 4.9a). The work was entirely recalculated with the remaining 11 valid specimens.

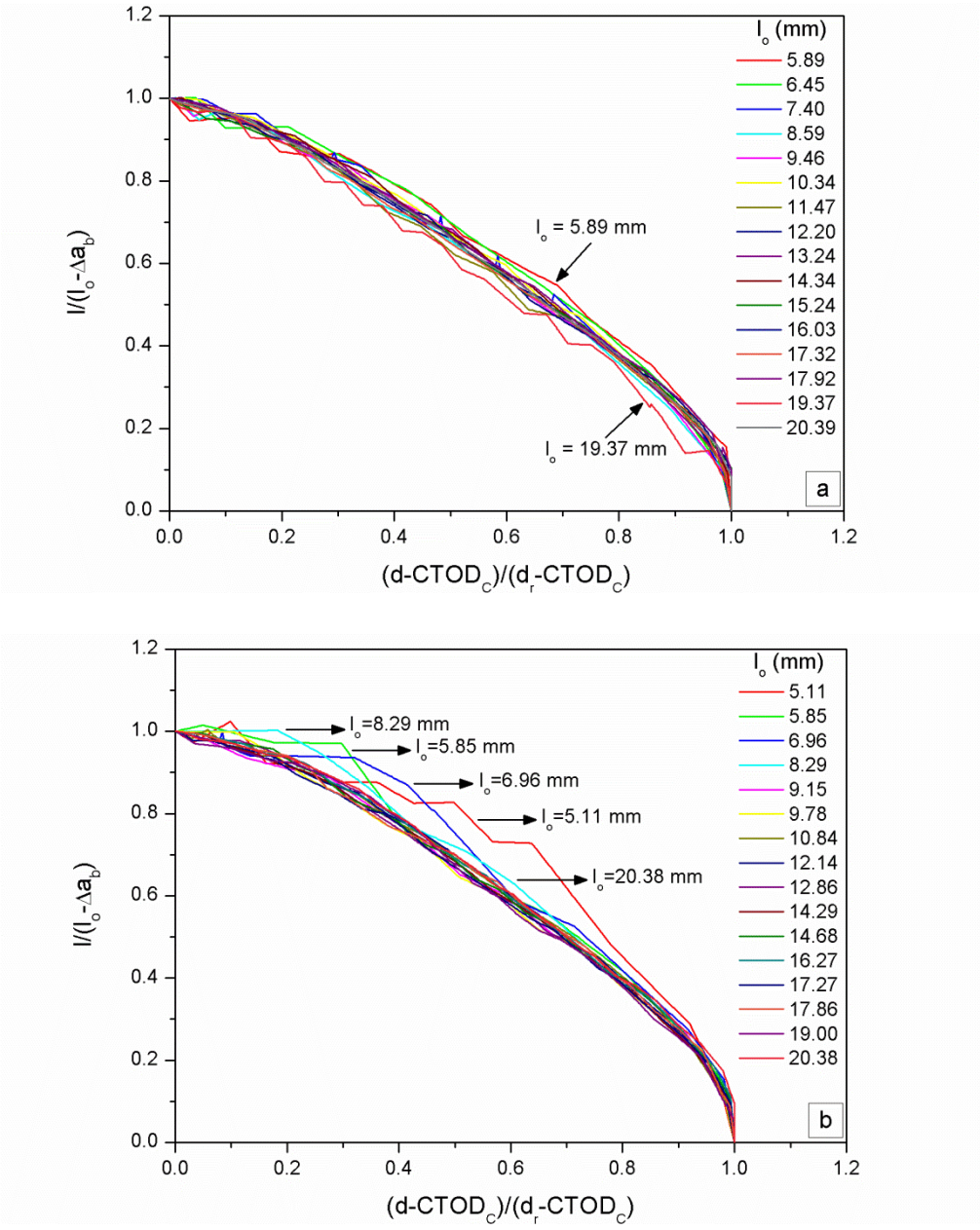

Figure 4.16 Normalization of crack growth for the EPBC2 specimens: a) Femtolaser, b) Razor blade

In the ECOZEN, a single graph of the normalized crack growth-displacement curves was done for both notch sharpening methods, a complete overlap of the curves was observed for all specimens,

indicating the same propagation behavior, which is independent of the initial ligament length (Figure 4.17).

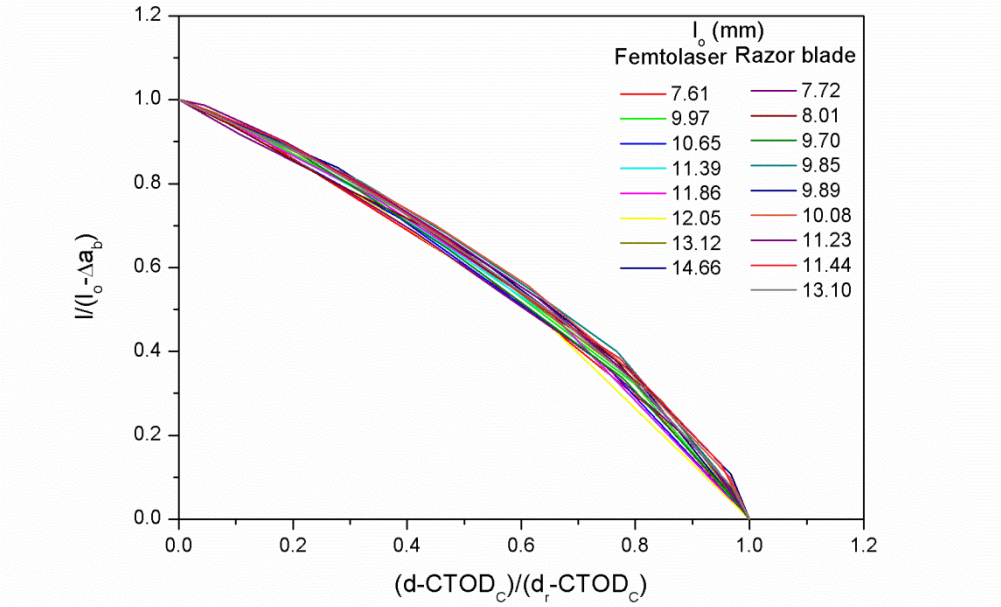

Figure 4.17 Normalized propagation curves for the ECOZEN specimens

For each material used in this work, if a single graph of the normalized crack growth-displacement curves is made for both notching techniques, the normalized crack growth range will overlap well enough considering the experimental variability, confirming that both sets of specimens present the same propagation behavior. These normalized crack growth-displacement plots are helpful to reject those specimens with different quality notches.

During the crack propagation, when the registered load (P) is represented as a function of the crack length (a), a straight line with slope $-t\sigma_i$ should be found. The linear dependence indicates that all propagations follow the same trend except at higher values, near the complete specimen rupture, where the slope increases, probably due to orientation hardening. As an example, Figure 4.18 presents the load-crack length plots for the PET material.

For the EPBC2 femtolaser specimens, when P is represented as a function of a (Figure 4.19a), 2 curves were deviated from the others that were directly related to the 2 previously discarded specimens in the normalized crack growth-displacement plot. In the case of the razor blade sharpened specimens (Figure 4.19b), 5 curves were deviated from the others, which correspond to the 5 specimens that were discarded in the stress-displacement and normalized crack growth-displacement plots.

In the PET, PETG, and ECOZEN, the load-crack length curves overlapped for each notch sharpening procedure.

Table 4.8 shows the σ_i values as found in the load-crack length plots, which match with the σ_i values of the stress-displacement plots for both notch sharpening procedures.

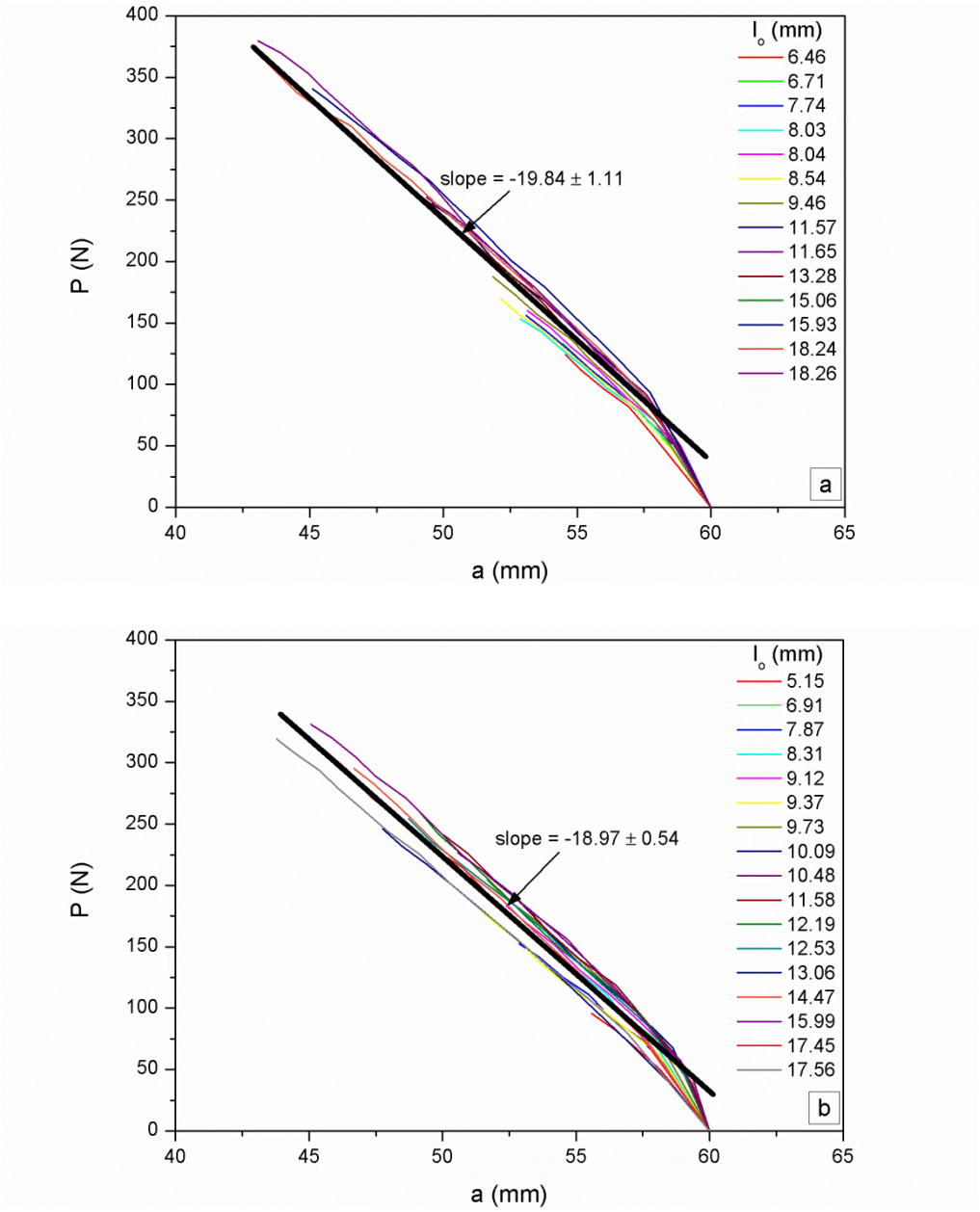

Figure 4.18 Tails of load versus crack length for PET specimens: a) Femtolaser, b) Razor blade

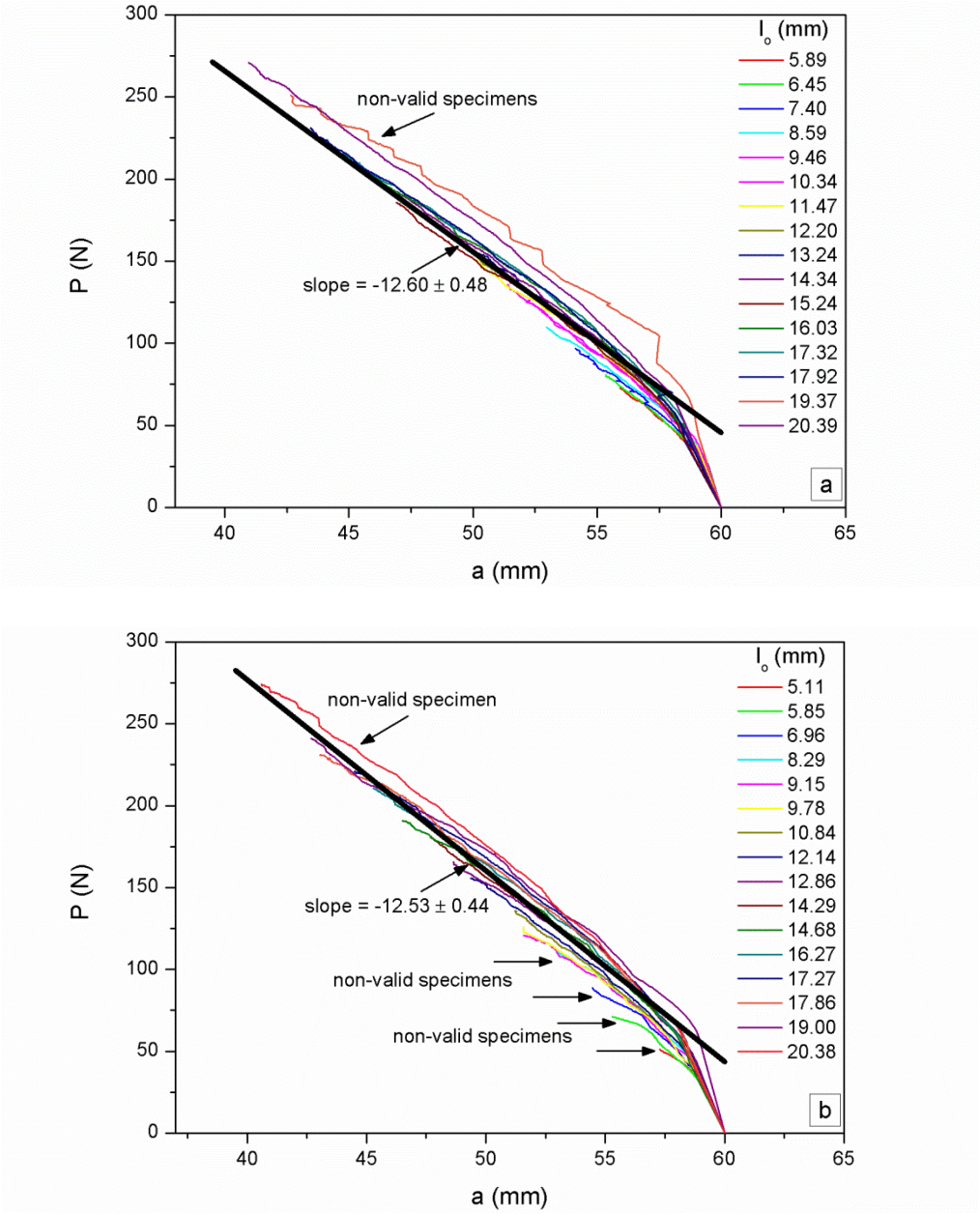

Figure 4.19 Load versus crack length for EPBC2 specimens: a) Femtolaser, b) Razor blade

Table 4.8 Slope value in the load-crack length graphs

Sharpening procedure	σ_i (MPa)				
	PET	PETG	ECOZEN	EPBC1	EPBC2
Femtolaser	39.68±2.22	36.98±1.44	34.37±1.50	---	25.20±0.96
Razor blade	37.94±1.08	32.16±1.10	35.18±2.15	---	25.06±0.88

4.4.2 w_e as inherent material parameter

The load-displacement, stress-displacement, and ligament length-displacement plots together with a careful observation of the frames stored by the DIC system and the analysis of the crack growth range via the normalized crack growth-displacement and load-crack length plots were used to eliminate specimens that do not satisfy the EWF key requirements.

In the PET, PETG, and ECOZEN, for both notch sharpening procedures, once the non-valid specimens were discarded, the key assumptions of the EWF analysis were thoroughly satisfied, including very sharp notches without plastic deformation, specimens in a plane state of stress and ligaments completely yielded before the onset of crack initiation. As such, w_e was considered as an inherent material property.

In the EPBCs, the specimens sharpened by femtolaser had fully yielded ligaments prior to the onset of crack initiation, sharpened notches with a radius of curvature of 1 μm and without plastic deformation ahead of the crack tip. The fracture was under plane stress conditions as well. Thus, w_e represented an inherent material parameter.

In the case of the EPBC razor blade sharpened specimens, the valid specimens satisfied the plastic zone radius and the alternative upper ligament length criterion, then two of the key requirements were fulfilled, i.e., the ligament lengths were completely yielded prior to the onset of crack initiation and fracture was under plane stress conditions.

However, in spite of the repetitive sharp notches, these specimens had plastic deformation ahead of the crack tip, and therefore the third requirement (good quality notches) is not accomplished. Thus, w_e is not an inherent material property, that is, it is a fracture toughness value useful only for comparison purposes. The relationships between w_e, J_{IC}, $CTOD_C$ and σ_i were completely fulfilled. These values depend on the notch quality, and their relationships were maintained.

4.5 J analysis

The Begley and Landes method [8] was used to determine the J-values. This method requires two steps.

The first step consists of the graphical representation of the energy (the area the under the load-displacement curve) divided by the specimen thickness as a function of the crack length when the displacement is fixed. In the resultant plot, the points belonging to the same displacement show linearity and can be fitted by a straight line. The slope of this regression line is –J. Figure 4.20 shows two of these plots for two different materials and the same notch sharpening procedure.

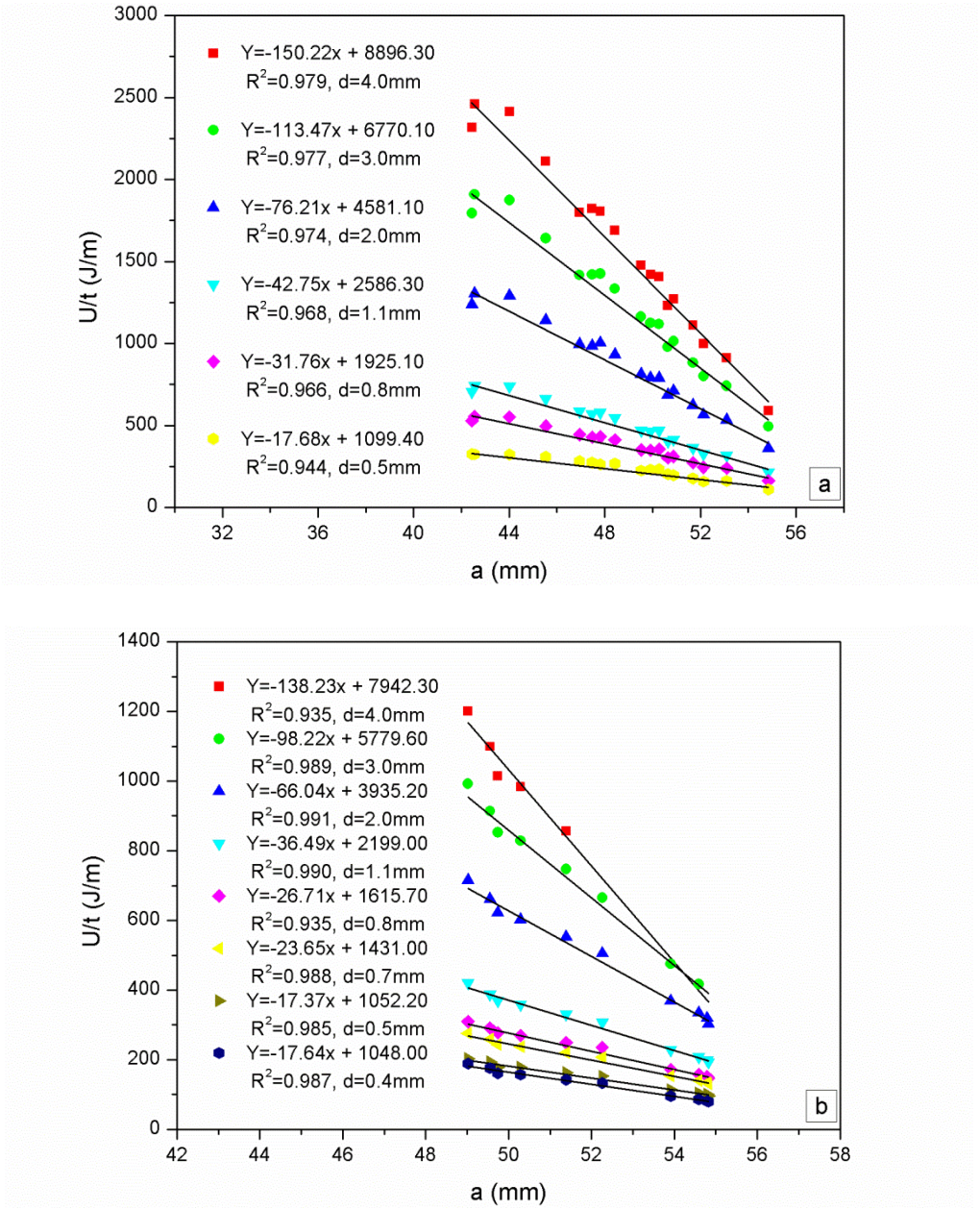

Figure 4.20 Input energy divided by thickness versus crack length for razor blade sharpened specimens: a) PET, b) PETG

The second step consists of plotting the J-values found in the U/t – a plot as a function of the displacement (J-plot). The points on this plot were adjusted by a regression line where the slope was equal to σ_i [9], which agreed reasonably well with the σ_i values as found in the stress-displacement plots.

Figure 4.21 depicts the J-plots corresponding to the same materials of Figure 4.20, and Table 4.9 presents the σ_i values as obtained in the J-plots.

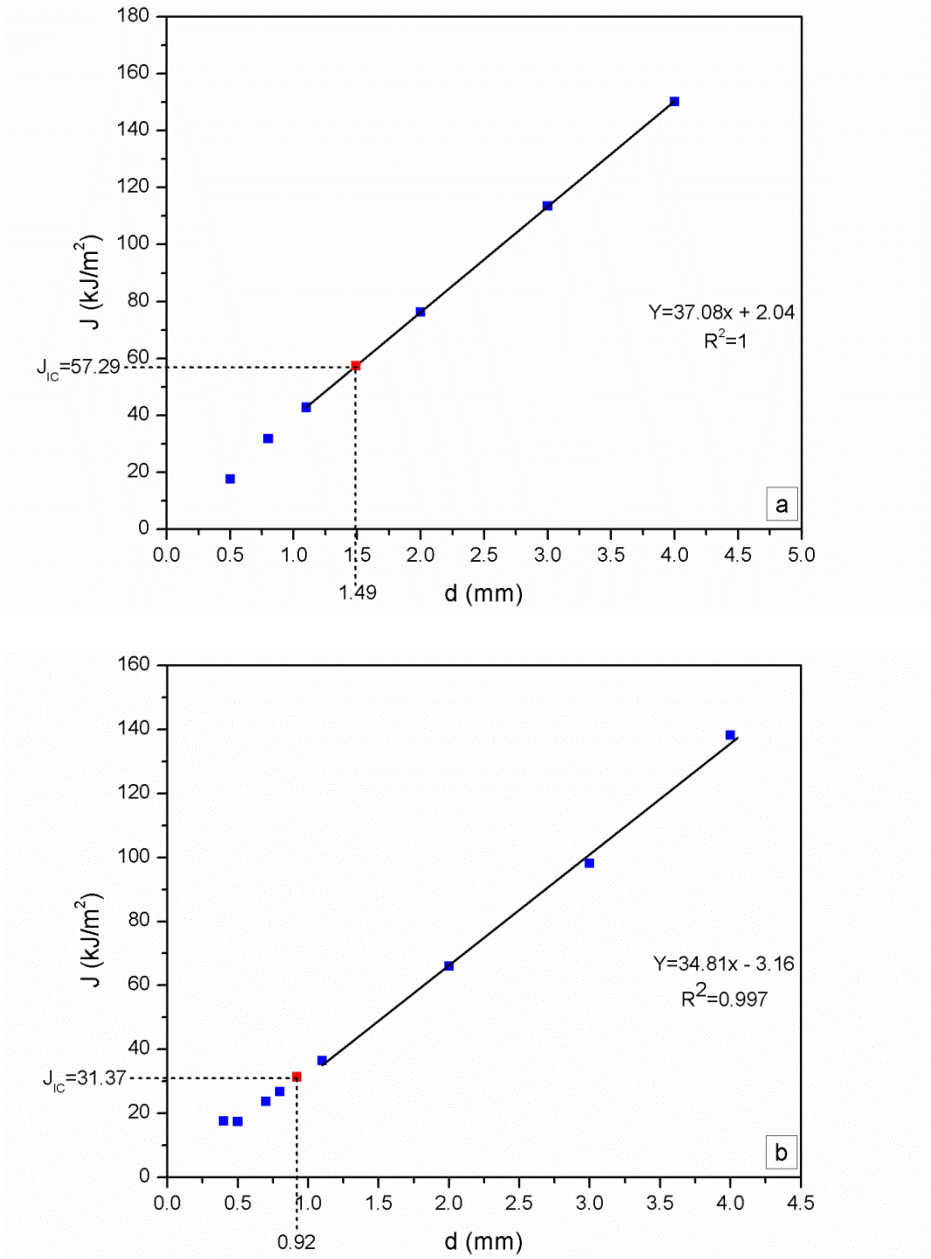

Figure 4.21 J-plots for razor blade sharpened specimens: a) PET, b) PETG

Table 4.9 Slope value in the J-plots

Sharpening procedure	σ_i (MPa)				
	PET	PETG	ECOZEN	EPBC1	EPBC2
Femtolaser	39.30	36.71	38.97	---	22.76
Razor blade	37.08	34.81	38.98	---	22.04

The J integral value at crack initiation (J_{IC}) is obtained by introducing the $CTOD_C$ value in the J-plot (Figure 4.21). This provided a value J_{IC} that matched well with w_e. Table 4.10 shows the J_{IC} values for all materials and both notch sharpening procedures.

Table 4.10 J integral values at crack initiation

Sharpening procedure	J_{IC} (kJ/m^2)				
	PET	PETG	ECOZEN	EPBC1	EPBC2
Femtolaser	63.15	29.13	28.00	---	126.49
Razor blade	57.29	31.37	29.64	---	166.01

There is a unique relationship between J_{IC} and $CTOD_C$. For a non-hardening material in plane stress, assuming that the stress in the plastic zone is σ_i [10], then

$$J_{IC} = \sigma_i . CTOD_C = w_e \qquad \text{Eq. (4.1)}$$

This last relationship is entirely fulfilled in our experimental results. In all cases, $w_e = J_{IC}$.

4.6 Femtolaser versus razor blade

All of the femtolaser sharpened notches had very consistent, sharp notches without plastic deformation in front of the notch tip and non-crossing stress-displacement (tails) curves. The ligament length-displacement curves also had self-similarity.

The razor blade sharpened notches had very sharp cracks, as sharp as the femtolaser ones, but the different compressive component of the sliding force that is applied by the operator generated three different levels of plastic deformation ahead of the notch tip. There were specimens with negligible plastic deformation ahead of the notch tip, similar to the femtolaser specimens, which gave equal results to the femtolaser. In other specimens, notches of the same specimen, but with different levels of plastic deformation caused non-simultaneous crack propagation and, in consequence, these specimens had to be discarded. Finally, specimens, where the two edge notches had the same high level of plastic deformation ahead of the notch tip, caused that the shapes of the stress-displacement curves were different when compared to specimens with no plastic deformation. These specimens had also to be discarded.

In polymer films less ductile than EPBC, as can be PET, PETG, and ECOZEN, it had been possible to generate notches with and without plastic deformation in front of the notch root using the razor blade sliding technique. Once specimens containing plastic deformation were discarded, the fracture parameters were coincident with those obtained in femtolaser specimens.

The non-destructive inspection of the notches in an optical light microscope can be helpful before testing in order to eliminate specimens with different levels of plastic deformation ahead of the notch tip.

For the EPBC (1 and 2) and the ECOZEN materials, the registered stress-displacement curves from two equal initial ligament lengths specimens, one sharpened by femtolaser and the other by razor blade were chosen to be analyzed.

It can be seen that the stress-displacement curves for the same ligament length but different notch sharpening procedure (femtolaser and razor blade) overlapped in the range comprised between the displacements d = 0 and the displacement corresponding to σ_{max} ($d_{\sigma max}$). The difference between both curves occurred in the range comprised between the displacement corresponding to σ_{max} and the displacement at the onset of crack initiation (d_i), where the razor blade specimen had a larger distance and larger d_i and Δa_b values. In spite of this, σ_i was the same for both notch sharpening procedures (Figure 4.22a).

The stress-displacement curves were also shifted along the displacement axis so that the rupture displacements coincided. Doing so, the d_i values fell in the same place, and the tails overlapped. With such representation, it can be deduced that the crack growth and the propagation energy are the same for both notch sharpening methods, and then the slope βw_p of the EWF plot would have the same value for both sets of specimens (Figure 4.22b).

If there is a set of specimens with the same notch tip radius, but has some specimens with, and others without plastic deformation ahead of the notch tip, then, after testing, all specimens would have the same σ_{max} and σ_i but different d_i. This results in crossing curves in the load-displacement and ligament length-displacement plots. The same behavior is expected if the set contains specimens that have different extents of plastic deformation.

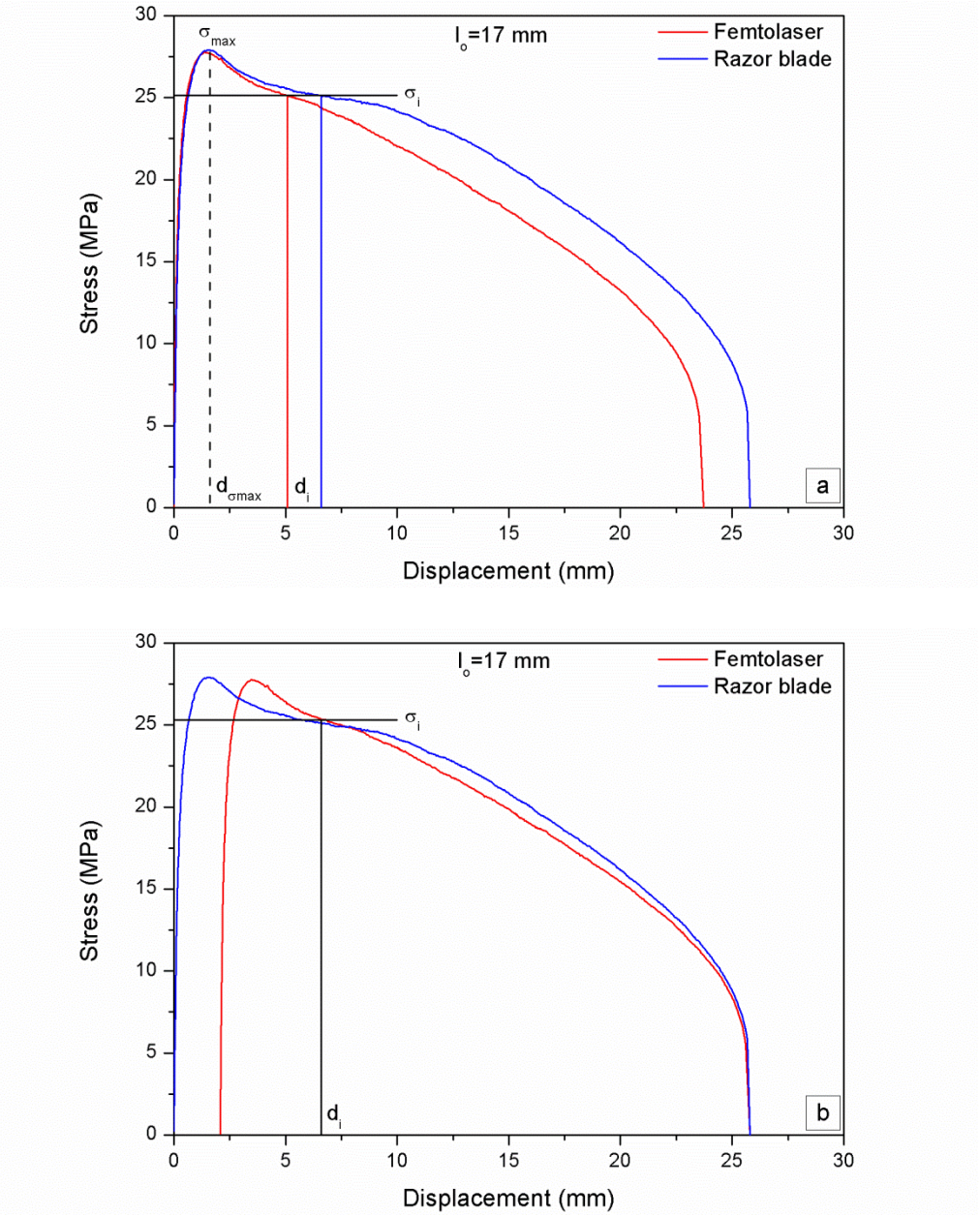

Figure 4.22 Femtolaser and razor blade specimens comparisons: a) Stress-displacement curve, b) Stress-displacement curve shifted to displacement at rupture

4.7 Shape of the stress-displacement curves

From the analysis of the femtolaser and razor blade sharpened specimens, it is clear that the shape of the stress-displacement curves is influenced by the plastic deformation ahead of the notch tip. In this case, the main differences between both sets are the larger Δa_b and rupture displacement (d_r) values for the razor blade sharpened specimens, resulting in a higher w_e value but the same βw_p. The equivalence of the slopes of the EWF plots is a consequence of identical crack propagation behavior, which is independent of the plastic deformation in front of the notch root.

The shape and size of the stress-displacement curves obtained from specimens that were notched in different ways allow analyzing their EWF behavior when they are compared with the femtolaser and razor blade sharpened specimens.

In order to investigate this influence, specimens that have the same ligament length but different kinds of sharpened notches were prepared. This analysis was performed on the EPBC (1 and 2) specimens.

In the EPBC1 specimens, the notch sharpening procedures included: pre-notches forming saw cut slots (S), pre-notches forming saw cut slots that were deformed plastically (SD), pre-notches frozen by liquid nitrogen and after sharpened by sliding a fresh razor blade across the pre-notch tip (SGN), and pre-notches that were made with a scalpel and after sharpened by sliding a fresh razor blade on the notch root (BG). In addition, femtolaser (SF) and razor blade sharpened specimens (SG) were also used in the analysis.

A stress-displacement plot corresponding to the six different types of notches were made (Figure 4.23). It was observed that once the crack initiation point was reached, all curves (tails) overlapped. As expected, these curves had the same propagation behavior and thus the same βw_p values.

All curves had equal values of σ_{max} and $d_{\sigma max}$. The visual assessment of σ_i also provided equal values for all curves, but differences in their corresponding displacement d_i were found. For all notch sharpening procedures, the main difference was in the distance between the displacements corresponding to the σ_i and σ_{max} values, that is, d_i - $d_{\sigma max}$. The larger distance between these displacements was originated by the larger d_i ($CTOD_C$) values. These differences increased with the radius of curvature and/or with the extent of plastic deformation in front of the notch tip, which resulted in higher w_e values.

The same results were found for the EPBC2, but, in this case, were only compared pre-notches frozen by liquid nitrogen and after sharpened with a razor blade, femtolaser sharpened specimens, and razor blade sharpened specimens.

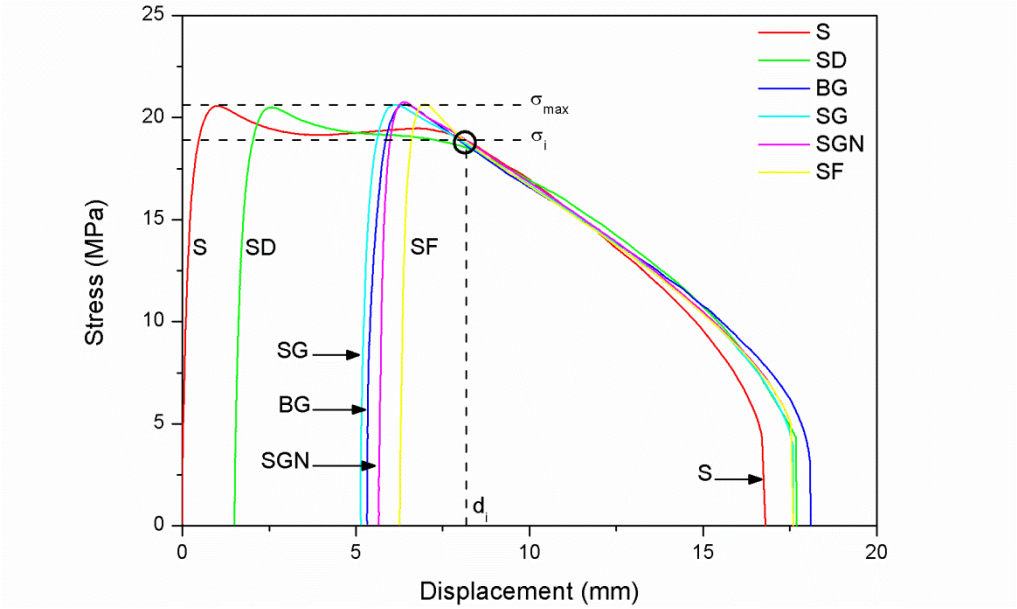

Figure 4.23 Notch sharpening comparison performed on the EPBC1 specimens

The effect on the shape of the stress-displacement curves of specimens with non-collinear notches was studied in the EPBCs. For do this, a specimen sharpened by razor blade sliding where the two edge notches were not collinear (they had 1 mm separation) was compared with a razor blade sharpened specimen with collinear notches.

The non-collinearity of the two edge notches can modify the stress distribution, and the results will be likely influenced.

In the EPBC1, the stress-displacement curves showed equal σ_{max} and σ_i values for both collinear and non-collinear specimens, but, in the specimen with non-collinear notches, the curve was shifted to the right, which implies a larger d_i and thus higher w_e value (Figure 4.24a).

In the EPBC2, the stress-displacement curves had approximately equal σ_{max} values and overlapped between d = 0 and d = d_i and also had equal σ_i values, which implied equal w_e values. However, the curve of the specimen with non-collinear notches had a larger d_i, causing that the tails of both curves did not overlap. This caused that the area under the curve between d_i and d_r was greater leading to a higher βw_p value for the specimen with non-collinear notches (Figure 4.24b).

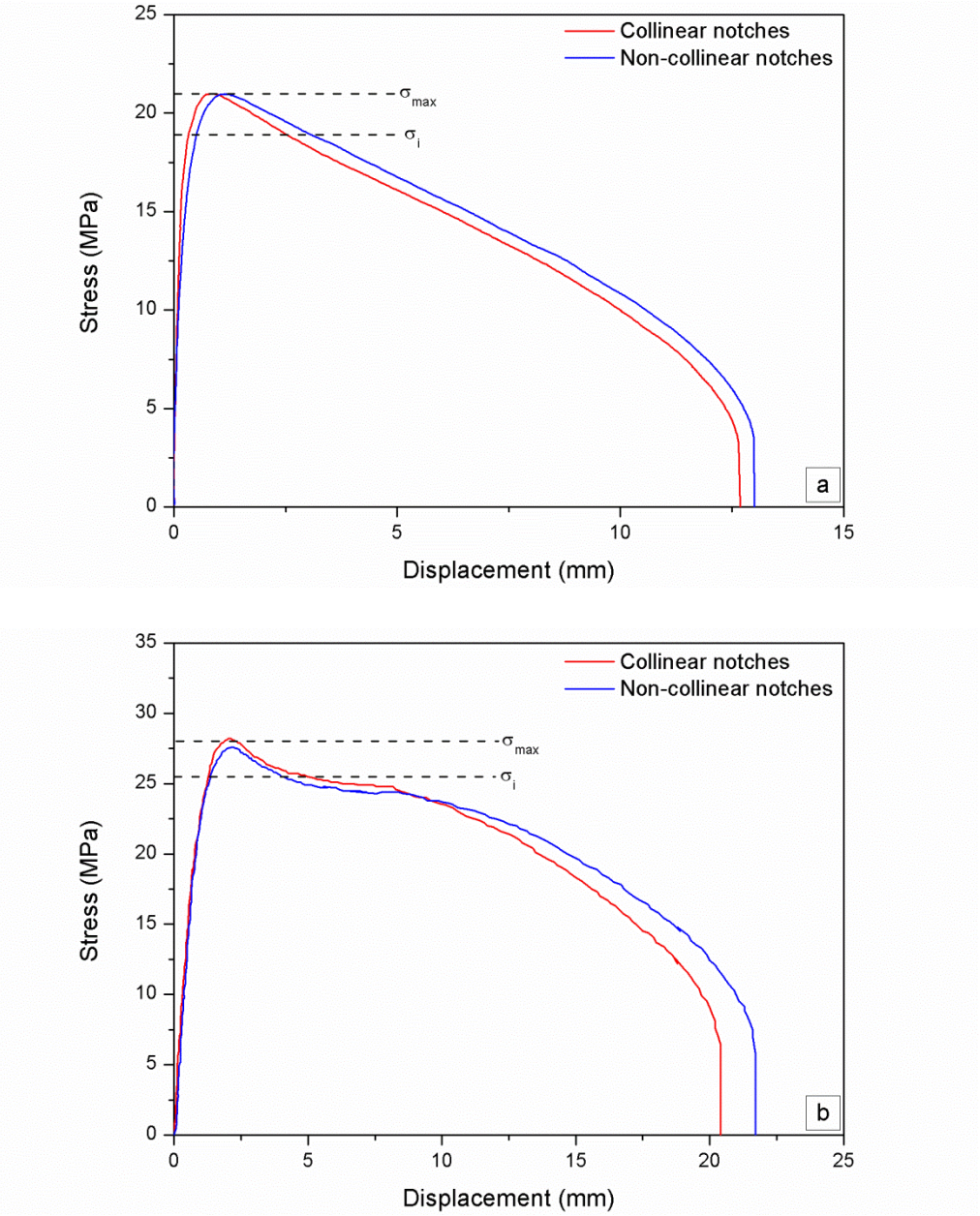

Figure 4.24 Effect of the non-collinearity of the two edge notches on the shape and size of the stress-displacement curves: a) EPBC1, b) EPBC2

The specimens have to be tested with the direction of tension perpendicular to the collinear notches. That is, the specimens must be properly mounted on the grips of the testing machine. If the specimens are tilted when they are mounted on the grips, then the collinear notches are not oriented perpendicularly to the direction of tension, and so the stress distribution in the ligament is modified.

A razor blade sharpened specimen tilted by 5° on the grips was tested and after compared with a razor blade sharpened specimen that was correctly mounted on the grips (Figure 4.25).

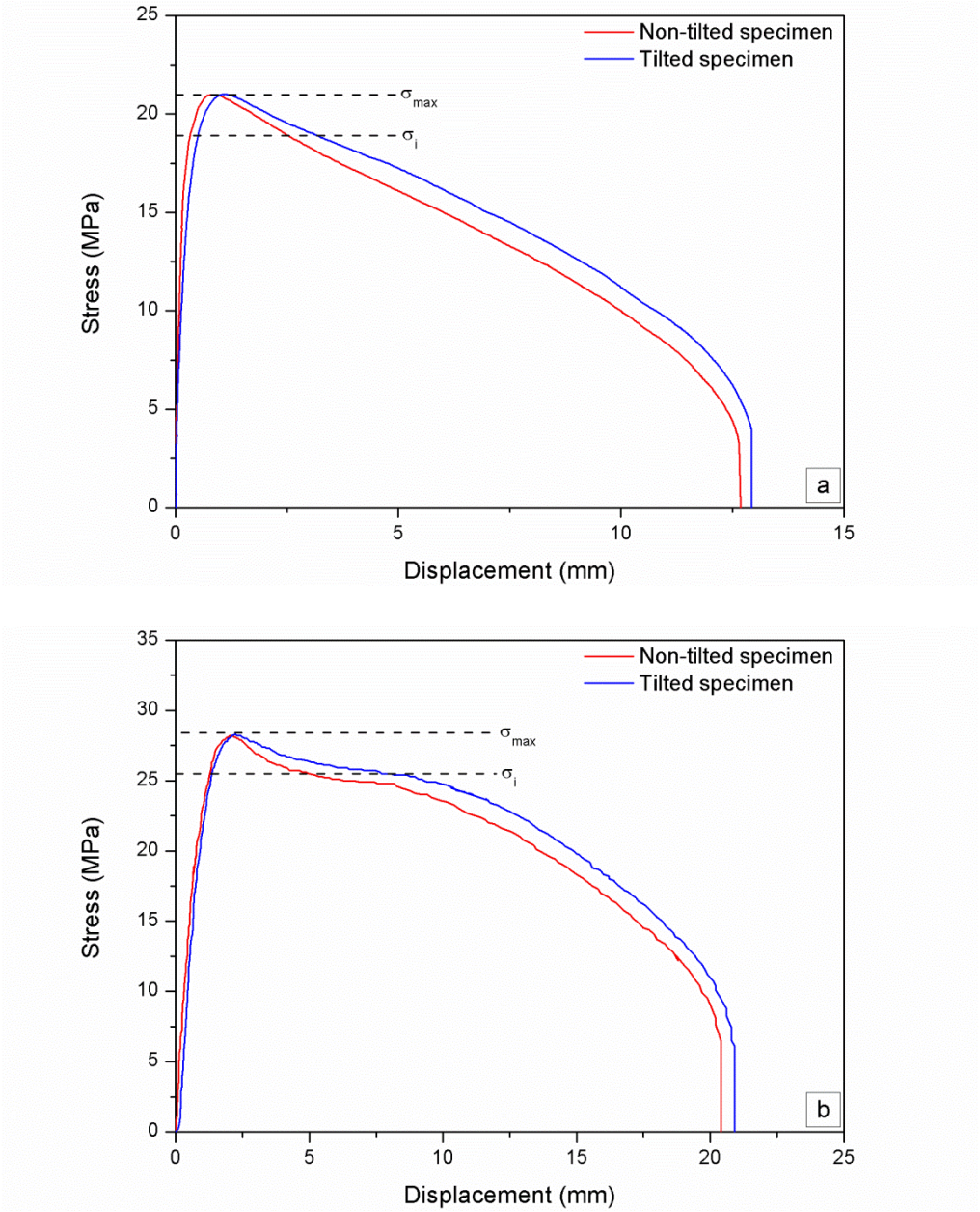

Figure 4.25 Effect of the specimen alignment on the shape and size of the stress-displacement curves: a) EPBC1, b) EPBC2

For both EPBCs, the stress-displacement curves overlapped well enough only up to σ_{max}. After this point, the curve of the tilted specimen was greater and had larger d_r than the non-tilted specimen. Considering that both the tilted and non-tilted specimens had the same σ_i, a higher w_e value can be found for the tilted specimen.

4.8 Analysis of the propagation range (tails) for the stress-displacement curves

The stress-displacement curves allow the partition into "head" or initiation and "tail" or crack propagation [5]. The shape of the "tail" can be approximated to be a half of a parabola, described by σ_i in the y-direction and (d_r – d_i) in the x-direction. Thus, the energy absorbed during the crack propagation per ligament section (U_p) can be estimated as:

$$U_p \cong \frac{\sigma_i.(d_r - d_i).2}{3} \quad \text{Eq. (4.2)}$$

The value of d_i ($CTOD_C$) can be obtained from either the stress-displacement plots or from the slope of the d_r – l_o plots. In our work, the following equation is generally used to obtain $CTOD_C$ [11]

$$d_r = CTOD_C + \alpha l_o \quad \text{Eq. (4.3)}$$

where α is the extension ratio at rupture.

Combining Eqs. (4.2) and (4.3), it can be found that

$$U_p \cong \frac{\sigma_i.\alpha.l_o.2}{3} \quad \text{Eq. (4.4)}$$

As w_e remains constant during crack propagation, the propagation energy per ligament length is a constant value and independent of the notch sharpening method. Then, considering the essential term w_e as the initiation energy, the propagation energy per ligament section is $W_p/(l_o.t)$, giving the equivalence:

$$U_p = \beta.w_p.l_o \quad \text{Eq. (4.5)}$$

Substituting Eq. (4.5) into Eq. (4.4) it provides

$$\beta.w_p \cong \frac{\sigma_i.\alpha.2}{3} \quad \text{Eq. (4.6)}$$

The parabola equation is given by

$$d = d_r + s\sigma^2 \quad \text{Eq. (4.7)}$$

where

$$s = \frac{d_i - d_r}{{\sigma_i}^2} \quad \text{Eq. (4.8)}$$

In a previous work, the stress-displacement curves in the propagation range were roughly approximated to be a quarter of an ellipse, which resulted in

$$\beta . w_p \cong \frac{\sigma_i . \alpha . \pi}{4} \qquad \text{Eq. (4.9)}$$

The βw_p values obtained through the slope of the EWF plot and the semi-parabola and the quarter ellipse approximations are presented in Table 4.11 along with the σ_i and α values for all materials studied in this thesis work.

It must be considered that the ellipse approach overestimates the area of the tails, thus giving higher βw_p values than the obtained by the slope of the EWF plot. However, the parabola approach fits well with the experimental βw_p values for all the materials, indicating a parabolic shape for the tails of the experimentally measured stress-displacement curves.

Table 4.11 Assessment of the plastic term

Material	Parameters		βw_p (MJ/m^3)		
	σ_i (MPa)	α	Slope EWF plot	Parabolic shape	Elliptical shape
PET	35.56	0.66	16.04	15.64	18.42
PETG	35.34	0.42	10.00	9.89	11.66
EPBC1	18.90	0.93	11.50	11.72	13.80
EPBC2	25.89	1.07	19.94	18.47	21.76
ECOZEN	34.82	0.26	5.93	6.03	7.11

In Figure 4.26, the modeled parabola (dashed line) together with its corresponding stress-displacement curve for a valid ECOZEN femtolaser sharpened specimen is represented. Here, it is observed that the parabolic shape fits well with the experimental stress-displacement curve in the propagation range.

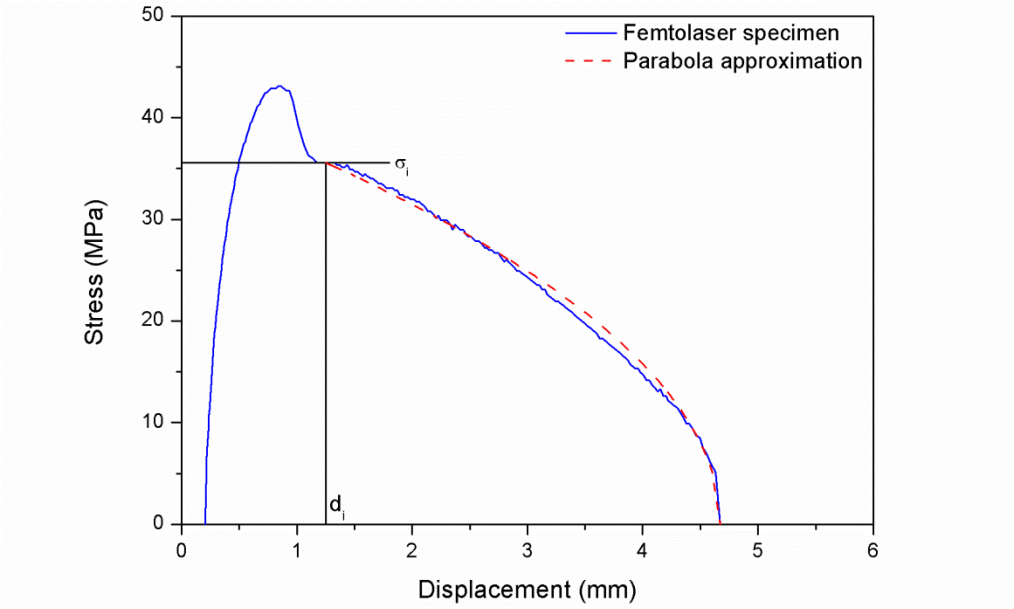

Figure 4.26 Graphical representation of a modeled parabola for an ECOZEN femtolaser specimen

4.9 References

[1] Clutton E. Essential work of fracture. In: Moore DR, Pavan A, Williams JG, editors. Fracture mechanics testing methods for polymers, adhesives and composites. Oxford: Elsevier Science, Ltd.; 2001, p. 177-195.

[2] Martínez AB, Arencón D, Rodríguez J, Salazar A. Influence of the notch sharpening on the impact fracture toughness of ethylene-propylene block copolymers. Polymer Testing 2014; 36: 75-81.

[3] Salazar A, Martín T, Navarro JM, Rodríguez J. Fracture behaviour of controlled-rheology ethylene-propylene block copolymers. Polymer International 2011; 60: 765-771.

[4] Martínez AB, Segovia A, Gamez-Perez J, Maspoch ML. Influence of femtolaser notch sharpening technique in the determination of essential work of fracture (EWF) parameters. Engineering Fracture Mechanics 2009; 76: 1247-1254.

[5] Martínez AB, Segovia A, Gamez-Perez J, Maspoch ML. Essential work of fracture analysis of the tearing of a ductile polymer film. Engineering Fracture Mechanics 2010; 77: 2654-2661.

[6] Hill R. On discontinuous plastic states, with special reference to localized necking in thin sheets. Journal of Mechanics and Physics of Solids 1952; 1: 19-30.

[7] Hashemi S, O'Brien D. The essential work of plane – stress ductile fracture of poly (ether – ether ketone) thermoplastic. Journal of Materials Science 1993; 28: 3977-3982.

[8] Begley JA, Landes JD. The J integral as a fracture criterion. In: Fracture toughness, ASTM STP 514, American Society for Testing and Materials. Philadelphia; 1972, p. 1-20.

[9] Hodgkinson JM, Williams JG. J and G_C analysis of the tearing of a highly ductile polymer. Journal of Materials Science 1981; 16: 50-56.

[10] Martínez AB, León N, Arencón D, Sánchez-Soto M. Essential work of fracture, crack tip opening displacement, and J-integral relationship for a ductile polymer film 2016; 55: 247-256.

[11] Mai YW, Powell P. Essential work of fracture and j-integral measurements for ductile polymers. Journal of Polymer Science part B: Polymer Physics 1991; 29: 785-793.

Chapter 5

Conclusions and future research lines

5.1 Conclusions

As polymers films are being increasingly used in engineering applications, their fracture toughness characterization becomes a basic requirement. In this sense, the present research study conducts a deep analysis of the appropriate approaches to characterize the ductile fracture behavior of thin polymer films.

The EWF approach has been successfully applied to all materials selected for this research study, including three materials that neck before the onset of crack initiation (PET, PETG, and ECOZEN) and two different grades of a rubber-toughened semicrystalline polymer (EPBC) that deform via multiple shear yielding.

w_e was verified an inherent material parameter and equal to J_{IC} under plane stress conditions. New methods were developed to discard specimens with poor notch quality. The parabolic shape in the propagation range of the stress-displacement curve (tail) was defined.

The general conclusions of this thesis work can be summarized as follows:

Notch sharpening procedure

The femtosecond pulsed laser ablation technique generates highly consistent, sharp notches, without plastic deformation in the region surrounding the crack tip. This sharpening technique is the most appropriate to sharpen notches of ductile polymer films, giving the lowest values for the fracture parameters.

The razor blade sliding technique can generate notches with different quality, which depends on the operator, the material ductility, and the compressive component of the sideways sliding force that is applied.

It is confirmed that a key requirement to obtain valid results is to have consistent notches without plastic deformation surrounding the crack tip. The notch tip radius has a strong influence on the fracture parameters as well.

EWF parameters

Three key assumptions must be satisfied for w_e to be an inherent material parameter: completely yielded ligament prior to the onset of crack initiation, plane stress conditions for the fracture process, and good quality notches.

The w_e, J_{IC}, and $CTOD_C$ values obtained from specimens with plastic deformation at the crack tip, being the only key assumption not accomplished, satisfy the relationships among w_e, $CTOD_C$, J_{IC}, and σ_i, but these values are not inherent properties of the material.

In DENT specimens, the crack growth and the propagation energy do not depend on the plastic deformation ahead of the crack tip. Thus, equal values for the slope of the EWF plot (βw_p) would be expected for both notch sharpening methods (femtolaser and razor blade).

Essential work of fracture, J-integral, and crack tip opening displacement relationships

The use of the DIC system has allowed the successful application of the EWF, J-integral and CTOD methods on a unique set of specimens.

It has been proved that the specific essential work of fracture (w_e) is the energy per unit ligament surface just up to crack initiation and has the same conceptual meaning and quantitative value that the J-integral at crack initiation (J_{IC}) when the crack initiates and propagates in a fully yielded ligament under plane stress conditions. The relationship of w_e and J_{IC} with the crack tip opening displacement at the onset of crack initiation ($CTOD_C$) was also confirmed.

The displacement at crack initiation (d_i) as found in the new stress-displacement plot coincides with the crack tip opening displacement at crack initiation $CTOD_C$.

Notch quality

In polymer films, the dispersion in the w_e, J_{IC}, and $CTOD_C$ values obtained in the same laboratory and especially between laboratories can be attributed to differences in the quality of the notches that can be generated by different operators. This is especially significant when the notch sharpening is performed using the razor blade sliding technique.

When the razor blade sliding is used as notch sharpening technique, three different kinds of specimens can be obtained. Specifically, Specimens with sharp notches and without plastic deformation ahead of the crack tip, specimens where the two notches have different levels of plastic deformation, and specimens with high, equal levels of plastic deformation ahead of the crack tip for both notches can be manufactured.

Razor blade sharpened specimens with sharp notches and without plastic deformation ahead of the notch tip yield fracture parameters equal to the femtolaser sharpened specimens. In razor blade sharpened specimens where the two notches have different levels of plastic deformation, the crack initiation does not happen at the same time. Specimens with high, equal levels of plastic deformation ahead of both notches provide higher w_e values than the femtolaser sharpened specimens and stress-displacement curves with different shapes and sizes.

The stress-displacement, ligament length-displacement, normalized crack growth-displacement, and load-crack length plots were used to eliminate specimens with poor notch quality.

Shape of the stress-displacement curves

The shape of the stress-displacement curves depends on the notch quality. Consistent notches have the same σ_{max}, σ_i, d_i, $CTOD_C$ and Δa_b values. In this case, the normalized curves in the propagation region overlap. Non-overlapping curves belong to specimens with different quality notches and can be discarded.

If there is a set of specimens with the same notch tip radius, but has some specimens with and others without plastic deformation ahead of the notch tip, after testing all specimens would have the same σ_{max} and σ_i, but the range comprised between (d_i - $d_{\sigma max}$) will be different, resulting in higher w_e values for the specimens with plastic deformation in front of the notch tip.

Non-collinear notches and misalignment of the specimens on the grips affect the stress-displacement curves and the results. Small differences of less than 1 mm in the collinearity of the notches can be unintentionally generated during the specimen manufacture and have a small effect on the results. More care is necessary when mounting the specimens on the grips because the shape of the stress-displacement curve is more affected and thus the results. Specimens with non-collinear notches and/or incorrectly aligned can also be detected by normalizing the curves in the propagation region.

Propagation range shape

The stress-displacement curves in the propagation range (tails) have a parabolic shape, which modeled results in βw_p being directly related to the stress at crack initiation (σ_i) and the extension or displacement ratio (α).

5.2 Future research lines

Most of the current research does not consider the effect of the quality of the notches on the results. Thus, the methodology here developed to separate specimens with poor quality notches must be extended to the materials studied in those research works.

We have proved that the propagation energy can be perfectly described and quantified by the initiation stress (σ_i) and the extension ratio at rupture (α). Therefore, the meaning of β, if any, must be investigated more in depth.

Acknowledgments

Quisiera empezar agradeciendo al Profesor Antonio Martínez Benasat por su paciencia y apoyo para guiarme, todo lo que he aprendido y he logrado durante esta tesis doctoral ha sido gracias a usted. Le agradezco también las charlas y experiencias personales y profesionales que me ha transmitido, me han servido de mucho y me han ayudado a tener una visión más amplia y profunda de las cosas, sus consejos siempre serán valorados y espero poner en práctica la metodología y forma de trabajo que me ha transmitido. Le deseo todo lo mejor que se merece.

Agradecer a la Profesora Maria Lluisa Maspoch, directora del Centre Català del Plàstic (CCP), por permitirme hacer uso de los equipos e instalaciones, así como por los conocimientos transmitidos en su función como catedrática de la Universitat Politècnica de Catalunya (UPC) y por los consejos brindados a lo largo del doctorado. Asimismo, a los profesores José Ignacio Velasco y Orlando Santana.

A todos y cada uno del personal de staff del CCP, con especial atención a:

Dr. David Arencón por todos los conocimientos transmitidos y las vivencias compartidas, incluidas las del gimnasio… nos pusimos fuertes ehhh.

Dr. Marcelo de Sousa por su ayuda y ejemplo como investigador, ahhh y por enseñarme el restaurante mexicano que tantas veces me ha salvado la vida.

Dra. Vera Realinho por los momentos compartidos dentro y fuera del CCP, incluidas esas comidas en familia en el mexterra.

Dr. Miguel Sánchez por sus consejos puntuales que en momentos precisos me han ayudado mucho.

A mis compañeros cuasi-doctores Hooman Abbasi, Javier Gómez, Mohammad Reza, Kian Habibi, Raja Hakim porque con su trabajo y continuo esfuerzo me inspiraron a trabajar más arduamente para lograr el objetivo final.

A continuación agradecer especialmente a las personas que sin su apoyo me hubiera sido imposible concluir esta gran experiencia de vida:

Annita Carreras: No tengo las palabras suficientes para agradecer todo lo que has hecho por mí, sin tu ayuda y comprensión esto hubiera sido imposible, gracias por soportar todas mis locuras (y mira que fueron muchas) y mis malos momentos, siempre tuviste las palabras y actitud correctas para hacerme seguir adelante. Me has ayudado a ser mejor persona y eres sin duda el mejor ser humano que he conocido, todos los que están a tu lado son bendecidos y seguramente lo saben. Te doy también las gracias por dejarme conocer a Berni me ayudo a ver que la bondad pura si existe, el jugar con el terremoto me brindo mucha paz mental. Finalmente, solo quiero decirte que te deseo lo mejor hoy y

siempre, deseando que tu vida sea tan maravillosa e inspiradora como lo ha sido hasta ahora. P.D: Berni tiene a su lado a la mejor madre que se puede tener.

Alba Giménez: Aunque al final de mi tesis ya no estabas en el CCP, no podía dejar de agradecerte. Gracias por brindarme tu amistad y dejarme conocer a una persona tan íntegra y con tan fuertes convicciones. Te agradezco que siempre me hayas escuchado y comprendido, tus hijos son muy bendecidos de tenerte como madre. Muchas gracias por todos los momentos compartidos dentro del CCP y por esas comidas en el mexterra y con tu familia que tanto me ayudaron mentalmente y que tanto disfrute.

Pilar Castejón: Sin duda la compañera de doctorado con la que compartí gran parte de mi tesis fue contigo, tuvimos momentos muy duros y muchas dudas pero siempre se resolvieron favorablemente. Conocí muchas de tus facetas, algunas me hicieron reír más que otras, te considero una persona humilde y muy trabajadora que siempre sabe lo que quiere y a hacia dónde quiere ir. Estoy 100% seguro que terminarás logrando todos tus objetivos de vida, que te harán sentirte orgullosa a ti y a los tuyos… ahhh y recuerda “no eres un vegetal”.

Agradecer a mi familia (padres y hermanos), especialmente a mi hermano Antonio León Albiter, por el apoyo que me han brindado en todos los aspectos, siempre los tengo presentes y me dan el aliento que necesito para darlo todo y un poco más.

Finalmente, agradecer al consejo nacional de ciencia y tecnología (CONACYT) por creer en mí al otorgarme el sustento económico que me ha servido a lo largo de estos años.

Annex

NOTCH EFFECT ON THE FRACTURE OF A POLYMERIC FILM (under review)

N. León,[a]* A.B. Martínez,[a] P. Castejón,[a] P.P. Martínez,[b] D. Arencón[a]

[a] Centre Català del Plàstic, Departament de Ciència dels Materials i Enginyeria Metal-lúrgica. Universitat Politècnica de Catalunya. BARCELONATECH. C/Colom 114, 08222, Terrassa, Spain.

[b] NUDEC SA. C/ Pintor Vila Cinca, 24-28, Pol. Ind. Can Humet de Dalt, 08213, Polinyà, Spain.

* noel.leon@estudiant.upc.edu
Tel.: +34 93 783 70 22
Fax: +34 93 784 18 27

ABSTRACT

The fracture behavior of a bio-based thermoplastic copolyester film has been studied by combining the essential work of fracture, the J-integral, and the crack tip opening displacement characterization methods on double edge notched tension specimens, in an attempt to provide a better understanding of the details that play an important role in the repeatability and the reproducibility of the essential work of fracture test, with particular attention to the effect of the quality of the notches generated by two different notch sharpening techniques. Specifically, the femtosecond pulsed laser ablation and the classic razor blade sliding techniques have been applied. The equivalence between the specific essential work of fracture and the J value at crack initiation, as well as their relationship with the crack tip opening displacement have been found again. It is also identified the parabolic shape of the stress-displacement curves, which modeled relates the specific non-essential work of fracture with the stress at initiation and the extension ratio during the crack growth.

Keywords: Essential work of fracture, J-integral, crack tip opening displacement, femtolaser ablation, notch mechanics, bio-based copolyester

1. Introduction

Films of polymers are used in a wide variety of applications. Their toughness is often a basic requirement to meet some applications.

The Linear Elastic Fracture Mechanics (LEFM) approach is used to study fractures occurring at nominal stresses well below the material's yield stress. The main assumption of LEFM is that the dissipated energy is confined to a small area near the crack tip (small scale yielding), and that brittle fracture occurs without extensive deformation. LEFM characterizes toughness using the critical stress intensity factor (K_{Ic}), and the energy per unit area of crack growth (G_{Ic}), at fracture initiation. There is a direct relationship between both parameters.

The LEFM approach is not applicable when the plasticity around the crack tip becomes too large; in those cases Elastic Plastic Fracture Mechanics (EPFM) applies and the crack tip opening displacement (CTOD) and J-integral are appropriate methods to characterize fracture.

Based on the deformation theory of plasticity, Cherepanov [1] and Rice [2] developed a new fracture parameter, the J-integral. This theoretical concept represents an energy contour path integral that is independent of the path around the crack. Rice [2] showed that the J-integral is essentially equal to the energy release rate of work done on a nonlinear elastic body containing a crack per unit surface area of crack growth, which can be expressed as

$$J = -\frac{1}{t}\left(\frac{dU}{da}\right)_{d=cte} \qquad \text{Eq. (1)}$$

where U is the external work done up to a given constant displacement, d, and a is the crack length.

Another important concept, first proposed by Wells in 1963 [3], is the CTOD. This method is used to determine a fracture parameter for ductile materials. It essentially measures the resistance of the material to the propagation of a crack. A direct relationship between the J-integral and CTOD concepts exists.

When the crack propagates through a highly deformed and yielded material, then Post-Yield Fracture Mechanics (PYFM) can also be applied and the Essential Work of Fracture (EWF) is a suitable method for characterizing fracture. For ductile polymers where crack propagation occurs through a fully yielded ligament, the EWF, the CTOD, and the J-integral methods are commonly used. The EWF method is becoming more widely used to characterize the plane stress toughness of ductile polymer films in mode I, primarily using the double edge notched tension (DENT) configuration. The widespread use of the EWF technique is due to the apparent ease with which DENT specimens may be prepared and tested.

It has been experimentally found that w_e, the specific energy just up to crack initiation, is equivalent to the J-integral [4-7] value at crack initiation in plane stress, J_o, when the complete ligament yielding of the sample precedes the onset of crack initiation. The specific essential work of fracture, w_e, becomes an inherent material parameter only if the ligament fully yields before the crack initiation. However, this condition is rarely met, in most publications it is not satisfied, and w_e is an apparent toughness that is only valid for comparison purposes.

There is a European Structural Integrity Society (ESIS) test protocol [8] for the EWF method, and several round-robin exercises [8,9] have been performed under the guidance of the ESIS technical committee 4 (TC4). In spite of the apparent simplicity of the test, some aspects of the validity of this technique remain controversial; there are intricate details that seem to play an important role in the repeatability and reproducibility of the EWF test. This problem has been, and still is, a topic of much debate, and these concerns indicate that EWF procedure is not yet sufficiently defined to be considered as a standard.

Some of the aspects of the test and specimen validity are related to the specimen manufacture, particularly the notch quality [4,5,10], and they are studied here in more depth. Two sets of DENT specimens were prepared. In one set the notches were sharpened using the femtosecond pulsed laser ablation technique (femtolaser), and the second set was sharpened using the classical razor blade sliding technique. Both sharpening techniques are able to generate notches with different quality.

A combination of several methods for fracture characterization is used, in an attempt to provide a better understanding of the EWF approach for characterizing the fracture toughness of thin ductile polymer films.

All of these methods are utilized to characterize the fracture behavior of a bio-based copolyester film.

2. The EWF approach

2.1. The EWF concept

The EWF approach was firstly proposed by Cotterell and Reddell [11] after Broberg's work on stable crack growth was published [12-14]. It is based on the hypothesis that the total energy involved in the ductile fracture of a pre-cracked specimen (W_f) can be separated into two terms.

$$W_f = W_e + W_p \qquad \text{Eq. (2)}$$

where W_e, the essential work of fracture, represents the energy required for the creation of two new surfaces during the crack propagation, whereas the second term, W_p, is called the plastic work or the

non-essential work of fracture and collects all other sources of energy produced throughout the fracture process (plastic deformation around the crack, heat dissipation, etc.).

The term W_e is considered to be proportional to the area of the Inner Process Zone (IPZ) while W_p is proportional to the volume of the Outer Plastic Zone (OPZ). These zones are schematized in Figure 1 for a DENT specimen.

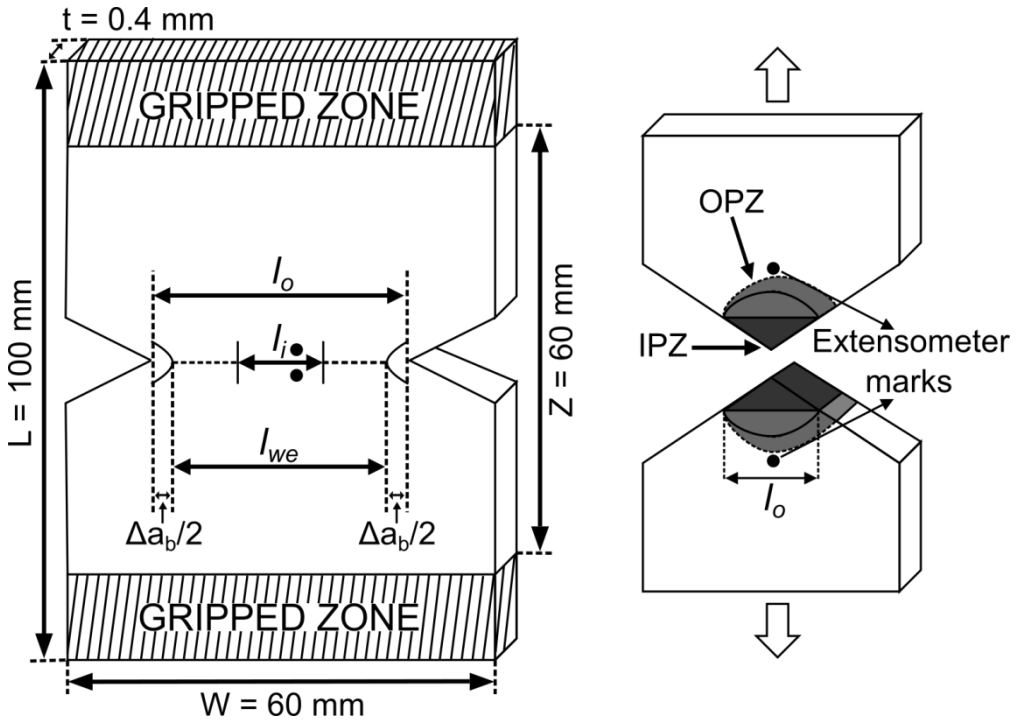

Figure 1 Double edge notched tension geometry

The DENT geometry is the most appropriate for mode I testing because the transverse stresses between the notches are tensile and therefore buckling problems are avoided [15].

Rewriting Eq. (2) using specific terms, i.e., dividing all terms by the area of the ligament cross-section, the following expression can be obtained:

$$w_f = \frac{W_f}{l_o.t} = w_e + \beta w_p.l_o \qquad \text{Eq. (3)}$$

where t is the specimen thickness, l_o is the original ligament length and β is a factor that depends on the shape of the OPZ.

It is possible to assess Eq. (3) by performing a series of tests on specimens with different ligament lengths and plotting the specific total work of fracture values, w_f, as a function of their ligament

lengths. A simple regression analysis of this plot shows that the specific essential work of fracture, w_e, and the specific non-essential work of fracture, βw_p, are the intercept for a zero ligament length and the slope of the linear regression line, respectively.

The EWF technique was originally developed for metals [16] and later extended to polymers by Mai [17]. A more detailed description of the procedure can be found elsewhere [18].

The value which represents the toughness, namely, w_e, is an inherent material parameter only if the ligament fully yields before the onset of crack propagation and is independent of the specimen geometry, as verified first by Mai and Cotterell [19].

2.2. Key requirements

In the EWF analysis, the following three basic key assumptions are made:

a) The ligament length is fully yielded prior to the onset of crack propagation.

This requirement ensures that the fracture mechanism is the same irrespective of the ligament length and that w_e is an inherent material parameter. However, this key assumption is rarely realized, even in most of the published articles this requirement is not satisfied, and thus the w_e values become an apparent toughness only useful for comparison purposes. In a DENT specimen, the ligament length will be completely yielded prior to the onset of crack propagation if it is less than twice the size of the plastic zone radius, r_p, under plane stress conditions:

for a linear plastic zone

$$2r_p = \frac{\pi}{8}\left(\frac{Ew_e}{{\sigma_y}^2}\right) \qquad \text{Eq. (4)}$$

and for a circular plastic zone

$$2r_p = \frac{Ew_e}{\pi{\sigma_y}^2} \qquad \text{Eq. (5)}$$

where E is the elastic modulus, σ_y is the uniaxial yield stress, and w_e is the specific essential work of fracture.

Although having a ligament length that is less than twice the plastic zone radius is a reasonable size criterion, it appears to be too restrictive considering the evidence encountered in amorphous copolyesters [5,20].

b) Fracture occurs under plane stress conditions.

There are constraints on the ligament length to ensure a pure plane stress state in the specimens.

Hill [21,22] has demonstrated for rigid, perfectly plastic materials in the DENT geometry, under plane stress conditions, that no stress can exceed the value of 1.15 σ_y. This value rises to 2.97 σ_y in a pure plane strain state, where σ_y is the uniaxial tensile yield stress. Thus, the maximum stress registered during the DENT test, σ_{max}, has to be maintained between σ_y and 1.15 σ_y, and its value is equal for all the ligaments, when there are pure plane stress conditions.

Theoretically, at small values of l_o, the specimen can be in a mixed state of stress, which increases σ_{max}, and so this Hill criterion could be employed to determine the lower limit of l_o. Nevertheless, in practice, the experimental variability in the σ_{max} values creates difficulties for the application of this criterion.

Clutton [8] suggested another criterion, which does not use the yield stress but uses the mean of the maximum stresses (σ_{max}) as follows

$$0.9\sigma_{max} < \bar{\sigma}_{max} < 1.1\sigma_{max} \qquad \text{Eq. (6)}$$

The Clutton criterion only removes data where an error in dimensional measurement or load exists, although these load errors can be undetected if the same load cell is used for all tests [9-23].

The polymer films have a thickness of less than 1 mm. A practical lower limit of 5 mm [9] in the ligament length has been accepted when preparing DENT specimens, which facilitates handling of specimens. The upper limit in the ligament requires full-ligament yielding before crack propagation. Hence, l_o has to be less than twice the plastic zone radius in DENT specimens.

Another upper limit is given by the relationship:

$$l_o \leq \frac{W}{3} \qquad \text{Eq. (7)}$$

where W is the specimen width. This last condition is necessary to prevent edge effects.

c) Good quality notches.

Good quality entails identical and consistently sharp notches without plastic deformation in front of the notch tip. This requirement guarantees self-similar load-displacement and ligament length-displacement curves for the tested specimens [4,5].

The notch sharpening is of critical importance in obtaining good results. There is evidence [9] that the larger notch tip radius, the higher the w_e values. Thus, the notches should be sharpened as much as

possible without significantly lowering the value of w_e. However, the smallest notch tip radius that was reached was about 1 μm.

It has also been demonstrated [10,24,25] that the larger plastic deformation in front of the notch tip, the higher the w_e values.

Several methods can be found in the literature that are used for sharpening notches in polymer films. Further, it appears that the notch quality is dependent on the technique used, and even on the skill of the operator.

The femtosecond pulsed laser ablation technique (femtolaser) is a non-contact method useful for sharpening the pre-notches. This powerful technique can be used to micromachine practically any material, with negligible thermal damage to the surface surrounding the ablated areas [26,27]. With proper set-up, the femtolaser ablation technique produces consistent notches that have negligible thermal damage, no plastic deformation, and a notch tip radius of approximately 1 μm [4,5,10]. A limitation of the femtolaser technique is the high cost per notch.

The most popular method used to sharpen notches is the razor blade sliding technique. In this technique, the notches are sharpened by drawing a fresh razor blade across the pre-notch tip. It is advisable to do this in a single pass so that the notch follows the same track avoiding bifurcations. Very small notch tip radius of around 1 μm can be manufactured.

Unintentional introduction of residual stresses and/or the development of a plastic zone ahead of the notch tip can be easily induced by the compressive component of the sideways sliding force. The higher the yield stress of the ductile polymer, the smaller the extent of the plastic deformation ahead of the notch tip.

Cooling specimens below their glass transition temperature (T_g) prior to the application of the razor blade sliding technique can be helpful.

The razor blade sliding is a manual procedure, which regularly results in differently sharpened notches. These differences can be in the notch tip radius and/or the extent of the plastic deformation [8].

In a set of DENT specimens, it is possible to have three different specimen populations that show distinct behaviors from one another, which are responsible for the non-similarity and crossing of the curves in the load-displacement, stress-displacement, and ligament length-displacement plots. These include specimens with two different notches, specimens with two equal notches and negligible plastic deformation, and specimens with two equal notches both of which have noticeable plastic deformation [5].

When the specimen has two different notches, crack initiation does not begin at the same time in both notches. Conversely, when the two notches are equal, the crack initiation happens at the same time (simultaneously). When comparing specimens with and without plastic deformation at the notch root [4,5] but with the same notch tip radius, it is noticed that the heads of the stress-displacement curves have different shapes. Specimens without plastic deformation yield a lower value for CTOD, that is, a lower w_e value. However, the tails of theses curves are independent of the notches and therefore show the same slope βw_p in the EWF plots. Clearly, the EWF results are not only affected by the notch sharpness, but also by the plastic deformation ahead of the notch tip.

Other procedures for generating notches have been tried unsuccessfully, which include cuts made by scissors or die-punch and scalpel cuts generated starting from the notch tip. These techniques generate greater plastic deformation ahead of the notch tip and result in higher w_e values than does the razor blade sliding method [8] or scalpel sliding method [25].

In single phase homopolymers and copolymers, full-ligament yielding must show a load and stress drop (necking) in the related load-displacement and stress-displacement curves [4,5,18].

3. Experimental details

3.1. Material

This study has been conducted on an amorphous thermoplastic copolyester, ECOZEN (SKYGREEN chemicals, Korea), produced by the polymerization of terephthalic acid, ethylene glycol, 1.4-cyclohexanedimethanol, and a bio-based monomer that is derived from renewable resources [28].

The material was kindly supplied by Nudec S.A (Spain) in the form of films with a thickness of 0.4 mm. The copolyester is slightly hygroscopic and the film had the water absorption at saturation.

Differential scanning calorimetry measurements (DSC) were conducted on a Q2000 equipment from TA instruments. The samples were heated at a scanning rate of 10 ºC/min. The DSC test revealed a T_g at 101 ºC at midpoint.

3.2. Specimen manufacture

Two kinds of specimens were prepared: dumbbell shaped and DENT specimens to perform uniaxial tensile testing and plane stress fracture toughness (EPFM and PYFM) testing, respectively.

All specimens were prepared with the longitudinal axis in the machine direction of the cast-extruded film.

3.2.1. Dumbbell shaped specimens

Eleven dumbbell shaped specimens were prepared from the 0.4 mm thick films using a cutting press, with the shape and dimensions of a Type V specimen in accordance with the ISO standard 527-3.

3.2.2. DENT specimens

The DENT geometry is shown in Figure 1, where W**,** t, L, and Z correspond to the specimen width, specimen thickness, specimen length, and the distance between clamps, respectively. Most published research has been performed using this geometry. There is experimental evidence that when W and Z are more than twice the largest ligament value, the w_e values do not change [9,29,30]. However, when Z is more than twice W, the specimens can become wavy in their own plane during the test [29] and thus modify the stress distribution in the ligament zone. Values of Z that are smaller than W seem to be far from the infinite plate case, where the result is probably influenced by the close proximity of the cross-heads to the fracture region.

Taking these pieces of evidence into consideration, the DENT specimens were obtained by cutting rectangular coupons from the 0.4 mm thick films with the dimensions shown in Figure 1. In order to minimize the plastic deformation at the notch root, a sandwich was formed by compressing a copolyester coupon between two layers of 1-mm-thick polymethyl methacrylate coupon, and was subsequently pre-notched with a saw. In this way, pre-notched specimens with different original ligament lengths (l_o) were obtained.

The notches must be collinear and placed opposite of one another at the midpoint of L [10].

The notch sharpening of the DENT specimens was carried out using two different methods, the non-contact femtosecond pulsed laser ablation technique and the manual razor blade sliding technique. This resulted in two sets of DENT specimens, femtolaser and razor blade, on which to perform the plane stress fracture toughness testing.

In one set of 10 specimens, the machined pre-notch was extended by the application of the femtolaser with the same set-up and other variables, as previously defined for polyethylene terephthalate (PET) [4] and polyethylene terephthalate glycol-modified (PETG) [5].

A second set of 22 specimens was sharpened manually by sliding a new razor blade across the pre-notch in a single pass, as the accepted method to sharpen notches in polymer films.

Prior to testing, one surface of each DENT and dumbbell shaped specimens was adequately spray painted in order to achieve a speckle pattern. The original ligament length of each specimen was measured after testing in an optical microscope.

3.3. Test details

All tests were carried out at 23 ± 1°C. The DENT and dumbbell shaped specimens were tested on a Zwick servo-hydraulic testing machine, which was fitted with a two-camera digital image correlation (DIC) system and Aramis software (GOM, Germany).

In general, DIC is based on the principle of comparing speckle patterns on the surface of the deformed and the undeformed samples, or between any two deformation states. Surfaces with high contrast are required to avoid image distortion and therefore inaccurate data. Hence, before testing, one surface of each specimen was covered with a thin white coating before being sprayed in order to obtain black points, as required by the DIC system.

3.3.1. Uniaxial tensile testing

Uniaxial tensile tests were performed on the dumbbell shaped specimens until complete failure at a cross-head speed of 1 mm/min, in accordance with the guidelines provided by the ISO standard 527. The load was registered by the load cell, and the deformation and displacements were measured by the DIC system.

3.3.2. DENT tests

The DENT specimens were tested in mode I until complete failure at a cross-head speed of 1 mm/min. The DENT specimens were tested with the tensile direction perpendicular to the collinear notches. The specimens were properly mounted on the grips with an initial distance between clamps of Z = 60 mm (Figure 1).

DIC system images obtained during the tests were recorded for all the specimens. These images were also analyzed with the Aramis software to measure the displacement and the ligament length evolution throughout the test.

There is experimental evidence that w_e is insensitive to changes in the gauge length chosen for displacement measurements. Nonetheless, the slope βw_p of the EWF plot and the rupture displacement (d_r) increase slightly with increasing gauge length [24]. The elastic deformation outside the plastic zone is recovered upon unloading; so that the d_r values would be expected to be equal at least that the total recovery of other displacements, as viscoelastic, does not happen before specimen rupture.

The displacement d was measured with two reference points very near to each other, but outside the largest OPZ, which corresponds to the largest original ligament length specimen. The distance between these two reference points was always the same for all specimens of a given set.

Then, by using the registered loads, displacements, and ligament lengths, two sets of data can be plotted for each specimen. Specifically, the stress is plotted as a function of the displacement, and the ligament length as a function of the displacement.

4. Results and discussion

The DENT test generates two different kinds of plots. Specifically, the stress-displacement and the ligament length-displacement plots for each tested specimen have been obtained. The same results can be used to perform EWF, CTOD, and J-integral analyses.

4.1. Deformation behavior

σ_y, E, and ν of the ECOZEN material were measured from the dumbbell shaped specimens.

The tensile stress-strain curves, represented in Figure 2, show an extensive amount of plastic deformation. A yield point (maximum load) can be seen where necking starts, followed by a sudden load drop where the neck develops. Afterwards, there is a drawing of the necked region (cold drawing), during which the tensile deformation continues at a constant stress (engineering flow stress, σ_{fs}), followed by a stress drop when the specimen ruptures.

The results obtained from the test of 11 specimens were: $E = 1.91 \pm 0.42$ GPa, $\sigma_y = 44.48 \pm 0.42$ MPa, $\sigma_{fs} = 33.77 \pm 0.44$ MPa, and $\nu = 0.44 \pm 0.01$.

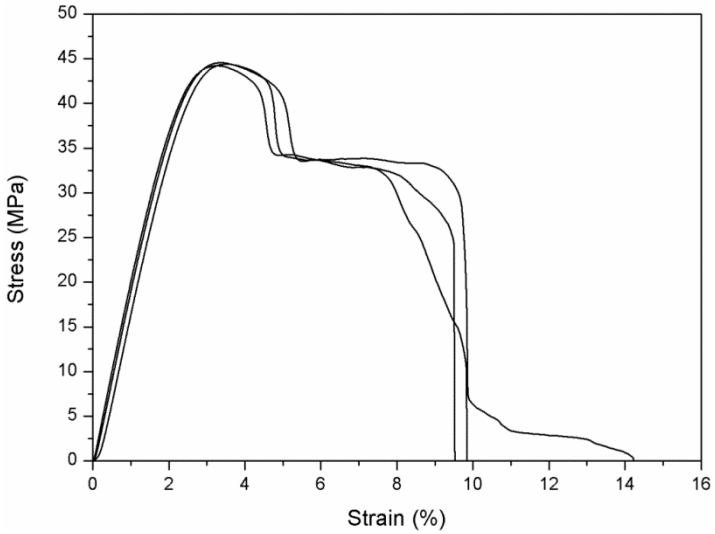

Figure 2 Uniaxial tensile stress-strain curves

4.2. DENT tests

4.2.1. Femtolaser sharpened DENT specimens

Four notches in two specimens were observed by scanning electron microscopy (SEM). The SEM samples had to be cut; hence, they could not be tested. All of the femtolaser sharpened notches observed through the SEM turned out to be virtually identical, as shown in Figure 3, with a notch tip radius of less than 1 μm and a sharpening depth of 1 mm. It was also observed that there was no plastic deformation and negligible thermal damage ahead of the notch tip.

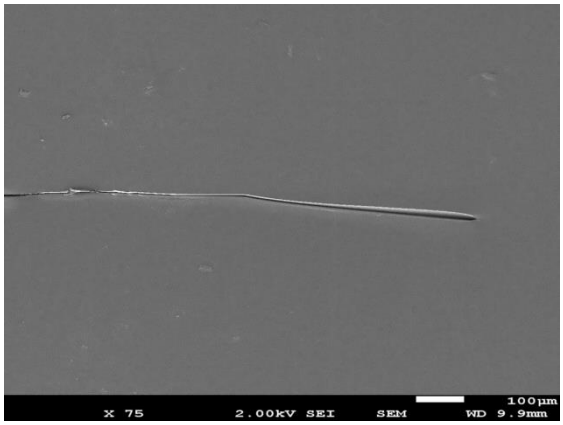

Figure 3 SEM micrograph for a femtolaser DENT specimen

A servo-hydraulic testing machine was used to measure the applied load, while the displacements were simultaneously measured by the DIC system. The registered load can be divided by the area of the cross-section of the ligament length to give stress. As such, the stress-displacement curves are represented in Figure 4, for each one of the 8 tested specimens. The images collected from each specimen by the DIC system in the DENT tests were analyzed to measure the ligament lengths, l, and their associated displacements. These data are represented in Figure 5.

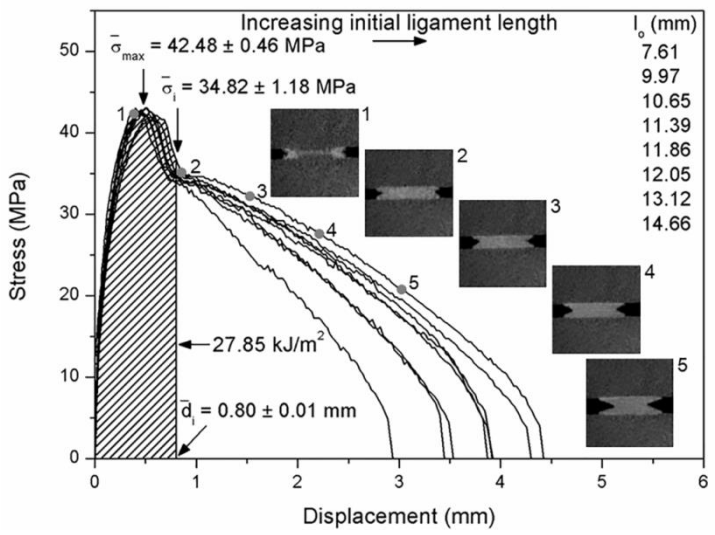

Figure 4 Registered stress-displacement curves for the femtolaser DENT specimens

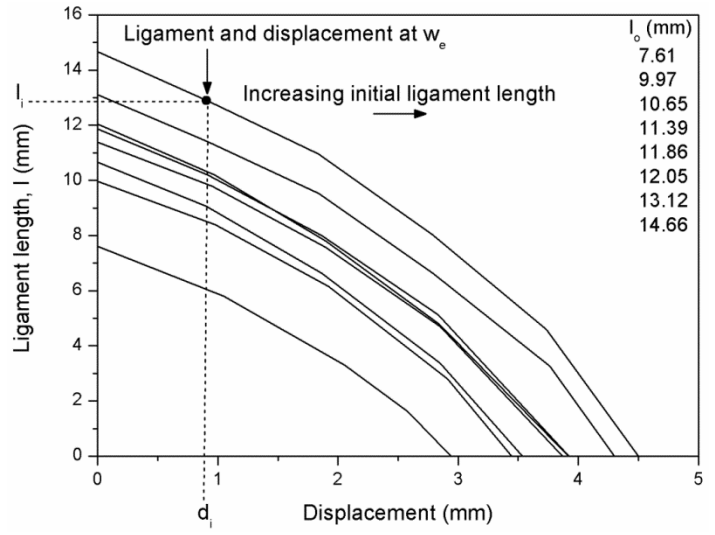

Figure 5 Registered stress-displacement curves for the femtolaser DENT specimens

w_f can be calculated by integrating each curve represented in Figure 4. In Figure 6, the w_f values are represented as a function of their corresponding l_o. A regression analysis of this plot shows that w_e = 27.85 KJ/m^2 and βw_P = 5.91 MJ/m^3 with a coefficient of determination R^2 = 0.968.

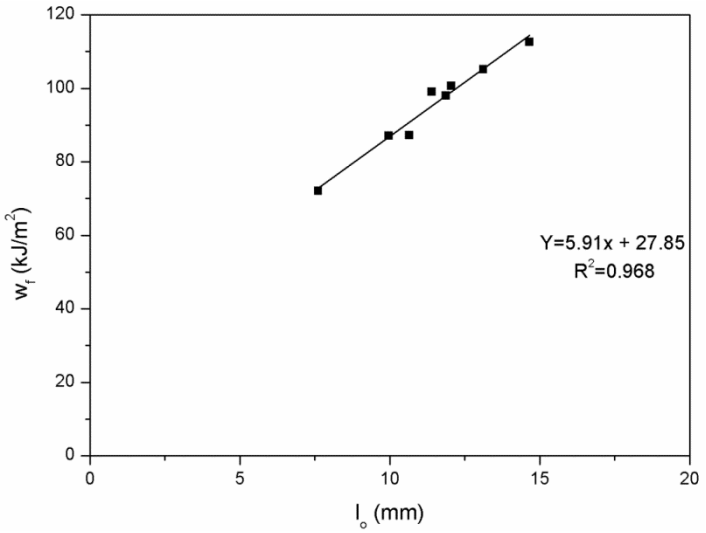

Figure 6 EWF plot for the femtolaser specimens

The hatched area under the stress-displacement curves in Figure 4 is equal to w_e = 27.85 KJ/m^2. In this figure, a set of overlapping curves (heads) can be observed in the low displacement range up to a fairly well recognizable displacement value, d_i, from which the curves (tails) start to diverge. The hatched area begins at d = 0 and continues until the displacement d_i, where the crack initiation begins. When the displacements are larger than d_i there is crack propagation and the curves diverge from each other. From the analysis of Figure 4, the crack initiation displacement d_i = 0.80 ± 0.01 mm and the crack initiation stress σ_i = 34.82 ± 1.18 MPa are identified. The hatched area represents the specific energy up to crack initiation, and then w_e corresponds to an initiation specific energy. In other words, it represents the energy per surface unit area required to create two new surfaces in a cracked body. An identical behavior was previously found in other polymer films, including PET [4], PETG [5], and ethylene-propylene block copolymer (EPBC) [7].

Curve overlapping occurs in the uniaxial tensile tests (Figure 2) if the distance between the displacement reference points is constant for all the specimens and yielding occurs between the above mentioned reference points. In the DENT tests, the displacements are measured using as a reference two points located close to the initial sharpened notch, and such that the OPZ zone is contained between the two points. The distance between these reference points is taken to be constant for all specimens. In this way, the elastic and viscoelastic contributions due to the bulk polymer located

outside the fracture process are negligible. It is important to remark that the heads of the registered stress-displacement curves (Figure 4) overlap and closely resemble those of the uniaxial tensile tests displayed in Figure 2, including the decrease in stress, characteristic of necking.

The average of the maximum stresses, σ_{max} = 42.48 ± 0.46 MPa is practically equal to σ_y. The Hill and Clutton criteria are satisfied. The crack initiation stress σ_i = 34.82 ± 1.18 MPa is almost equal to σ_{fs}.

The sequence of events leading to the fracture of the DENT specimens, as observed in the frames shown in Figure 4, encompasses the opening and blunting of the notch tip with the yielding and necking of the ligament area (heads), followed by crack initiation and propagation until complete fracture (tails).

Prior to the onset of crack initiation, there is an increment of the crack length Δa_b due to blunting (Figure 1), where l_i is the remaining portion of the ligament length yet to be fractured. Thus

$$l_i = l_o - \Delta a_b \qquad \text{Eq. (8)}$$

When representing l_i as a function of l_o a linear dependence arises. The intercept is located at $-\Delta a_b$ and the slope is equal to 1. The l_i values taken from Figure 5 and their corresponding l_o, are plotted in Figure 7. The regression line in Figure 7 provides a slope of 1, as predicted, and Δa_b= 1.40 mm.

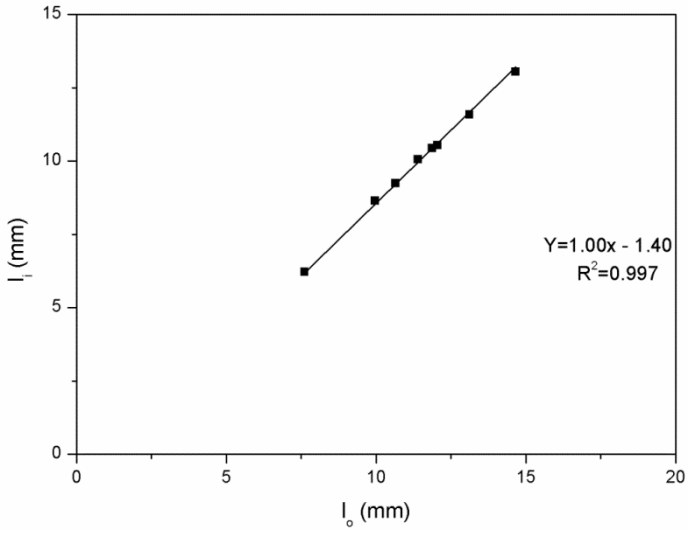

Figure 7 Determination of Δa_b for the femtolaser specimens

Even following a careful observation of the frames stored by the DIC system, we were not able to distinguish the exact frame in which blunting finishes and crack initiation begins. The recorded frames

shown in Figure 4 correspond to the tested specimen with the largest original ligament length (l_o = 14.66 mm). The second frame, which corresponds to d_i, clearly shows the full-ligament yielding and necking before the onset of the crack initiation. The plastic zone is wedge-shaped and narrow, which is consistent with a linear plastic zone. These observations were similar for all specimens.

Applying Eq. (4) results in $2r_p$ = 10.64 mm, which is the theoretical maximum ligament length, but specimens with larger values of l_o have been used in this work. Although Eq. (4) is a reasonable size criterion, it appears to be too restrictive considering the visual evidence observed in the second frame of Figure 4, and as indicated by the ligament necking and the stress drop, which happen before d_i is reached. Similar behaviors have been noted in other thermoplastic copolyesters [5,8,18,20].

Unfortunately, the strain fields at the point of crack initiation cannot be studied. The large deformations developed in the blunted crack-tip region lead to such distortion of the speckle pattern that they cannot be analyzed by the Aramis software.

The key assumptions of the EWF analysis were thoroughly satisfied, including very sharp notches without plastic deformation, specimens in a plane state of stress, and ligaments completely yielded before the onset of crack initiation. Thus, w_e represents and inherent material property.

Hashemi and O'Brien [31] applied to DENT specimens a method for obtaining the critical crack tip opening displacement $CTOD_C$ (CTOD value at the onset of crack propagation). Under plane stress conditions the following linear relationship exists

$$d_r = CTOD_c + \alpha . l_o \qquad \text{Eq. (9)}$$

where d_r is the displacement at rupture and α is the extension or displacement ratio from crack initiation until rupture.

In Figure 8, d_r is plotted as a function of l_o. A simple linear regression analysis of this plot shows that the $CTOD_C$ value is the intercept at zero ligament length, 0.85 mm. This $CTOD_C$ value, as can be expected, agrees very well with the d_i value previously found.

Using the Δa_b and $CTOD_C$ values makes it possible to normalize the ligament length-displacement curves shown in Figure 5 for the purpose of comparing the crack propagation of the DENT specimens. The normalized curves are represented in Figure 9. A complete overlap of the curves for all specimens can be observed, indicating the same propagation behavior, which is independent of l_o.

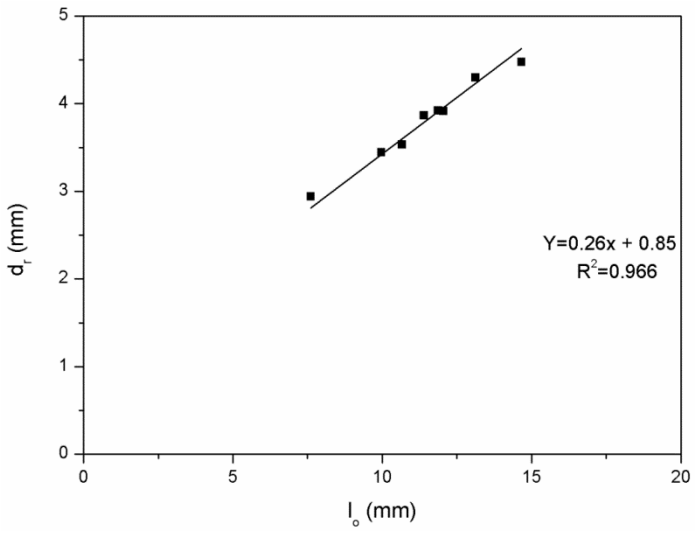

Figure 8 Determination of $CTOD_C$ for the femtolaser specimens

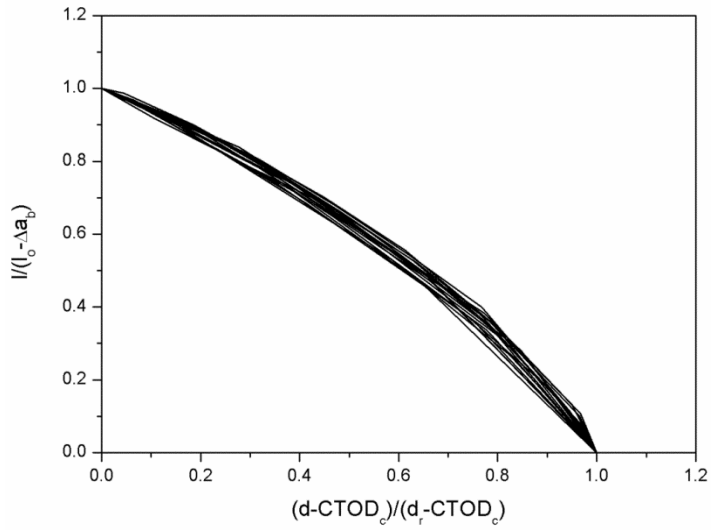

Figure 9 Normalized propagation curves

The crack propagation can also be analyzed. When the ligament length is completely yielded and necked, the following relationship applies:

$$P = t\,(W - a) \cdot \sigma_i \qquad \text{Eq. (10)}$$

where P is the load, and a the crack length. The derivative yields

$$\frac{dP}{da} = -t\,\sigma_i \qquad \text{Eq. (11)}$$

Thus, a linear dependence of the load on a is predicted for the propagation region (tails).

According to Figure 1, a can be represented by

$$a = W - l \qquad \text{Eq. (12)}$$

Thus, after combining Figures 4 and 5 with Eq. (12), the load is represented as a function of a for the tails in Figure 10. Here, a linear dependence can be observed except at higher a-values, close to the complete fracture where the slope and hence σ_i increases, probably as a consequence of orientation hardening. From the slope, it is found that σ_i = 34.37 MPa, coinciding with the previously found value of σ_i = 34.82 ± 1.18 MPa from Figure 4.

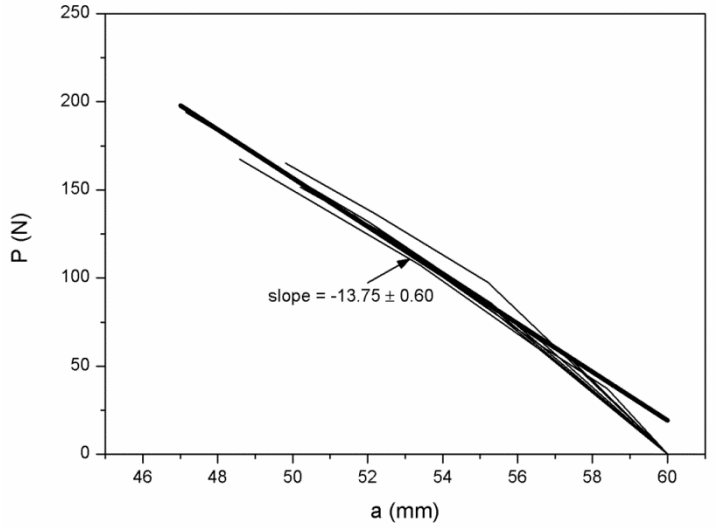

Figure 10 Load-crack length for the femtolaser specimens

There are several approaches to evaluating the J-integral, but for the sake of simplicity, the Begley and Landes experimental method [32] is used here because it can be adequately applied to the previous DENT test results.

This experimental method requires two steps. The first step consists of the graphical representation of the energy divided by the specimen thickness as a function of the crack length when the displacement is fixed. This method consists of taking a constant displacement value d, in Figure 5, where only one l-value is found for each specimen. Then, using Eq. (12), each l value is transformed into a crack length value. The energy is found through numerical integration of the load over the constant displacement value d in Figure 4. This same procedure is applied to a new set of constant displacements adequately chosen. This graphical representation is shown in Figure 11. The points belonging to the same displacement show linearity and can be modeled by a straight line. Following Eq. (1), the slope of the regression lines are –J.

The second step consists of the representation of the J values as a function of the displacement as shown in Figure 12.

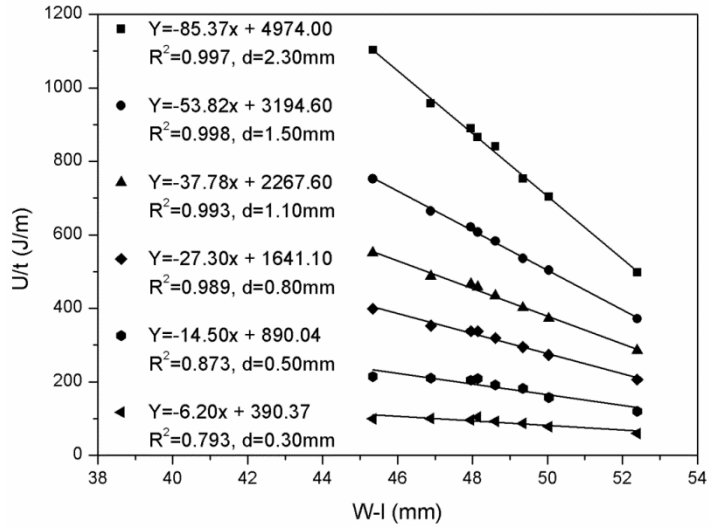

Figure 11 Input energy divided by thickness versus crack length at constant displacement for the femtolaser specimens

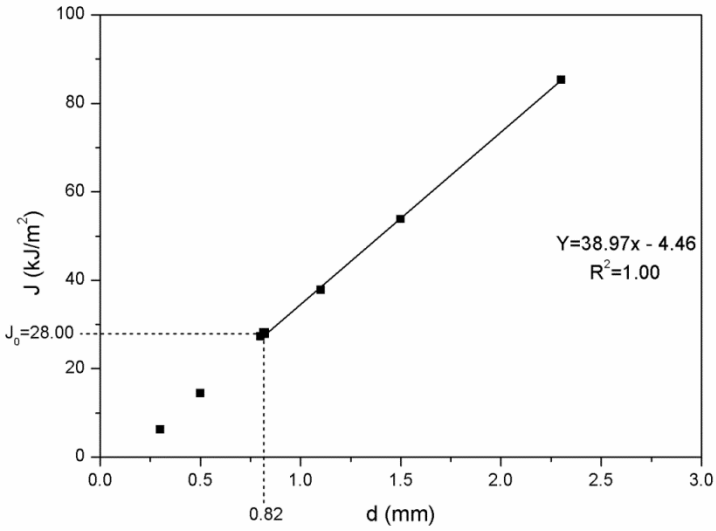

Figure 12 J-integral plot for the femtolaser specimens

Following Hodgkinson and Williams [33], the total energy U for a non-work hardening full yielding of the ligament is

$$U = P \cdot d \qquad \text{Eq. (13)}$$

which, combined with Eq. (10), results in

$$U = t\,(W - a)\sigma_i \cdot d \qquad \text{Eq. (14)}$$

That is, U/t is a linear function of the crack length at a constant fixed displacement, and this is verified in Figure 11.

Equation 1 merged with Eq. (14) gives

$$J = -\frac{1}{t}\left(\frac{dU}{da}\right)_{d=cte} = \sigma_i \cdot d \qquad \text{Eq. (15)}$$

From the slopes of the regression lines in Figure 11 and the slope in Figure 12, Eq. (15) is verified. From the slope in Figure 12, it is found that σ_i = 38.97 MPa, a value that matches reasonably well with the σ_i values obtained before.

The J value at crack initiation J_o is obtained by introducing the $CTOD_C$ value into the J plot, as shown in Figure 12. The resulting value J_o = 28.00 KJ/m^2 coincides with w_e = 27.85 kJ/m^2. This result confirms the equivalence between w_e and J_o when the ligament length is fully yielded prior to the onset of crack initiation.

The Shih analysis [34] shows that there is a unique relationship between J_o and $CTOD_C$. For a non-hardening material in plane stress and assuming that the stress in the plastic zone is σ_i, then

$$J_o = \sigma_i \cdot CTOD_c \qquad \text{Eq. (16)}$$

In the present study this relationship is completely fulfilled. Moreover, our analysis shows a complete relation between w_e, J_o, and $CTOD_C$.

The specific energy as a function of a for the femtolaser sharpened specimens is represented in Figure 13. The curves are obtained as follows. For each a-value a corresponding l-value is obtained [Eq. (12)]. For each l-value the corresponding displacement d can be found through Figure 4. Finally, the specific energy is obtained by the numerical integration of the curves shown in Figure 4 up to the above mentioned displacement d. This procedure is repeated for increasing a-values, and for each specimen.

In Figure 13, it can be observed that though there is not a unique curve, the termination points indicate a linear dependence on l_o. At the termination points, l_o is equivalent to Δa at complete fracture. The regression line is the same that was found in the EWF plot (Figure 6). If the increment of crack length just prior to crack initiation Δa_b is introduced in Figure 13, a coincidence between the specific initiation energy and w_e is again observed.

The $w_e = J_o = 27.85$ kJ/m^2 value for the ECOZEN is slightly lower than the value reported [5] for PETG (32 kJ/m^2), as can be expected, due to its chemical structure as a modified PETG.

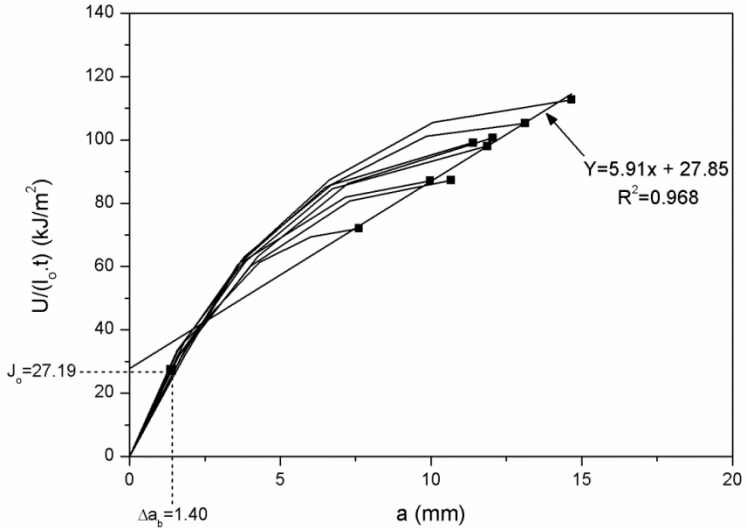

Figure 13 Specific energy as a function of the crack length for the femtolaser specimens

4.2.2. Razor blade sliding sharpened specimens

In the second set of DENT specimens, the pre-notch was extended by the popular contact method of sliding a fresh razor blade across the pre-notch tip in a single pass.

Eight notches from 4 specimens were observed by SEM. Figure 14(a,b) shows the micrographs of the two notches from the same specimen. In Figure 14a, a volume accumulation of plastically deformed material ahead of the notch tip induced by the compressive component of the sideways sliding force can be observed, whereas this feature is absent in Figure 14b.

All of the analyzed notches were very sharp with a notch tip radius less than 1 μm, but with different sharpening depths, ranging between 100 μm and 250 μm.

The razor blade sliding sharpening method generates notches of different quality, which are strongly dependent on the operator's skill. Thus, 3 kinds of specimens can be produced. Specifically, specimens with both notches as those in Figure 14a, specimens with both notches as those in Figure 14b, and finally specimens with one notch as that in Figure 14a and the other one as that in Figure 14b were obtained.

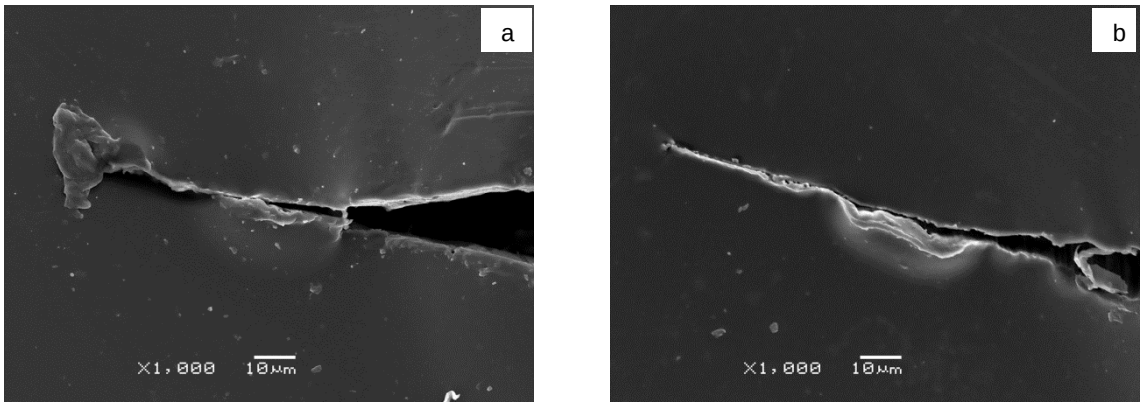

Figure 14 SEM micrographs of a razor blade sharpened specimen: a) Notch tip with plastic deformation, b) Notch tip without plastic deformation

The remaining 18 specimens were tested in the same way as the femtolaser sharpened specimens. The obtained EWF parameters were w_e = 35.86 KJ/m^2 and βw_p = 5.94 MJ/m^3, with R^2 = 0.960.

Careful observation of the frames collected by the DIC system showed that in 5 specimens the two edge notches did not propagate at the same time and therefore were discarded. It has been demonstrated that in the specimens with both notches of different quality, they do not propagate simultaneously.

The registered stress-displacement and ligament length-displacement curves of the remaining 13 specimens are shown in Figures 15a and 16, respectively.

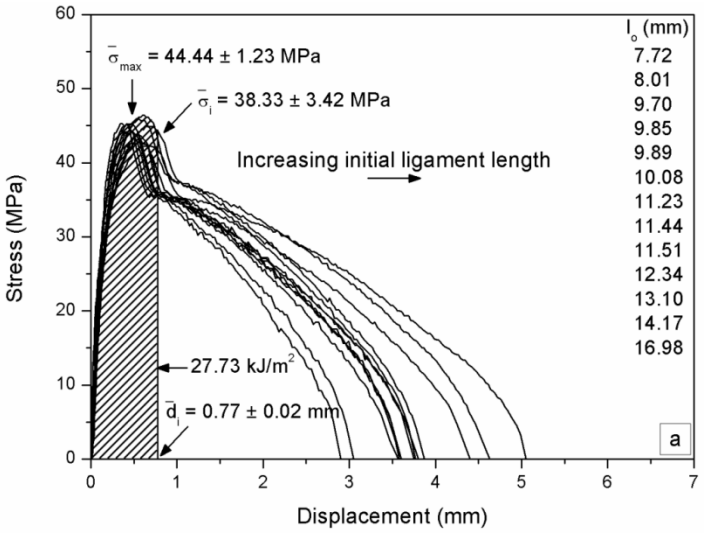

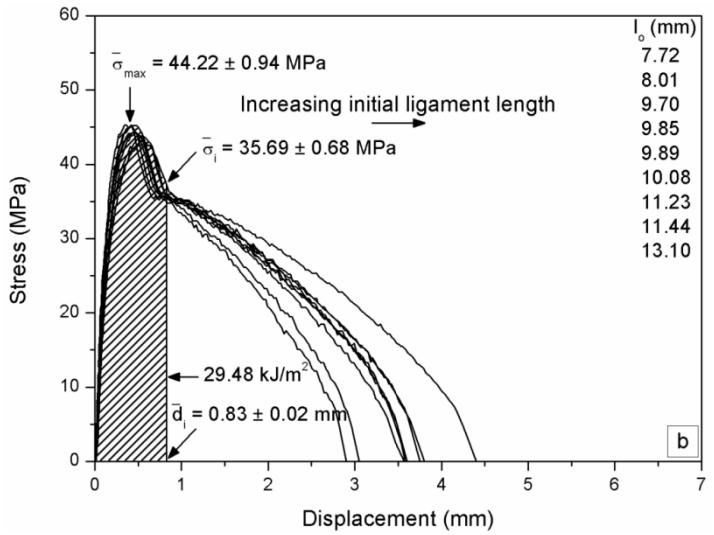

Figure 15 Stress-displacement curves for the razor blade sharpened specimens: a) Thirteen specimens, b) Nine selected specimens

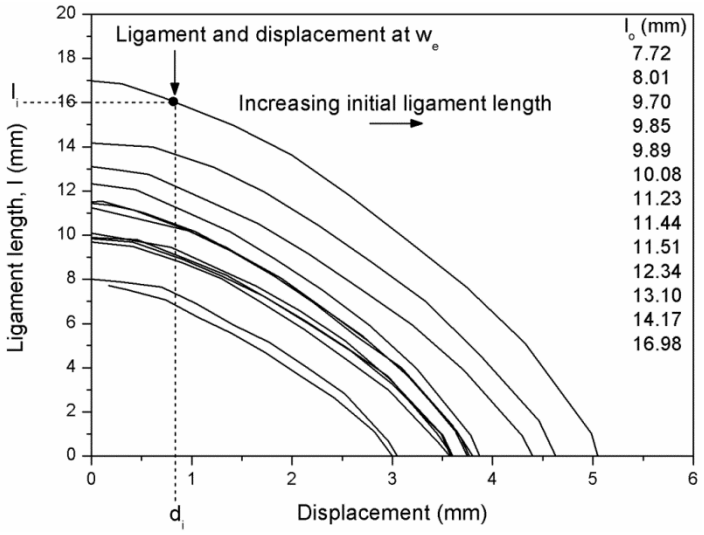

Figure 16 Ligament length-displacement curves for the razor blade sharpened specimens

For the 13 specimens, the EWF parameters were (Figure 17a) w_e = 27.73 KJ/m^2 and βw_p = 6.40 MJ/m^3, with R^2 = 0.972.

The hatched area in Figure 15a corresponds to w_e = 27.73 KJ/m^2 and, proceeding as before with the femtolaser sharpened specimens, it is found that σ_{max} = 44.44 ± 1.23 MPa, σ_i = 38.33 ± 3.42 MPa and d_i = 0.77 ± 0.02 mm.

In Figure 15a, two different populations of curves can be observed. In the first one (9 specimens), the heads overlap, and d_i occurs after the necking of the ligament length. In the second one (4 specimens), the heads do not completely overlap, and d_i occurs before the complete necking of the ligament length, resulting in a large standard deviation for σ_i.

These two sets of curves can be explained by differences between the two populations in the plastic deformation ahead of the notch tip. As has been recently demonstrated [10], it occurs between specimens with and without plastic deformation ahead of the notch tip.

As has been shown [10], when specimens with the same l_o and notch tip radius but with different levels of plastic deformation at the notch root are tested, the stress-displacement curves are equal in the range between d = 0 and the displacement corresponding to σ_{max} ($d_{\sigma max}$), but the distance between d_i and $d_{\sigma max}$ increases with the plastic deformation at the notch root. However, the tails are equal.

Once the population of the specimens with excessive plastic deformation in front of the notch tip was separated, the stress-displacement curves for the 9 specimens with small or negligible plastic deformation are presented in Figure 15b, and the corresponding EWF plot is shown in Figure 17b.

The parameters obtained with the EWF method were w_e = 29.48 KJ/m^2 and βw_p = 6.19 MJ/m^3, with R^2 = 0.942. The w_e value (29.48 kJ/m^2) is represented by the hatched area in Figure 15b. The stress-displacement curves (heads) overlap just in this hatched area until a d_i value of 0.83 ± 0.02 mm. After this point, the curves (tails) start to diverge from one another. The σ_{max} = 44.22 ± 0.94 MPa and σ_i = 35.69 ± 0.68 MPa values are also found by analyzing this plot.

The l_o values of these 9 specimens were in a plane stress state, completely yielded, and necked before crack initiation. The Hill and Clutton criteria were also satisfied. Finally, the key requirements of the EWF approach were fulfilled. Thus, w_e is an inherent material property.

The w_e, σ_{max}, σ_i, and d_i values of these 9 specimens agree reasonably well with the corresponding values of the set of femtolaser sharpened specimens presented before, which had no plastic deformation ahead of the notch tip.

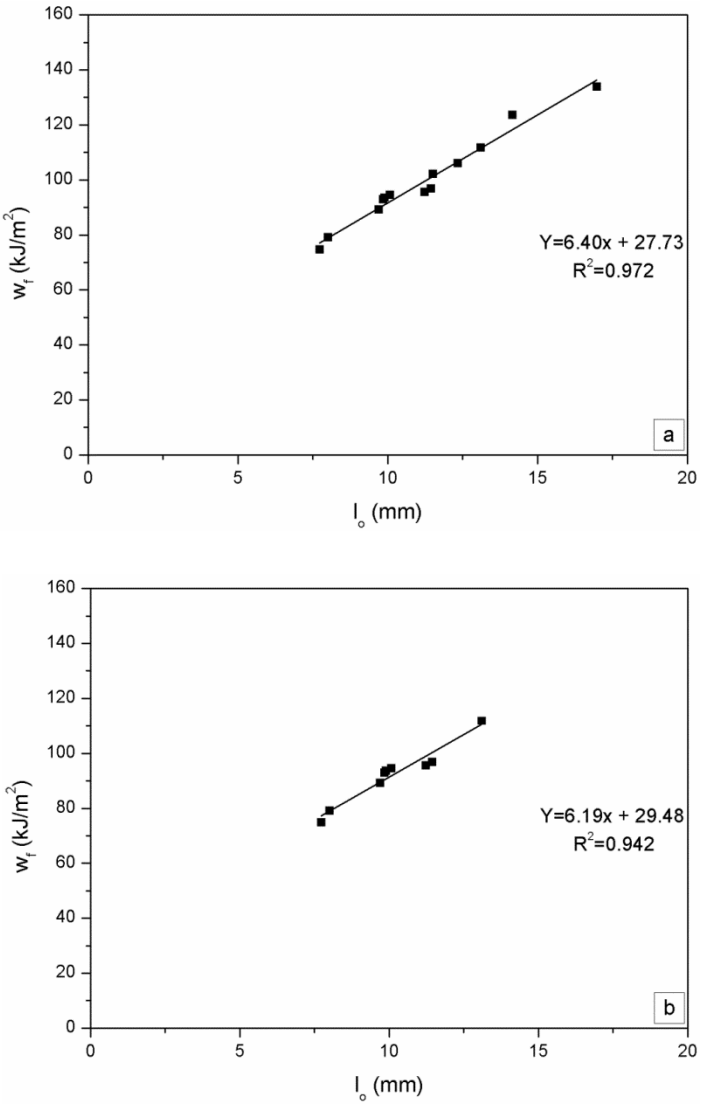

Figure 17 EWF plot for the razor blade sharpened specimens: a) Thirteen specimens, b) Nine selected specimens

The l_i-l_o and d_r-l_o plots are presented for the 9 valid razor blade sharpened specimens in Figures 18 and 19, respectively. A simple linear regression analysis of both plots leads to Δa_b = 1.42 mm and $CTOD_C$ = 0.85 mm. As can be expected, the $CTOD_C$ value matches the value obtained from the femtolaser sharpened specimens.

The ligament length-displacement curves of the razor blade sharpened specimens shown in Figure 16 can be normalized for the propagation region. The normalized curves are represented in Figure 9 together with the normalized curves of the femtolaser sharpened specimens. A complete overlap of all the normalized propagation curves is observed in Figure 9.

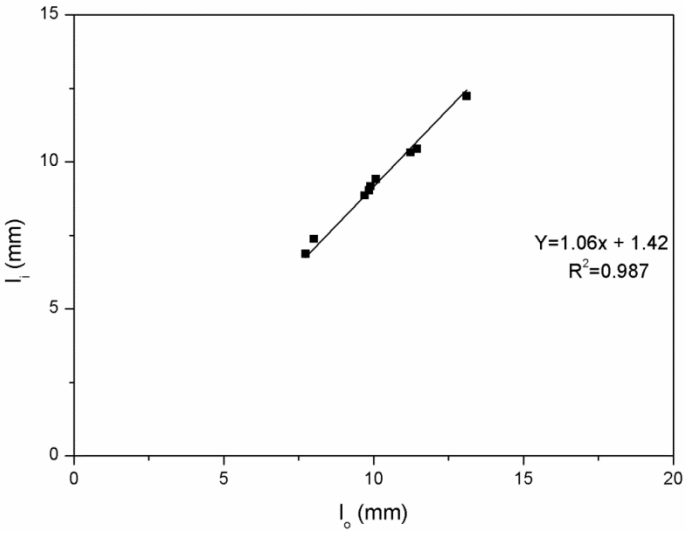

Figure 18 Determination of Δa_b for the nine selected razor blade sharpened specimens

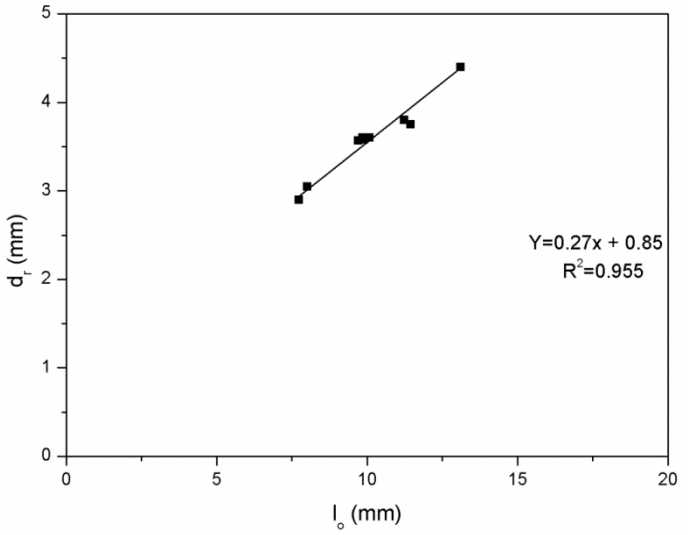

Figure 19 Determination of $CTOD_C$ for the nine selected razor blade sharpened specimens

The load-crack length curves for these 9 specimens are represented in Figure 20. From the slope and applying Eq. (11), it can be found that σ_i = 35.18 MPa, which is nearly equal to the value previously found for the femtolaser sharpened specimens.

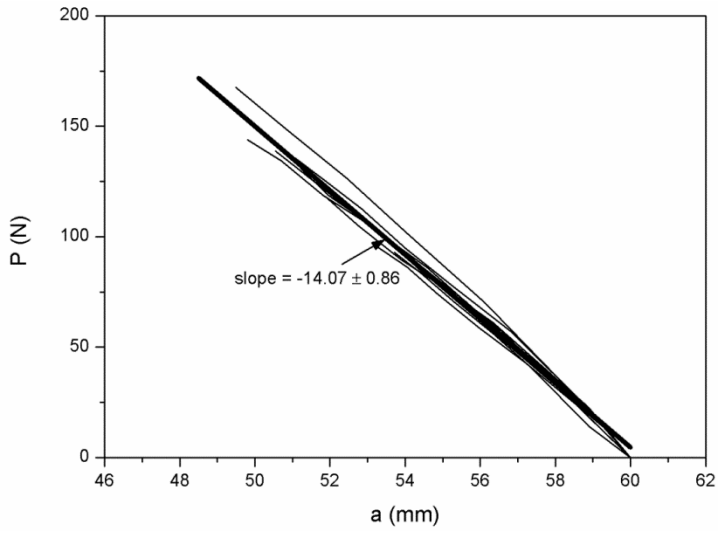

Figure 20 Load-crack length for the nine selected razor blade sharpened specimens

As in the case of the femtolaser sharpened specimens, the Begley and Landes method is used to evaluate the J-integral. The two steps required for the application of this method lead to Figures 21 and 22. In Figure 21, it can be observed that U/t is a linear function of the crack length at a constant fixed displacement. From the slope of the regression line in Figure 22, applying Eq. (15), it is found that σ_i = 38.98 MPa, which practically matches the value calculated for the femtolaser specimens. J_o is obtained by introducing the $CTOD_C$ value in the J-integral plot. This provides a value of J_o = 29.64 KJ/m^2 equal to w_e and coincident with the value obtained for the femtolaser sharpened specimens. Equation 25 is also satisfied.

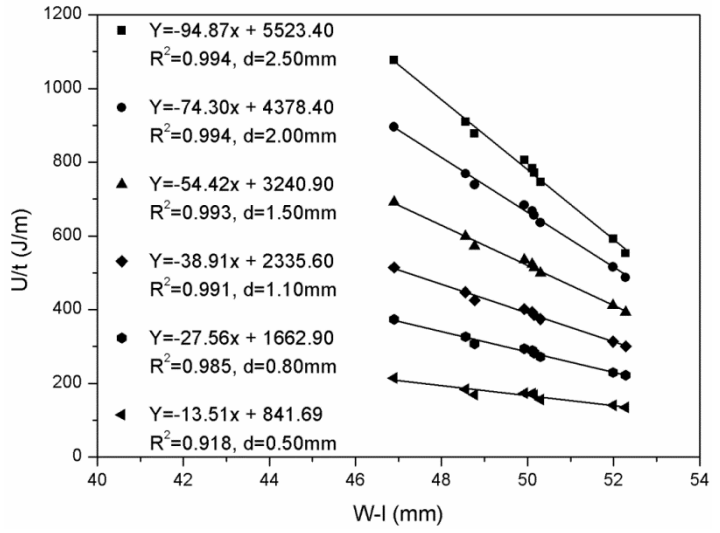

Figure 21 Input energy divided by thickness versus crack length at constant displacement for the razor blade sharpened specimens

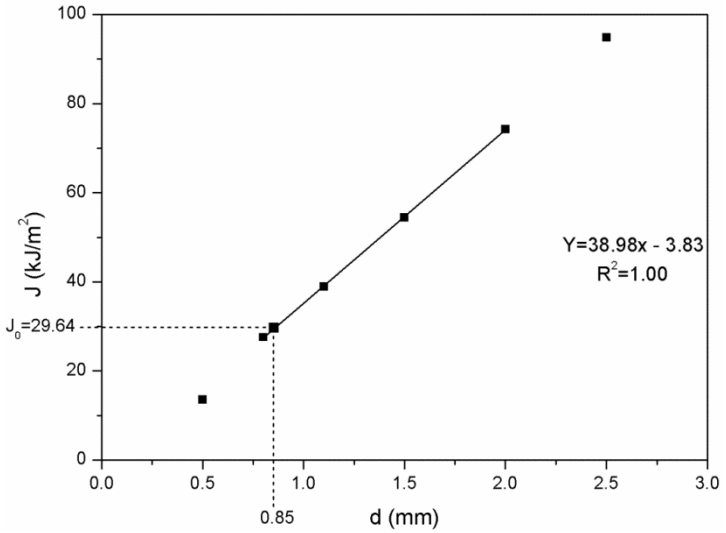

Figure 22 J-integral plot for the nine selected razor blade sharpened specimens

4.2.3. Femtolaser versus razor blade

All of the femtolaser sharpened notches had very consistent, sharp notches without plastic deformation in front of the notch tip and non-crossing stress-displacement (tails) curves. The ligament length-displacement curves also had self-similarity.

The razor blade sharpened specimens had very sharp notches, as sharp as the femtolaser ones, but the different compressive component of the sliding force that is applied by the operator generates three different levels of plastic deformation ahead of the notch tip.

There are specimens with negligible plastic deformation ahead of the notch tip, similar to the femtolaser specimens, which give equal results to the femtolaser. In other specimens, notches of the same specimen, but with different levels of plastic deformation cause non-simultaneous crack propagation and, in consequence, these specimens must be discarded. Finally, specimens where both notches have the same high level of plastic deformation ahead of the notch tip cause that the shapes of the stress-displacement curves to be different when compared to specimens with no plastic deformation. These specimens also must be discarded.

Figure 23a represents the stress-displacement curves for the femtolaser l_o = 14. 66 mm and the razor blade l_o = 14.17 mm specimens. The razor blade sharpened specimen was 1 of the 4 non-valid specimens. In Figure 23b, the femtolaser curve is shifted to the right.

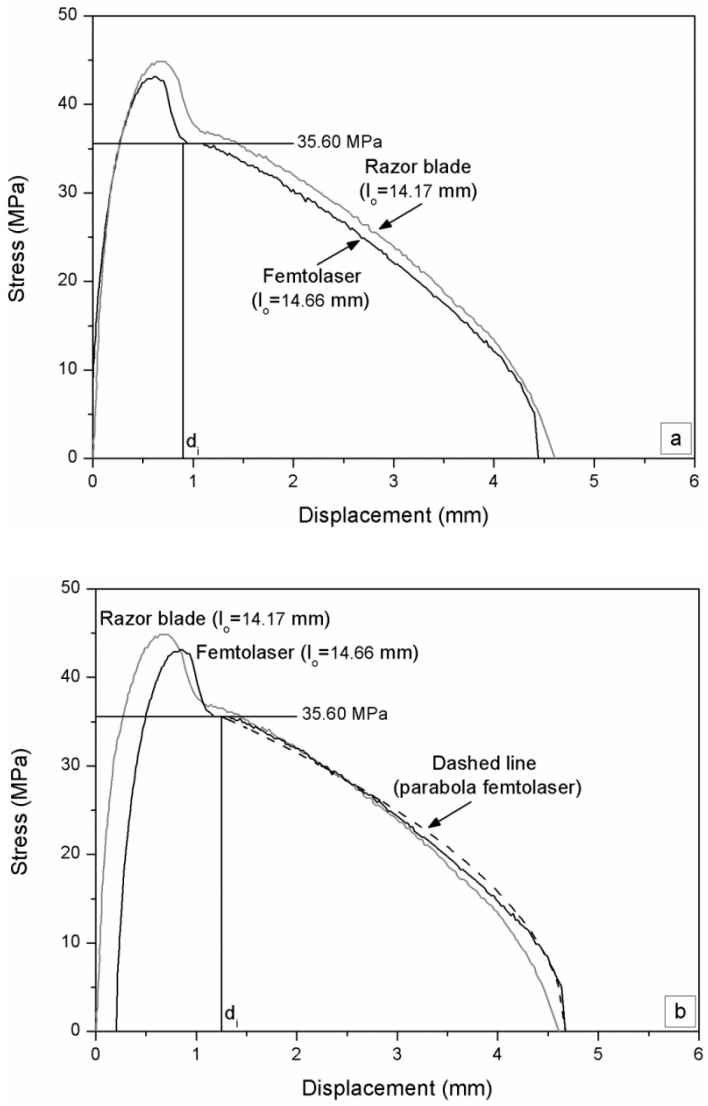

Figure 23 Femtolaser and razor blade sharpened specimens with $l_o \approx 14$: a) Measured displacement, b) Displacement shifted to d_r.

Analyzing Figure 23(a,b), it is found that both specimens have practically the same σ_{max} and σ_i values. Nevertheless, the $CTOD_C$ and d_r values of the razor blade specimen are larger than those of the femtolaser specimen, resulting in a higher w_e value for the razor blade sharpened specimen. The same trends have been observed in other polymer films [4,5,10] between specimens with different levels of plastic deformation ahead of the notch tip. The shapes of the stress-displacement curves are influenced by the plastic deformation surrounding the crack tip, but the tails remain equal. Thus, βw_p and the propagation behavior are independent of the notch quality.

The stress-displacement curves in Figures 4 and 15b, allow the partition into “head” (or initiation) and “tail” (or crack propagation), as described previously: The shape of the “tail” can be approximated

to be a half of a parabola, described by σ_i in the y-direction and (d_r-d_i) in the x-direction. Thus, the energy absorbed during the crack propagation per ligament section (U_p) can be estimated as:

$$U_p \cong \left(\frac{\sigma_i \cdot (dr - di) \cdot 2}{3}\right) \quad \text{Eq. (17)}$$

The value of d_i can be obtained from either the stress-displacement plots (Figures 4 and 15b) or from the slope of the d_r-l_o plots (Figures 8 and 19). In any case, combining with Eq. (9), it results in

$$U_p \cong \left(\frac{\sigma_i \cdot \alpha \cdot l_o \cdot 2}{3}\right) \quad \text{Eq. (18)}$$

As w_e remains constant during crack propagation, the propagation energy per ligament length is a constant value, independent of the notch sharpening method. Then, considering the essential term w_e as the initiation energy, the propagation energy per ligament section is $W_p/(l_o \cdot t)$, giving the equivalence:

$$U_p = \beta \cdot w_p \cdot l_o \quad \text{Eq. (19)}$$

Substituting into Eq. (18) gives [7]

$$\beta \cdot w_p \cong \left(\frac{\sigma_i \cdot \alpha \cdot 2}{3}\right) \quad \text{Eq. (20)}$$

The parabola equation is given by

$$d = d_r + s\sigma^2 \quad \text{Eq. (21)}$$

where

$$s = \frac{d_i - d_r}{{\sigma_i}^2} \quad \text{Eq. (22)}$$

In Figure 23b, the modeled parabola (dashed line) for the femtolaser sharpened specimen with l_o = 14.66 mm is also represented. It is observed that the parabolic shape fits well with the experimental stress-displacement curve in the propagation range (tails).

The stress-displacement curves were previously roughly approximated to be a quarter of an ellipse [13] during the crack growth (tails), which results in

$$\beta \cdot w_p \cong \left(\frac{\sigma_i \cdot \alpha \cdot \pi}{4}\right) \quad \text{Eq. (23)}$$

The βw_p, σ_i, and α values obtained for this bio-based copolyester, as well as the values obtained for other polymer films, PET [4], PETG [5], and three different commercial grades of EPBC [10,13,35], are presented in Table I along with the obtained βw_p values using the semi-parabola [Eq. (20)] and the quarter of an ellipse [Eq. (23)].

Table I Assessment of the plastic term

Material	Parameters		βw_p (MJ/m^3)		
	σ_I (MPa)	α	Slope EWF plot	Parabolic Eq. (20)	Elliptical Eq. (23)
ECOZEN	34.82	0.26	5.93	6.03	7.11
PET [4]	35.56	0.66	16.04	15.64	18.42
PETG [5]	35.34	0.42	10.00	9.89	11.66
EPBC [10]	18.90	0.93	11.50	11.72	13.80
EPBC [13]	21.00	0.96	14.00	13.74	16.83
EPBC [35]	25.89	1.07	19.94	18.47	21.76

It must be considered that the ellipse approach [Eq. (23)] overestimates the area of the tails, thus giving higher βw_p values that the obtained by the slope of the EWF plot. However, the parabola approach [Eq. (20)] fits well with the experimental βw_p values for the six polymer films, indicating a parabolic shape for the tails of the experimentally measured stress-displacement curves. Eq. (20) relates the plastic term βw_p to the crack initiation stress σ_i and the extension ratio α at rupture.

5. Conclusions

The femtosecond pulsed laser ablation technique generates highly consistent, sharp notches, without plastic deformation in the region surrounding the crack tip. This sharpening technique is the most appropriate to sharpen notches of the most ductile polymer films, giving the lowest values for the fracture parameters. Limitations of this technique include the availability of the equipment and the high cost per notch.

Notch sharpening of polymer films using the razor blade sliding technique can generate notches with different quality, which depends on the material ductility and the compressive component of the sideways sliding force that is applied. Three different types of specimens can be obtained. Specimens with sharp notches and without plastic deformation near to the crack tip can be obtained, which yield fracture parameters equal to the femtolaser sharpened specimens. Generally, however, specimens with plastic deformation around the crack tip are obtained. When the two notches in the specimen have different levels of plastic deformation, the crack propagation from both notches does not happen at the same time. Specimens with sharp notches, but equal levels of plastic deformation ahead of both notches can be also obtained. These specimens result in stress-displacement curves with different shapes and higher w_e values than those of specimens without plastic deformation in front of the notch tip.

In DENT specimens, the crack propagation does not depend on the plastic deformation surrounding the crack tip, and equal values for βw_p will be obtained.

In polymer films, the variability of the w_e, J_o, and $CTOD_C$ values obtained in the same laboratory and especially between laboratories can be explained by differences in the quality of the notches that can be generated by different operators. This is especially significant when the notch sharpening is performed using the razor blade sliding technique.

The equivalence between w_e and J_o, as well as their relationship with the $CTOD_C$ is again confirmed.

The stress-displacement curves in the propagation range (tails) have a parabolic shape, which modeled results in βw_p being directly related with the stress at initiation σ_i and the extension or displacement ratio α.

References

[1] Cherepanov GP. Crack propagation in continuous media. Journal of Applied Mathematics and Mechanics 1967; 31: 476-488.

[2] Rice JR. A path independent integral and the approximate analysis of strain concentration by notches and cracks. Journal of Applied Mechanics 1968; 35: 379-386.

[3] Wells AA. Application of fracture mechanics at and beyond general yielding. British Welding Journal 1963; 10: 563-570.

[4] Martínez AB, León N, Arencón D, Sánchez-Soto M. The post-yield fracture of a ductile polymer film: Notch quality, essential work of fracture, crack tip opening displacement, and J-integral. Engineering Fracture Mechanics 2017; 173: 21-31.

[5] Martínez AB, León N, Arencón D, Sánchez-Soto M. Essential work of fracture, crack tip opening displacement, and J-integral relationship for a ductile polymer film. Polymer Testing 2016; 55: 247-256.

[6] Mai YW, Powell P. Essential work of fracture and j-integral measurements for ductile polymers. Journal of Polymer Science Part B: Polymer Physics 1991; 29: 785-793.

[7] Martínez AB, Segovia A, Gamez-Perez J, Maspoch ML. Essential work of fracture analysis of the tearing of a ductile polymer film. Engineering Fracture Mechanics 2010; 77: 2654-2661.

[8] Clutton E. Essential work of fracture. In: Moore DR, Pavan A, Williams JG (editors). Fracture mechanics testing methods for polymers, adhesives and composites. Oxford: Elsevier Science, LTD.; 2001, p. 177-195.

[9] Williams JG. Rink M. The standardisation of the EWF test. Engineering Fracture Mechanics 2007; 74: 1009-1017.

[10] Martínez AB, León N, Segovia A, Cailloux J, Martínez PP. Effect of specimen notch quality on the essential work of fracture of ductile polymer films. Engineering Fracture Mechanics 2017; 180: 296-314.

[11] Cotterell B, Reddel JK. The essential work of plane stress ductile fracture. International Journal of Fracture 1977; 13: 267-277.

[12] Broberg KB. Critical review of some theories in fracture mechanics. International Journal of Fracture 1968; 4: 11-19.

[13] Broberg KB. Crack-growth criteria and non-linear fracture mechanics. Journal of the Mechanics and Physics of Solids 1971; 19: 407-418.

[14] Broberg KB. On stable crack growth. Journal of the Mechanics and Physics of Solids 1975; 23: 215-237.

[15] Cotterell B, Pardoen T, Atkins AG. Measuring toughness and the cohesive stress-displacement relationship by the essential work of fracture concept. Engineering Fracture Mechanics 2005; 72: 827-848.

[16] Mai YW, Cotterell B. The essential work of fracture for tearing of ductile metals. International Journal of Fracture 1984; 24: 229-236.

[17] Mai YW, Cotterell B. On the essential work of ductile fracture in polymers. International Journal of Fracture 1986; 32: 105-125.

[18] Bárány T, Czigány T, Karger-Kocsis J. Application of the essential work of fracture (EWF) concept for polymers, related blends and composites: a review. Progress in Polymer Science 2010; 35: 1257-1287.

[19] Mai YW, Cotterell B. Effect of specimen geometry on the essential work of plane stress ductile fracture. Engineering Fracture Mechanics 1985; 21: 123-128.

[20] Karger-Kocsis J. For what kind of polymer is the toughness assessment by the essential work concept straightforward?. Polymer Bulletin 1996; 37: 119-126.

[21] Hill R. On discontinuous plastic states with special reference to localized necking in thin sheets. Journal of the Mechanics and Physics of Solids 1952; 1: 19-30.

[22] Hill R. The mathematical theory of plasticity. New York: Oxford University Press; 1998.

[23] Tuba F, Oláh L, Nagy P. On the valid ligament range of specimens for the essential work of fracture method: the inconsequence of stress criteria. Engineering Fracture Mechanics 2013; 99: 349-355.

[24] Martínez AB, Segovia A, Gamez-Perez J, Maspoch ML. Influence of femtolaser notch sharpening technique in the determination of essential work of fracture (EWF) parameters. Engineering Fracture Mechanics 2009; 76: 1247-1254.

[25] Pegoretti A, Castellani L, Franchini L, Mariani P, Penati A. On the essential work of fracture of linear low-density-polyethylene. I. Precision of the testing method. Engineering Fracture Mechanics 2009; 76: 2788-2798.

[26] Chichkov BN, Momma C, Nolte S, von Alvensleben F, Tünnermann A. Femtosecond, picosecond, and nanosecond laser ablation of solids. Applied Physics A: Materials Science and Processing 1996; 63: 109-115.

[27] Moreno P, Méndez C, García A, Arias I, Roso L. Femtosecond laser ablation of carbon reinforced polymers. Applied Surface Science 2006; 252: 4110-4119.

[28] Kim JH, Kim JR, Kim SK, Lee YJ, Kim J. S. Dongbang, ECOZEN®, A New Bio-based, BPA-Free and High-T_g Copolyester, SK chemicals Research Center, Korea.

[29] Maspoch ML, Ferrer D, Gordillo A, Santana OO, Martínez AB. Effect of the specimen dimensions and the test speed on the fracture toughness of iPP by the essential work of fracture (EWF) method. Journal of Applied Polymer Science 1999; 73: 177-187.

[30] Arkhireyeva A, Hashemi S, O' Brien M. Factors affecting work of fracture of uPVC film 1999; 34: 5961-5974.

[31] Hashemi S, O' Brien D. The essential work of plane-stress ductile fracture of poly (ether-ether ketone) thermoplastic. Journal of Materials Science 1993; 28: 3977-3982.

[32] Begley JA, Landes JD. The J integral as a fracture criterion. In: Fracture toughness ASTM STP 514. Philadelphia: American Society for Testing and Materials; 1972, p. 1-20.

[33] Hodgkinson JM, Williams JG. J and G_c analysis of the tearing of a highly ductile polymer. Journal of Materials Science 1981; 16: 50-56.

[34] Shih CF. Relationships between the J-integral and the crack opening displacement for stationary and extending cracks. Journal of the Mechanics and Physics of Solids 1981; 29: 305-326.

[35] León N, Martínez AB, Castejón P, Arencón D, Martínez PP. The fracture testing of ductile polymer films: Effect of the specimen notching 2017; 63: 180-193.